RESCUE AND REPAIR OF COLLAPSED REPLICATION FORKS

by

Kelvin William Pond

A dissertation submitted in partial fulfillment
of the requirements for the Doctor of Philosophy
degree in Cellular and Molecular Medicine in the
Graduate College of
The University of Arizona
2019

THE UNIVERSITY OF ARIZONA
GRADUATE COLLEGE

As members of the Dissertation Committee, we certify that we have read the dissertation prepared by Kelvin William Pond, titled Rescue and Repair of Collapsed Replication Forks and recommend that it be accepted as fulfilling the dissertation requirement for the Degree of Doctor of Philosophy.

[Dr. Nathan Ellis] Date: 05/03/2019

[Dr. Catherine Smith] Date: 5/3/2019

[Dr. Eric Weterings] Date: 05/03/2019

[Dr. Curtis Thorne] Date: 05/03/2019

Final approval and acceptance of this dissertation is contingent upon the candidate's submission of the final copies of the dissertation to the Graduate College.

I hereby certify that I have read this dissertation prepared under my direction and recommend that it be accepted as fulfilling the dissertation requirement.

[Dr. Ted Weinert] Date: 05/5/019
Dissertation Committee Chair
[Cellular and Molecular Medicine]

Acknowledgments

Thanks to all the shared resources at the Arizona Cancer Center, mainly the flow cytometry shared resources and the microscopy alliance. Thanks to my colleagues outside of the lab: Dr. Ghassan Mouneimne and Dr. Marco Padilla-Rodriguez for their help with image analysis, Dr. Gregory Rogers and Dr. Mengdie Wang for their help with microscopy, and Dr. Ted Weinert and Dr. Keith Maggert for their helpful comments and continued mentorship. Thanks to my committee members for taking the time to listen and evaluate my work and progress. Thanks to Dr. Carol Gregorio for continually putting the needs of the students first and always being willing to listen. Thanks to Dr. Christelle DeRenty, Hanen Alassady, and Mary Yagle for their help in the lab. Special thanks to Dr. Nathan Ellis for being the greatest mentor any student could ever want (or deserve), I would have never gotten here without you. Extra special thanks to my parents Dr. Gerald Pond and Dr. Anne Cress for their unconditional support and love from day 1, those are some big shoes to fill, I am continually inspired by your accomplishments.

TABLE OF CONTENTS

Abstract

NSMCE2 is an E3 SUMO ligase and a subunit of the SMC5/6 complex that associates with the replication fork and protects against genomic instability. Here, we study the fate of collapsed replication forks generated by prolonged hydroxyurea treatment in human NSMCE2-deficient cells. Double strand breaks accumulate during rescue by converging forks in normal cells but not in NSMCE2-deficient cells. Un-rescued forks persist into mitosis, leading to increased mitotic DNA damage. Excess RAD51 accumulates and persists at collapsed forks in NSMCE2-deficient cells, possibly due to lack of BLM recruitment to stalled forks. Despite failure of BLM to accumulate at stalled forks, NSMCE2-deficient cells exhibit lower levels of hydroxyurea-induced sister chromatid exchange. In cells deficient in both NSMCE2 and BLM, hydroxyurea-induced double strand breaks and sister chromatid exchange resembled levels found in NSCME2-deficient cells. We conclude that the rescue of collapsed forks by converging forks is dependent on NSMCE2. DNA damage encountered by the replication fork causes fork stalling and is a major source of mutations when not adequately repaired. Fork stalling can lead to fork collapse, that is, a state of the fork in which normal DNA synthesis cannot be resumed at the site of stalling. Collapsed forks must be rescued by replication forks initiated nearby, but little is known about the rescue mechanism by which an active fork merges with a collapsed fork. We used an inhibitor of DNA replication to generate collapsed replication forks and then studied genetic control of collapsed-fork rescue. We found that NSMCE2, which is a gene product that is known to regulate repair responses to replication stress, is required for cells to effectively rescue collapsed replication forks in order to complete DNA synthesis. DNA double strand breaks that are associated with normal collapsed-fork rescue do not accumulate in cells that are deficient for NSMCE2, suggesting that DNA breakage is part of

the rescue and repair mechanism. Failure to rescue collapsed forks leads to DNA damage in mitosis and DNA damage in the following cell cycle. Our work highlights a unique role for NSMCE2 in rescue of collapsed replication forks. We then used the basic information about NSMCE2 and its role in the rescue of collapsed forks to generate the hypothesis that NSMCE2-deficient cells would reply more on topoisomerase proteins to help resolve excess topological stress. We used this to hypothesis to screen for potential NSMC2 inhibitors and discovered four potential compounds which sensitized a human cancer cell line to topoisomerase 1 poison. The finding that NSMCE2 inhibited cells rely more on topoisomerases has a clear impact. As an adjuvant therapy, NSMCE2 inhibition could significantly lower the effective dose of clinically approved, but highly toxic chemotherapies.

CHAPTER I: Introduction

i. Genomic Instability and Cancer

The maintenance of the human genome is essential in both the prevention of cancer initiation and cancer development. Most cancers display genomic instability, and it is considered a hallmark of cancer. However, because genomic instability could be caused by other oncogenic processes, it is difficult to define when this process plays a role in cancer. Mammalian models such as cultured human cell lines, organoids, and murine systems have made provided detailed evidence which shows that genome instability can promote the development of cancer. Detailed analysis of patient DNA has also shown that the onset of genomic instability is tightly associated with cancer development (Ben-David et al., 2019), poor prognosis (Witkiewicz et al., 2015), and therapeutic response (Andor et al., 2017). The study of rare genetic disorders has clearly shown that several different DNA repair genes are essential to prevent cancer. Loss of any one of these DNA repair genes in the germline is sufficient to cause multiple different types of cancer (Cunniff et al., 2017; Lebel and Monnat, 2018; Lynch et al., 2015; Natale and Raquer, 2017; Nepal et al., 2017; Rothblum-Oviatt et al., 2016). The autosomal recessive disorder Blooms syndrome (BS), which results from mutations in the BLM gene, is one such example (German, 1995). Most patients with BS die from cancer related illness as they are 99 times more likely to be diagnosed compared to the general population. Many different types of cancer can occur in BS patients and the mean age of cancer diagnosis is 23 (de Renty and Ellis, 2017). The BLM protein is a potent suppressor of homologous recombination and protects the cells from hyper-recombination. This is evidenced by BLM mutant cells having a 10-fold increase in sister chromatid exchange (SCE), which is a readout for homologous recombination (Chaganti et al., 1974).

SCEs are dependent on RAD51 recombinase, which is essential for homologous recombination. *In vitro*, BLM suppresses the single strand DNA binding of RAD51 to prevent this hyperrecombination phenotype (Bugreev et al., 2007). The study of rare genetic disorders resulting from loss of DNA repair proteins is perhaps the most convincing evidence that genomic instability is sufficient to cause cancer. The hyper-evolutionary state that occurs after a DNA repair mutation in a population of cells would be an essential advantage to a disease that thrives on its ability to persist in multiple different environments, de- and re-differentiate into different cell types, and survive toxic insults that would wipe out a clonal population.

A major source of genomic instability is DNA damage (Jeggo et al., 2016). Cells are constantly challenged by multiple forms of DNA damage, and they have evolved sophisticated DNA repair systems to recognize and repair these lesions. DNA damage repair can be low fidelity due to use of alternative repair-specific polymerases which are more likely to make mistakes compared to canonical nascent DNA synthesis proteins. DNA repair factors can also obstruct transcription and DNA replication machinery, which can lead to development of more serious DNA damaging lesions. Double stranded breaks (DSBs) are the most toxic form of DNA damage that a cell can sustain, and a major source of double strand breaks (DSBs) in proliferating cells originates from the process of DNA replication.

ii. Replication Fork Collapse and Dormant Origin Activation

The replication complex can be destabilized at DNA lesions, difficult to replicate DNA structures, or proteins that have engaged the DNA. These events can to activation of various DNA repair pathways, potentially lethal replication-associated DSBs, and genomic instability. Due to the availability of a homologous sequence, replication-associated DNA damage events are primarily repaired by the high-fidelity homologous recombination (HR)

pathway. To effectively recover from replication-associated DNA damage, cells have multiple mechanisms that stabilize and protect the replication fork during DNA repair.

More than 250 proteins are actively associated with the replication fork during normal DNA replication (Dungrawala et al., 2015). The stopping of the replisome as it encounters an obstruction or lesion is known as fork stalling. During fork stalling, the helicase continues to unwind the parental DNA while the polymerases dissociate as they are unable to produce nascent DNA (Byun et al., 2005). This process, known as uncoupling, results in the exposure of roughly 100 bp of single stranded DNA at each fork, which is double the amount seen at normal replication forks (Zellweger et al., 2015). After uncoupling, the single stranded binding protein replication protein A (RPA) binds the free single stranded DNA (ssDNA) and initiates the DNA damage response via recruitment of repair effector proteins, such as the ataxia telangiectasia and Rad3 related (ATR) kinase. ATR will then facilitate the recruitment of many downstream repair factors and limit the activation of new replication origins to prevent exhaustion of the nuclear RPA pool (Toledo et al., 2013). The recruitment of over 60 repair factors is associated with the dissociation of many of the initial replisome components after prolonged blockade (Dungrawala et al., 2015). The result of prolonged blockade is the inability of the fork to resume DNA synthesis, and is termed fork collapse.

During a normal cell cycle, many more potential origins are licensed in G1 than are used in S-phase. This is because these dormant origins can become activated in situations where normal forks become collapsed. If two convergent replication forks collapse before termination and no dormant origins are present in the un-replicated region, DNA synthesis cannot be completed (Moreno et al., 2016). Failure to complete DNA synthesis in S-phase results in DNA damage in mitosis when sister chromatids attempt to separate. Commonly

damaged loci within the genome often lie within late replicating "origin deserts" and are common sources of DNA damage, presumably due to their frequency of under-replication or repetitive nature (Glover et al., 2017). The frequency of damage at these sites becomes increased when cells are placed in environments where the replication process is slowed (Chan et al., 2009). This is because cells no longer have time to complete replication in regions of the genome which have a low density of origins, such as within heterochromatin.

iii. RAD51 and Replication Fork Stalling

A central factor in the HR process is the RAD51 recombinase. The ancestor of this strand exchange protein, RecA, was originally identified using *E. coli* (Willetts et al., 1969). Mutations in the gene were then identified using yeast screens for radiation sensitive mutations, and the protein was given the name RAD51 (Calderon et al., 1983). The ~43kDa protein contains an ATPase domain, which is stimulated by its binding to single stranded DNA (ssDNA) at the N-terminus. Interestingly, in both humans and yeast, ATP binding but not ATP hydrolysis is required for RAD51 DNA binding (Forget et al., 2007). Hydrolysis of ATP-RAD51 promotes the disassembly of RAD51 from DNA filaments (Hilario et al., 2009). RAD51 binds both ssDNA and double stranded DNA (dsDNA) with comparable affinity (Benson et al., 1994), and in either case each monomer covers three nucleotides of DNA. RAD51 then polymerizes along the DNA to form right handed filaments. The resulting RAD51-bound DNA filament is ~1.5 times its normal B-form length (Chen et al., 2008; Ogawa et al., 1993). During replication-specific DNA repair (Figure 1-1A), RAD51 must initially displace the single stranded binding protein RPA with the help of mediators (Carreira et al., 2009; Godin et al., 2016; Sullivan and Bernstein, 2018). Once properly loaded, the RAD51 ssDNA filament can catalyze a reaction known as strand exchange, where the ssDNA will invade and displace homology-containing dsDNA to form a structure

known as a displacement loop (D-loop) (McEntee et al., 1979; Shibata et al., 1979). During replication specific DNA damage, the replication fork will stop moving to allow for repair by HR. The replication fork backs away from the site of DNA damage during a process known as replication fork reversal (Higgins et al., 1976). The replication fork is then resected to produce a 3' overhanging DNA segment, which is the eventual substrate of RAD51 (Cotta-Ramusino et al., 2005; Thangavel et al., 2015). D-loop formation allows for the re-initiation of DNA replication where the 3' strand has invaded into the homologous sequence ahead of the replication fork. This process eventually leads to break induced replication (BIR) by Holiday Junction resolvases (Mayle et al., 2015) or migrating D-loop repair (Saini et al., 2013). With only one known exception (Ira and Haber, 2002), all HR pathways require RAD51-mediated strand exchange, which results in a heteroduplex DNA structure. If RAD51 is not removed from the heteroduplex DNA, the later steps of HR are inhibited (Solinger et al., 2002). RAD51 plays critical roles at the replication fork both upstream and downstream of its strand exchange activity. For example, RAD51 protects the replication fork from pathological resection independently of the RAD51 mediator, breast cancer type 2 susceptibility protein (BRCA2) (Mijic et al., 2017). Separation of function mutations of RAD51 will need to be more thoroughly investigated in order to determine which activities of RAD51 are required for DNA repair during replication-associated damage.

iv. Collapsed-Fork Rescue

Fork collapse is a rare event, occurring at less than 10% of replication forks, in dividing mammalian cells (Petermann et al., 2010; Pond et al., 2019). However, if cells are exposed to replication associated DNA damaging agents or have high levels of replication stress, fork collapse becomes quite common (Pond et al., 2019). Fork collapse is relevant in cancers because it is triggered by many chemotherapies (Kitao et al., 2018). Cancer cells also

have higher levels of replication stress due to display differential fork speed, metabolic changes, and excessive transcription (Gaillard et al., 2015; Kitao et al., 2018). Although it is well known that forks collapse frequently after prolonged fork stalling in mammalian cells, much less is known about the repair mechanism that occurs as the newly activated dormant origins collide with the collapsed forks. We have termed this process collapsed-fork rescue.

Very little is known about collapsed-fork rescue in mammalian cells, but extremely useful information has been gathered in yeast systems due to the ability of researchers to isolate and study fragments of replicating DNA (Villwock and Aparicio, 2014). This is possible because, unlike human cells, yeasts activate origins of replication at specific loci and therefore robust model systems can be engineered with relative ease. However, it is unclear whether replication forks actually collapse in such a way that they depend on rescue by new origins, as restart of collapsed replication forks occurs and is independent of DSB formation (Lambert et al., 2010; Mizuno et al., 2009). Moreover, the barriers to the replication fork which are used in many yeast systems are somewhat artificial, as many do not activate canonical replication checkpoint responses (Mohebi et al., 2015). Nevertheless, yeast systems have provided useful insights about how collapsed-fork rescue might work in human cells.

The main insight for our work that was provided by yeast systems was the reliance on induction of a DSB for collapsed-fork rescue to occur properly. The MUS81 structure-specific endonuclease (MUS81) is responsible for the cleavage of 4-way branched DNA structures that occur during HR (Boddy et al., 2001). The result of MUS81 activity is the production of a DSB that can be resected to allow for the later stages of HR to occur properly (Whitby et al., 2003). If MUS81 is inhibited in human cells, then cells cannot resolve recombination intermediates which occur as a result remodeling of the stalled replication fork, and mitotic DNA damage occurs (Duda et al., 2016). Three key pieces of

evidence were provided by yeast systems which connect the activity of MUS81 to the BLM helicase and structural maintenance of chromosomes protein 5/6 (SMC5/6). (1) breaks at collapsed forks are dependent on cutting by Mus81 and processing by the BLM ortholog Rqh1 (Froget et al., 2008). (2) fork convergence at a stalled fork is also Mus81 dependent (Mayle et al., 2015). (3) The SMC5/6 is required for Mus81-dependent resolution of recombination intermediates in meiosis (Copsey et al., 2013).

In 2010 Petermann and Helleday discovered that after fork collapse, DSBs are associated with release of cells from prolonged fork blockade, and that these DSBs are far more abundant than DSBs resulting from fork collapse itself (Petermann et al., 2010). Our main goal was to address the gap in knowledge regarding the essential factors required for the production of DSBs during collapsed-fork rescue in mammalian cells.

v. Topoisomerases and their Effects on the Replication Fork

Topoisomerase proteins are essential for proper DNA repair due to their ability to induce a transient break in the DNA in order to relax supercoiled DNA or untangle catenated DNA. The six human Topoisomerases act at various DNA structures and are associated with proper relaxation and untangling of supercoiled DNA occurring during DNA replication, transcription, and segregation of chromosomes. The collective roles of the topoisomerases are too numerous to be described here, but have been excellently reviewed (Pommier et al., 2016). I will focus on topoisomerase 1 and topoisomerase 2α as those are the targets we have investigated. Although Top1 and Top2α mutants are inviable, these proteins are popular as anti-cancer targets due to the high level of DNA damage and repair occurring in many cancer types (Delgado et al., 2018). Topoisomerase poisons, such as Camptothecin (Hsiang et al., 1985) and Etoposide (Minocha and Long, 1984) are a class of topoisomerase inhibitors which stabilize the broken DNA intermediate of the topoisomerase

catalytic cycle. These nicked cleavage complexes can manifest into DSBs and result in cell death as they are encountered by the replication fork. Other inhibitors of topoisomerases will impede different stages of the catalytic cycle resulting in inactive protein, which does not associate with DNA breaks Topo2 inhibitor ICRF-187 (Lyu et al., 2007). These inhibitors are far less toxic to cells, providing a useful differentiation between toxicity caused by replication associated trapping of topoisomerases and the absence of the protein itself. In Chapter 4 we utilized both camptothecin and ICRF-187 to show that Non-structural maintenance of chromosomes element 2 (NSMCE2)-deficient cells rely more on topoisomerase proteins and are sensitized to topoisomerase inhibition. We utilized this defect as a readout to screen several candidate compounds for their potential to inhibit NSMCE2 activity.

vi. NSMCE2 and DNA Repair

Sumoylation is a post-translational modification. In humans, there are five small ubiquitin-like modifier (SUMO) paralogues, however SUMO4 and SUMO5 are only expressed in certain cell types (Bohren et al., 2004; Liang et al., 2016). Yeast possess a single SUNO homolog, Smt3, which is essential. In mice, SUMO1 and SUMO 2-null animals are viable, whereas SUMO 2 mice die during development (Wang et al., 2014; Zhang et al., 2008). SUMO2/3 are thought to be the main SUMO paralogs which respond to cellular stress (Saitoh and Hinchey, 2000). The 11 kDa human SUMO proteins attach to target substrates via their lysine residues. This reversible process, similar to ubiquitination, is catalyzed by three enzymatic steps which require E1, E2, and E3 enzymes. There are over six thousand sumoylation substrates in human cells (Hendriks et al., 2017). Most sumoylation occurs on nuclear proteins which are involved in transcription, mRNA processing, DNA replication, and the DNA-damage response (Hendriks and Vertegaal,

2016). The heterodimeric sumo-activating enzyme E1 (SAE2) is the sole E1 enzyme in humans, which is activated by ATP catalysis of a covalent bond between a cystine on SAE2 and the C-terminal glycine on SUMO. The active SUMO is then passed to the cystine on ubiquitin-conjugating 9 (UBC9), which is the sole E2 enzyme in yeast and humans. Activated UBC9 binds to SUMO substrates via their consensus motif ΨKxD/E (Rodriguez et al., 2001). Importantly, not all consensus sites are sumoylated, and sites outside this motif can be sumoylated (Pichler et al., 2005; Xu et al., 2008). The E3 SUMO ligases promote the substrate specificity of the SUMO modification by bridging the loaded UBC9 with the target substrate, promoting UBC9s SUMO-transfer conformation (Reverter and Lima, 2005; Streich and Lima, 2016). In humans, there are ten SUMO E3 Ligases, and others are continually being discovered. The yeast homolog of human NSMCE2, methyl methanesulfonate sensitivity gene 21 (MMS21), is an E3 SUMO ligase which was first identified in yeast cells that were found to be sensitive to the replication specific DNA damaging agent methyl methanesulfonate (Zhao and Blobel, 2005). Sumoylation mutant alleles of MMS21 accumulate X-shaped replication intermediates which depend on RAD51 recombinase for formation (Branzei et al., 2006). These recombination intermediates are structurally similar to those found in human Bloom's syndrome cells and yeast *sgs1* mutant cells (Liberi et al., 2005). BLM is regulated by sumoylation (Eladad et al., 2005) and contains a sumo-interaction site (SIS) that mediates its localization to promyelocytic leukemia protein (PML) nuclear bodies (Zhu et al., 2008). The yeast homolog of BLM, Sgs1, is recruited to stressed replication forks via interaction of a SIS on Sgs1 and auto-sumoylated MMS21 (Bermudez-Lopez et al., 2016; Bonner et al., 2016a). Similar to the data for yeast Sgs1 recruitment, BLM fails to accumulate at HU-induced stalled replication forks in NSMCE2-deficient cells (Pond et al., 2019), but SCE-inducing agents fail to induce SCEs in cultured

cells (Potts et al., 2006; Potts and Yu, 2007). The defect in the generation of SCEs after fork collapse is likely due to a defect in the formation of DSBs (Pond et al., 2019), which is potentially a prerequisite for HR after replication fork collapse.

Mms21 appears to play a unique role in murine model systems. The genetic ablation of NSMCE2 resulted in increased SCEs, genomic instability, and cancer development (Jacome et al., 2015). These phenotypes were complemented by both a normal and a SUMO-ligase dead allele, leading the authors to conclude that the sumoylation activity of NSMCE2 is independent of its role in genome stability and tumor suppression. This is a puzzling result because yeast, chicken, and human cells rely on the catalytic activity of NSMCE2/Mms21 to prevent genomic instability (Carlborg et al., 2015; Kliszczak et al., 2012; Payne et al., 2014; Potts, 2009; Potts and Yu, 2005, 2007; Wu et al., 2012; Xaver et al., 2013). Currently, it is unknown whether NSMCE2/MMS21 plays a structural role in the SMC5/6 complex in human cells, and model organism data is largely conflicting (Fernandez-Capetillo, 2016; Kliszczak et al., 2012; Tapia-Alveal et al., 2014).

Understanding the molecular mechanisms of repair at collapsed replication forks will facilitate the exploitation of DNA repair defects in cancer treatments. Studies in yeast and humans have given us potential targets for the regulation of replication intermediate processing, and our studies using human cancer cells has provided a translational link for the maintenance of genomic stability regulated by the SUMO pathway. The results gained from this dissertation have provided useful insights into mechanisms which regulate genomic stability through the SUMO pathway and could lead to the identification of novel targets for therapeutic intervention and prognosis.

Here I will present the collected discoveries I have gathered on NSMCE2 and its role in DNA repair during fork collapse and collapsed-fork rescue. In short, my work has led to

insights into a previously uninvestigated repair pathway. The defect in the collapsed-fork rescue pathway in NSMCE2-deficient cells has allowed me to understand how the repair process works in normal cells, and has provided information about a system that cancer cells rely on for survival. I will also present a detailed method on how we studied the successful rescue of collapsed replication forks, preliminary data on the role of NSMCE2 in resection, and its potential as an adjuvant therapy target for human cancers.

CHAPTER II: Rescue of collapsed replication forks is dependent on NSMCE2 to prevent mitotic DNA damage

Introduction

Replication-associated DNA damage is common in human cells and can lead to the development of somatic mutations. DNA damage during replication can be induced by DNA lesion-producing chemicals, proteins bound to the DNA, DNA polymerase inhibitors, or nucleotide limitation (Gaillard et al., 2015). Hydroxyurea (HU) triggers fork stalling due to nucleotide limitation through inhibition of ribonucleotide reductase (Stubbe and van der Donk, 1995). Human cells exposed to HU for up to six hours are capable of restarting 80% of their replication forks (Aggarwal et al., 2010; Leung et al., 2013; Thangavel et al., 2015; Ying et al., 2013). However, forks that are stalled for 16 to 24 h are unable to restart (Petermann et al., 2010), indicating they have collapsed. Collapsed replication forks must be rescued by active forks initiated at dormant origins to complete genome duplication. In both human cells and yeasts, the induction of a double strand break (DSB) is associated with repair of collapsed forks (Hanada et al., 2007; Mayle et al., 2015). Although factors essential for the formation of DSBs during fork collapse have been identified (Fugger et al., 2013), the mechanism generating DSBs when the new replication forks converge with the collapsed forks is unknown.

The DNA helicase mutated in Bloom's syndrome, BLM, possesses multiple functions in DNA replication fork stabilization and homologous recombination (HR), which is a mechanism that operates in the repair of replication-associated DSBs (de Renty and Ellis, 2017). Recruitment of BLM to replication forks is part of the mechanism that stabilizes forks in both unperturbed and replication-stressed cells (Davies et al., 2007; Hand and German, 1975). Excessive DSBs accumulate in BLM-deficient cells released from replication

blockade after prolonged fork stalling (Ouyang et al., 2009), suggesting that BLM plays a role in collapsed-fork rescue. In the absence of BLM, after fork collapse, under-replicated DNA and unresolved HR intermediates persist into mitosis where they cause DNA damage (Chan et al., 2009; Naim and Rosselli, 2009).

The E3 SUMO ligase NSMCE2 is a component of the SMC5/6 complex, which is present at stalled replication forks and a key component of the stalled fork proteome (Dungrawala et al., 2015). In budding yeast, deletion of the *NSMCE2* homolog *MMS21* is lethal; however, sumoylation-deficient hypomorphs are viable and have defects in replication-specific DNA repair (Zhao and Blobel, 2005). These cells also accumulate excess RAD51-dependent recombination intermediates during replication stress and are deficient in HR (Branzei et al., 2006; Zhao and Blobel, 2005). During fork stalling, MMS21 undergoes auto-sumoylation ~~during replication stress~~, after which it recruits the BLM homolog Sgs1 via SUMO binding sites on Sgs1 (Bermudez-Lopez and Aragon, 2016; Bonner et al., 2016b). Once recruited, Sgs1 resolves HR intermediates generated during repair of damaged replication forks.

In human cells, forks adopt a RAD51-dependent structure during stalling, which resembles a Holliday junction (Zellweger et al., 2015). RAD51 is required to prevent replication-induced DSBs, and RAD51 levels increase at stalled forks as they transition from a restart-competent state to a collapsed state (Petermann et al., 2010). BLM regulates the exchange of RAD51 recombinase for RPA (Bugreev et al., 2009; Bugreev et al., 2007), and in previous work we showed that sumoylation of BLM regulates a switch between BLM's pro- and anti-recombinogenic functions (Ouyang et al., 2009). If negative regulators of RAD51 such as BLM and the recently described RADX are ablated, excess RAD51 is loaded at stalled forks and excess DSBs accumulate (Dungrawala et al., 2017). In other situations,

however, induction of excessive RAD51 can instead trigger inhibition of HR repair (Parplys et al., 2015b). Because NSMCE2 regulates BLM recruitment, and RAD51-dependent HR intermediates accumulate in yeast *mms21* mutant cells, we hypothesized that NSMCE2 may be a critical regulator of RAD51 function at collapsed replication forks.

Here we studied the role of NSMCE2 in repair and rescue of collapsed replication forks. We found that NSMCE2 is essential for formation of DSBs during collapsed-fork rescue. Interestingly, lack of DSBs during collapsed-fork rescue is associated with hyper-accumulation of RAD51 and impaired sister chromatid recombination. Defects in the rescue of collapsed replication forks in NSMCE2-deficient cells lead to DNA damage in mitosis.

Results

We used two different siRNAs to deplete NSMCE2 in HeLa cells, resulting in an approximately 80% reduction in both RNA and protein levels (Supplementary Figure 1A). To corroborate key NSMCE2-deficient phenotypes, we also prepared *NSMCE2*-/- clones of HEK293T cells in which we targeted a single site in exon 2 of *NSMCE2* and isolated two clones with different frameshift mutations containing no detectable NSMCE2 protein (Supplementary Figure 1B). Hereafter, we refer to cells in which we have knocked down NSMCE2 as NSMCE2-deficient cells and we refer to *NSCME2*-/- cells as NSMCE2-null cells.

NSMCE2 is required for BLM sumoylation and its localization to stalled replication forks

Experiments in yeast suggested that NSMCE2 is required for efficient sumoylation of BLM (Bonner et al., 2016b; Branzei et al., 2006). To measure SUMO-BLM levels, we used human U2OS cells that express a His-tagged SUMO2 to carry out pull down assays. Analysis of SUMO-conjugates revealed that sumoylated BLM levels increased approximately eight fold after prolonged fork stalling by treatment with 2 mM HU for 16 hours (Figure 1A and 1B). We then tested if sumoylation of BLM is dependent on NSMCE2 by knockdown of endogenous NSMCE2. Depletion of NSMCE2 using two different siRNAs resulted in a 60% decrease in sumoylated BLM in HU-treated cells compared to HU-treated control cells (Figure 1A and B). These data indicate that BLM sumoylation is dependent on NSMCE2. Residual SUMO-BLM could result from the incomplete depletion of NSMCE2 or from residual sumoylation catalyzed by other E3 SUMO ligases.

We previously reported that a BLM protein mutated at its preferred sumoylation sites K317R and K331R is recruited normally to stalled replication forks (Ouyang et al., 2009); consequently, we hypothesized that BLM localization at stalled forks might be normal in NSMCE2-deficient cells. On the contrary, siRNA-mediated depletion of NMSCE2 in HeLa cells led to a three-fold reduction in BLM foci in cells treated with HU for 24 h compared to HU-treated control cells (Figure 1C). NSMCE2 depletion was not associated with a change in the levels of BLM protein in NSMCE2-deficient HeLa cells (Supplementary Figure 2A), and overexpression of siRNA-resistant *NSMCE2* in depleted HeLa cells substantially rescued the defect in localization of BLM at stalled forks (Supplementary Figure 3A; representative low power images of BLM localization are shown in Supplementary Figure 4A). These data show that efficient recruitment to, or retention of, BLM at collapsed replication forks is dependent on NSMCE2.

NSMCE2 prevents excessive accumulation of RAD51 and promotes HR

BLM can promote dissociation of RAD51 recombinase from ssDNA (Bugreev et al., 2009). Because BLM's role in dissociation of RAD51 at stalled forks could be defective in NSMCE2-deficient cells, we tested whether NSMCE2 plays a role in regulation of RAD51 accumulation. NSMCE2-deficient cells, both untreated cells and cells treated with HU for 24 hours, exhibited increases in the number, intensity, and size of RAD51 foci compared to controls (Figure 1D and 1E; Supplementary Figure 3B; representative low power images of RAD51 localization are shown in Supplementary Figure 4C). Western blot analysis showed that total cellular RAD51 protein levels were similar in NSMCE2-deficient and control cells (Supplementary Figure 2A). Because over 90% of stalled replication forks are unable to restart after 24 hours of HU treatment (Petermann et al., 2010; Sidorova et al., 2013), we tested whether the excess RAD51 was localized to collapsed replication forks. To test this, we labeled nascent DNA synthesis with 10 μM EdU for 12 min prior to HU treatment, treated cells with HU for 24 hours, and then analyzed RAD51 foci. As expected, RAD51 co-localized with EdU foci in HU-treated control and NSMCE2-deficient cells (Supplementary Figure 3C). These data show that NSMCE2 is required to prevent over-accumulation of RAD51 at forks under conditions that lead to their collapse.

RAD51 is normally loaded onto ssDNA by exchange with ssDNA binding protein RPA (Ma et al., 2017). We therefore tested whether the excess RAD51 accumulation in NSMCE2-deficient cells might correlate with a diminished accumulation of RPA at stalled forks. For this experiment, we measured the accumulation of chromatin-bound RPA after nucleoplasmic extraction of cells treated with HU for 24 hours. After siRNA-mediated depletion of NSMCE2 and HU treatment, cells displayed 40% fewer RPA foci in both HeLa (Figure 1F and 1G; representative low power images of RPA localization are shown in

Supplementary Figure 4B) and U2OS cells (Supplementary Figure 3D) compared to control cells. Overexpression of siRNA-resistant *NSMCE2* in depleted HeLa cells rescued the defect in RPA foci accumulation (Supplementary Figure 3E). In addition, HU-treated HEK293T NSMCE2-null cells displayed reduced levels of chromatin-bound RPA compared to control normal cells (Supplementary Figure 3F and G). We conclude that RAD51 accumulates in excess over RPA in NSMCE2-deficient and NSMCE2-null cells, perhaps due to a failure to recruit BLM to stalled forks.

The lower levels of RPA foci suggest that there are lower levels of ssDNA. To test this possibility, we measured the levels of ssDNA by incorporation of BrdU for two cell divisions prior to HU treatment, followed by immunodetection with anti-BrdU antibodies in non-denaturing conditions. Unlike control cells, which displayed at least a two-fold increase in BrdU foci after treatment with 2 mM HU for 24 hours, NSMCE2-deficient cells displayed no induction of BrdU foci after HU treatment (Supplementary 3H; representative low power images of BrdU localization are shown in Supplementary Figure 4D). Thus, the lower levels of focal RPA in HU-treated NSMCE2-deficient cells are evidence of lower levels of ssDNA detectable by anti-BrdU antibodies at collapsed replication forks. Because anti-BrdU antibodies cannot detect BrdU in the ssDNA-RAD51 nucleoprotein filament (Haas et al., 2018), these results do not rule out the possibility that the excess RAD51 is bound to ssDNA.

To test whether the RAD51-bound chromatin in NSMCE2-deficient cells is competent for HR, we measured the frequency of sister chromatid exchanges (SCEs) after prolonged fork stalling by 24-hour treatment with HU. The SCE assay measures crossovers generated after resumption of DNA synthesis that can be detected in the subsequent mitosis. NSMCE2-deficient cells had a 45% reduction in the number of HU-induced

SCEs/metaphase compared to control cells (Figure 1H). Thus, the excess RAD51 observed at stalled forks is not associated with increased sister chromatid recombination. Contrary to previous reports using murine cells (Jacome et al., 2015), we found that basal levels of SCEs in HEK293T NSMCE2-null cells were similar to normal HEK293T cells (Supplementary Figure 3I).

NSMCE2 is required for DSBs and RAD51 resolution during collapsed-fork rescue

Because HU-induced SCEs were suppressed in NSMCE2-deficient cells, we hypothesized that the excess RAD51 leads to a defect in DSB formation during rescue of collapsed forks. To test this possibility, we measured DSB accumulation in control and NSMCE2-deficient cells after prolonged exposure to HU. In HeLa cells exposed to control siRNA, a 16-hour treatment with HU did not induce DSBs; however, a 48-hour treatment with HU led to an accumulation of DSBs detectable by pulsed-field gel electrophoresis (PFGE) (Figure 2A). Interestingly, we found that NSMCE2-deficient cells failed to produce a detectable increase in DSBs after a 48-h exposure. Ionizing radiation with 4 Gy followed by a 30-min repair period results in equal levels of DSBs in both control and NSMCE2-deficient cells, indicating that NSMCE2-deficient cells are not defective in DSB formation per se but in replication stress-induced DSBs.

Because NSMCE2-deficient cells are defective in DSB formation at stalled forks after prolonged HU treatment, we tested whether the DNA damage response was also reduced. We measured γ-H2AX levels by analysis of DNA damage foci and flow cytometry. We found by both measures that NSMCE2-deficient cells accumulate two- to three-fold less γ-H2AX after prolonged HU treatment (Supplementary Figure 3J) despite normal levels of

phosphorylation of CHK1 and of RPA32 (Supplementary Figure 2A). Substantial rescue of the levels of γ-H2AX foci was observed by overexpression of siRNA-resistant *NSMCE2* (Supplementary Figure 3L).

To investigate the ability of cells to generate DSBs during collapsed-fork rescue, we measured the kinetics of accumulation of DSBs over time after release from HU. After release from the HU block, normal cells linearly accumulated DSBs, whereas NSMCE2-deficient cells failed to accumulate DSBs four and eight hours after release (Figure 2A). The accumulation appears to be replication-dependent, because normal cells released into 10 μM aphidicolin after HU arrest did not accumulate DSBs (Supplementary Figure 5A). Flow cytometry confirmed that control and NSMCE2-deficient cells show similar cell-cycle distributions 6 and 12 hours after release from HU, suggesting that differences in cell cycle progression after release from HU do not explain these results (Supplementary Figure 5B). Moreover, no significant differences in the levels of apoptosis were observed in control and NSMCE2-deficient cells after release from HU, ruling out apoptosis as a confounder of differences in DSBs (Supplementary Figure 5D). Levels of DSBs in untreated HEK293T NSMCE2-null cells were higher than in untreated normal HEK293T cells; however, similar to the results obtained with NSMCE2 depletion, after treatment with HU and during release we observed a defect in accumulation of DSBs (Supplementary Figure 5C). Similar to NSMCE2-deficient HeLa cells, NSMCE2-null cells were also defective in their γ-H2AX response after HU treatment (Supplementary Figure 5E). Collectively, the results suggest that in the absence of NSMCE2 the levels of DSBs that are normally generated during collapsed-fork rescue are reduced.

We next tested whether NSMCE2-deficient cells have a defect in the dynamics of RAD51 localization during collapsed-fork rescue. Because RAD51 protein accumulates

during HU treatment, we hypothesized that converging forks displace the RAD51 over time. We therefore released cells from prolonged fork stalling and measured levels of the RAD51 foci at collapsed replication forks in a time course. Two, four, and eight hours after release from HU, control HeLa cells exhibit a steady decrease in RAD51 foci whereas NSMCE2-deficient cells retained them (Figure 2B). RAD51 foci increased in normal cells between 8 and 12 h after release from HU, possibly due to RAD51-dependent DNA repair in late S or G2 phase. In addition, we also observed a persistence of RAD51 foci at stalled forks in NSMCE2-null cells compared to normal cells after release from HU treatment (Supplementary Figure 6A). In both normal and NSMCE2-null HEK293T cells, RAD51 foci co-localized with RPA and γ-H2AX foci (Supplementary Figure 6B).

We considered the possibility that persistence of excessive RAD51 at collapsed replication forks might disturb replication dynamics in S phase after release from HU. To measure replication fork dynamics, we performed microfluidics-assisted replication track analysis (maRTA)(Sidorova et al., 2009). We found that replication fork speed, fork restart, and dormant origin firing were similar in NSMCE2-deficient cells compared to control cells, after either 5 or 16 h of HU treatment (Figure 2C). These data indicate that both the replication dynamics of unperturbed forks and of dormant origin activation in replication-stressed cells are not adversely affected by NSMCE2 deficiency.

NSMCE2 prevents mitotic DNA damage resulting from replication stress

NSMCE2-deficient cells maintained normal cell cycle progression in the absence of HU treatment (Figure 2D); however, after release from prolonged HU treatment, NSMCE2-deficient cells displayed an arrest in the next G1 phase (Supplementary Figure 7A). Defects

in collapsed-fork rescue could lead to under-replicated DNA in S phase and DNA damage in mitosis. Similar to previously reported results (Jacome et al., 2015; Payne et al., 2014), we found increases in the frequencies of abnormal anaphases, micronuclei, and G1 53BP1 nuclear bodies after release from HU block in NSMCE2-deficient cells compared to controls indicating that excess mitotic DNA damage is induced in NSMCE2-deficient cells (Supplementary Figure 7B-F; representative low power images of 53BP1 localization are shown in Supplementary Figure 4E).

To investigate further the nature of the mitotic damage invoked in HU-treated, NSMCE2-deficient cells, we measured the frequency of ultra-fine bridge (UFB) formation in cells undergoing mitosis. In order to obtain a sufficient number of cells in anaphase, cells were pretreated or not with HU for 24 h; they were then blocked in G2 with 7.5 μM of the CDK1 inhibitor RO-3306 for 15 h and then finally released into metaphase for 1 h prior to fixation (Figure 3A). Flow cytometry confirmed effective G2 arrest by RO-3306 treatment (Supplementary Figure 7G). We visualized UFBs using the PICH repair helicase, which localizes to UFBs and DNA under tension (28). The number of UFBs measured by PICH staining was increased after HU treatment in NSMCE2-deficient cells but not control cells (Figure 3B and F). PICH-positive UFBs were also positive for BLM (Figure 3C), indicating that localization of BLM to these structures is not dependent on NSMCE2. The crosslink repair protein FANCD2 is sometimes associated with the ends of UFBs, and has been used as a marker for under-replicated DNA persisting into mitosis (16). FANCD2-flanked, PICH-positive UFBs (Figure 3D) were infrequently observed in both NSMCE2-deficient and control cells. Thus, the excess UFBs produced in NSMCE2-deficient cells are not equivalent to the UFBs produced in cells treated with low-dose aphidicolin (Chan et al., 2009; Naim and Rosselli, 2009).

We then tested whether mitotic DNA damage originated from collapsed forks in the previous S-phase. As a marker for damaged DNA and repair in anaphase cells, we counted the number of FANCD2 foci and found a 1.8 fold increase in NSMCE2-deficient cells treated with HU compared to control cells (Figure 3E and G). In order to monitor the location of collapsed forks generated by prolonged treatment with HU, we labeled cells with EdU for 20 min before treatment with HU. FANCD2 foci co-localized with the EdU label at a greater frequency in HU-treated, NSMCE2-deficient cells compared to control cells (Figure 3H), indicating that the recruitment of FANCD2 observed in mitosis had occurred in regions of chromatin where replication forks had previously stalled and collapsed. These data suggest that defective collapsed-fork rescue in NSMCE2-deficient cells leads to increased under-replicated DNA persisting into mitosis, which results in mitotic DNA damage.

In order to measure DNA damage in metaphase cells, we measured the levels of γ-H2AX associated with metaphase chromosomes and the levels of chromosome aberrations detectable at metaphase. For the analysis of γ-H2AX levels, normal HEK 293T and NSMCE2-null cells were treated with 2 mM HU for 24 h, released into medium with RO-3306 to block them in G2, then released into normal medium and prepared for analysis of γ-H2AX levels by immunofluorescence (Supplementary Figure 8A and B). HU-treated NSMCE2-null cells exhibited a nearly 50% increase in median fluorescence intensity of chromosome-associated γ-H2AX in phospho-H3-positive cells compared to HU-treated HEK 293T normal cells. For the analysis of chromosome aberrations, cells were treated or not with 2 mM HU for 24 hours and then metaphase chromosomes were prepared and analyzed by fluorescence microscopy (Supplementary Figure 9). We identified increased frequencies of chromatid arm breaks, telomere fusions, and secondary constrictions in

NSMCE2-null cells compared to control cells. Chromatid arm breaks and secondary constrictions were induced by HU treatment (Supplementary Figure 9). The increase in secondary constrictions in HU-treated NSMCE2-nulls cells is consistent with increased under-replicated DNA and the increase in chromatid breaks could arise from chromosome breakage in mitosis or under-replication as seen at common fragile sites.

Epistasis relationships among *NSMCE2, BLM,* and *RAD51* during collapsed-fork rescue

Because NSMCE2 is essential for proper localization of BLM to stalled replication forks but displays phenotypes distinct from BLM-deficient cells, we asked whether *NSMCE2* is epistatic to *BLM* during rescue of collapsed forks. In these experiments, we used siRNAs to deplete BLM in NSMCE2-null and control cells (Figure 4A). In normal HEK293T cells depleted for BLM, Western blot analysis showed that levels of phosphorylated RPA and γ-H2AX are similar to control cells. In contrast, in NSMCE2-nulls cells depleted for BLM, the levels of phosphorylated RPA and γ-H2AX are reduced in comparison to control cells but similar to NSCME2-null cells. The data for phosphorylated H2AX were confirmed by analysis of focal γ-H2AX and flow cytometry (Figure 4B, D, and E). Prolonged HU treatment of BLM-deficient normal HEK293T cells resulted in a 2.6 fold increase in the levels of SCEs from 8.2 to 21.1 SCEs/metaphase, whereas prolonged HU treatment of BLM-deficient NSMCE2-null cells resulted in an only small increase in SCEs from 4.6 to 6.3 SCEs/metaphase (Figure 4C). Consistent with the suppression of HU-induced SCEs, the levels of HU-induced DSBs were also suppressed in BLM-depleted NSMCE2-null cells relative to BLM-deficient normal cells. These data indicate that NSMCE2 is epistatic to BLM with respect to HU-induced phenotypes.

Because DSB accumulation is suppressed in NSMC2-deficient cells, we tested whether depletion of RAD51 would restore HU-induced DSB levels to normal in NSMCE2-null cells. After transfection of control and RAD51 siRNAs, we treated cells with 2 mM HU for 24 hours, then released into normal medium for 6 hours and quantitated the DSB marker γ-H2AX by flow cytometry and measured DSBs by PFGE. In HU-treated, control-depleted normal HK293T cells, γ-H2AX levels increased approximately 10 fold compared to baseline after release into normal medium for 6 hours (Supplementary Figure 10A and C). Contrary to expectation, RAD51 depletion in normal cells resulted in much smaller induction of γ-H2AX, similar to the levels in HU-treated control and RAD51-depleted NSMCE2-null cells. Consistent with the results with γ-H2AX levels, in HU-treated, control-depleted normal HEK293T cells, DSB levels increased approximately three-fold compared to baseline after release into normal medium for 6 hours (Supplementary Figure 10B). In contrast, RAD51 depletion in normal cells resulted in almost no induction of DSBs compared to baseline, which again was similar to the levels of DSBs in HU-treated control and RAD51-depleted NSMCE2-null cells. Similar results on DSB formation were observed when we treated HEK293T cells with the RAD51 ssDNA binding inhibitor BO2 (Supplementary Figure 10E), which disrupts DNA strand exchange activity (Huang and Mazin, 2014; Huang et al., 2011). Treatment of cells with BO2 did result in an increase in the levels of DSBs in untreated cells but had very little effect on cells treated with or released from HU block. NSMCE2-null cells were largely unaffected by treatment with BO2. The formation of UFBs in HeLa cells after knockdown of RAD51 was increased compared to controls, and levels were similar to those seen in cells after NSMCE2 depletion. A further increase was also observed after treatment with HU in siR51 cells. Cells which were knocked down for both NSMCE2 and RAD51 showed no further increase in the level of UFBs formed after fork

collapse. These data suggest that, despite the fact that RAD51 has hyper-accumulated at collapsed replication forks, in the absence of NSMCE2, the RAD51 at collapsed forks is nonfunctional.

Discussion

DNA combing experiments in mammalian cells have shown that, after prolonged fork stalling due to HU exposure, DNA synthesis does not normally resume at the site where the fork stalled (see reference 2 and Figure 2). These data rule out rescue mechanisms, such as HR-mediated restart or break-induced replication, in which replication is re-established at the site of fork stalling. The majority of collapsed forks must therefore be rescued by converging forks initiated at dormant origins after release from prolonged replication arrest. DSBs have been previously associated with resumption of DNA synthesis after release from prolonged HU block (Ouyang et al., 2009; Payne et al., 2014; Petermann et al., 2010), but the mechanism by which these breaks are generated is not well understood. Here we show that normal rescue of collapsed replication forks is dependent on NSMCE2. After resumption of DNA synthesis, NSMCE2-deficient cells do not accumulate normal numbers of DSBs. The large increase in UFBs in mitosis indicates that many forks fail to complete DNA replication.

NSMCE2 deficiency is associated with a higher number of RAD51 foci at collapsed forks and persistence of foci after release from replication arrest. These results are consistent with results obtained in yeast mutants of the SMC5/6 complex and *MMS21*, in which excess RAD51-dependent recombination intermediates accumulate at stalled forks (Ampatzidou et al., 2006; Branzei et al., 2006; Sollier et al., 2009). Pathological accumulations of RAD51 have

been associated with DNA repair defects (Inano et al., 2017; Parplys et al., 2015a). We do not know the structure of the RAD51-bound DNA in NSMCE2-deficient cells, and the excess RAD51 could be at the fork itself, associated with ssDNA gaps behind the fork, or associated with other abnormal structures. There are established roles for RAD51 at stalled replication forks that do not involve DSBs. For instance, RAD51's role in reversal of the replication fork is epistatic to its BRCA2-mediated fork protection function (Mijic et al., 2017; Schlacher et al., 2011). Our experiments with RAD51 depletion in normal cells suggest that reversed fork structures, catalyzed by RAD51, are required for the formation of DSBs during fork rescue, very likely as substrates for nucleases such as MUS81. Biochemical studies suggest that BLM performs a quality control function on stressed replication forks by dissociating nonfunctional, ADP-bound RAD51 from the nucleoprotein filament. Because BLM does not accumulate normally to stalled forks in the absence of NSMCE2, it is possible that the RAD51 that accumulates excessively in NSMCE2-defcient cells is in the nonfunctional ADP-bound state. That said, the epistasis experiments indicate that NSMCE2 controls other factors besides BLM that contribute to the function of RAD51 at collapsed forks. We propose a model in which the excess nonfunctional RAD51 prevents DSB formation during the convergence of active replication forks with collapsed forks, leading to excess under-replicated DNA that is detectable at anaphase (Figure 5). However, more definitive tests of this proposition are required to rule out other possible models. For example, it could be informative to use molecular combing to monitor the replication dynamics of forks from newly fired origins as they converge upon collapsed replication forks.

We found that BLM sumoylation is dependent on the presence of NSMCE2. We and others (Payne et al., 2014) have shown that BLM does not accumulate normally at

stalled forks in NSMCE2-deficient cells. BLM has multiple functions in the resolution of recombination intermediates during replication stress, normally ensuring that recombination intermediates are resolved without exchange. Yet the levels of SCEs are low in the absence of NSMCE2, suggesting additional roles of NSMCE2 in promotion of crossover events when BLM is absent. Our evidence suggests that RAD51-associated intermediates in NSMCE2-deficient cells are not resolved until M phase, whereas RAD51 foci are normally resolved during S phase. Because BLM localization to UFBs is not dependent on NSCME2, BLM could have a role in resolving RAD51-associated intermediates in mitosis. Our findings that excess γ-H2AX accumulated on metaphase chromosomes, but not during S phase, suggest that under-replicated DNA is not resolved until G2/M phase. For example, prometaphase DNA repair (Ying et al., 2013) or mitotic resolvases (Shah Punatar et al., 2017) could decatenate under-replicated DNA to permit disjunction of inter-linked sister chromatids.

We cannot rule out the possibility that the loss of NSMCE2 in cells affects the function of the SMC5/6 complex. However, in agreement with previous results in human U2OS and DT40 cells (Kliszczak et al., 2012; Verver et al., 2016), we found SMC5 levels were normal in NSMCE2-deficient HeLa cells (Supplementary Figure 2B). These data suggest that, unlike in *S. cerevisiae* (Duan et al., 2009), SMC5 levels are not dependent on the presence of NSMCE2 in human cells. Whether NSMCE2 plays a structural role in collapsed-fork rescue and other repair processes remains to be determined.

Our results here agree with previous results showing lower levels of SCEs in NSMCE2-deficient cells (Wu et al., 2012). Hypomorphic *NSMCE2* mutation in humans is associated with a syndrome characterized by short stature and acanthosis nigricans (Payne et al., 2014). Cells derived from these patients display increased micronuclei, nucleoplasmic

bridges at cytokinesis, and binucleated cells. Despite a defect in BLM localization at replication forks in patient cells, untreated cells have normal SCE levels, and UV treatment induces only a small increase in SCEs (Payne et al., 2014). We found that cells deficient for both NSMCE2 and BLM exhibit reduced levels of HU-induced DSBs and SCEs, indicating that NSMCE2 is epistatic to BLM during collapsed-fork rescue. In contrast to results with human cells, murine cells that are null for *Nsmce2* exhibit increased SCEs, and *Blm* knockdowns in the murine *Nsmce2*-null cells display an additive increase in SCE levels (Jacome et al., 2015). The explanation for these different outcomes of NSMCE2 deficiency between humans and mice is unknown.

We used HU to generate and study collapsed forks and to block repair-coupled DNA synthesis (e.g., break-induced replication, gap filling, lesion bypass, etc.). We therefore cannot rule out the possibility that NSMCE2 plays other roles during the unperturbed cell cycle or in situations where template switching can bypass DNA damage during replication, such as in cells treated with methyl methanesulfonate or UV irradiation. We observed higher levels of DSBs in untreated NSMCE2-null cells (Supplementary Figure 4), but observed no increase in basal SCE levels (Figure 4C). Our analysis using maRTA indicated that deficiency of NSMCE2 did not alter replication dynamics in untreated cells, which is consistent with results reported in yeast (Menolfi et al., 2015). We suggest that the increased DSBs in untreated NSMCE2-deficient cells may originate from incomplete replication at common fragile sites, leading to DNA breakage in mitosis and the formation of micronuclei in the next cell cycle that are known to be prone to replication-associated DNA breakage (Zhang et al., 2015). HR-directed DSB repair is dependent on NSMCE2 (De Piccoli et al., 2006; Watanabe et al., 2009); consequently, these breaks would most likely be repaired by non-homologous end joining. Studies in both mammalian cells (Jacome et al., 2015; Potts et al.,

2006) and yeasts (Liang et al., 2018) indicate that HR can be increased in NSMCE2-deficient cells under some conditions, emphasizing the general complexity of NSCME2's roles in maintenance of genomic integrity.

The importance of mechanisms that regulate RAD51 protein levels is underscored by studies that have identified increased RAD51 protein levels as a negative predictor of patient outcome in several cancer types (Gachechiladze et al., 2017). The present work has uncovered a connection between NSMCE2 and the formation of DSBs at collapsed replication forks during rescue. The identification of NSMCE2 as a potential controller of HR-mediated fork rescue highlights NSMCE2's potential as a new therapeutic target for combinatorial therapy of HR-dependent cancers.

CHAPTER III: Analysis of Double Strand Breaks in Mammalian Cells using Pulsed Field Gel Electrophoresis

1. Introduction

Double strand breaks (DSBs) are a particularly cytotoxic type of DNA damage (Bennett et al., 1993). Generation of this toxic DNA damage in humans has important clinical applications, especially in cancer treatments (O'Connor, 2015). DSBs can be generated using DNA damaging agents, such as γ-irradiation and topoisomerase inhibitors, that are exogenously administered to cells in culture or to whole animals (van Gent et al., 2001). They can also be generated endogenously by normal cellular process (e.g., during immune cell gene rearrangements, DNA repair, and meiotic recombination) (Ashour et al., 2015; Hanada et al., 2007; Nitiss, 2009). Accurate measurement of DSBs in mammalian cells is a critical methodology, because understanding both how DSBs are generated and how they are repaired is a cornerstone in basic scientific investigations and in novel clinical applications.

Clinically relevant doses of γ-irradiation (1-2 Gray) generate approximately 40 DSBs per cell (Blocher, 1988; Elia et al., 1991), which is equivalent to 1-2 breaks per chromosome. Human chromosomes range from 50 to 250 million base pairs in length. Consequently, for a method to be truly useful in experimental investigations, it should be able to achieve a sensitivity to resolve DNA fragments in the 10 million base pair (Mb) range or longer. The pulsed-field gel electrophoresis (PFGE) method is the only technology that approaches this range. The PFGE method relies on the capacity to separate DNA fragments on the basis of their migration through an agarose gel. In standard agarose gel electrophoresis, which relies on application of an electric field of constant strength parallel to the direction of DNA migration, the limit of DNA length resolution is approximately 25 kb [8]. The limitation of

mobility is thought to arise from the parallel alignment of DNA molecules and an associated reduction in thermal motion of the molecules such that the larger molecules slither through the agarose sieve with the same mobility. PFGE differs from standard agarose gel electrophoresis in that DNA fragments are separated by application of varying field strengths at different angles for different times. The variation in field direction along with variation of both field strength and time prevents the parallel alignment of the DNA molecules and permits reorientation of the DNA molecules relative to the pores in the agarose sieve. Once the gel system and associated materials are acquired, PFGE provides a simple and quantitative method to measure DSBs in a population of cells.

The PFGE method was developed in tandem with methods that preserve chromosome DNA intact. In standard DNA preparations, the DNA molecules are sheared to lengths shorter than 500,000 bp. The method used for PFGE relies on embedding cells in low-melt agarose then lysing cells and digesting the proteins on the DNA in the agarose. This procedure spares the DNA from shear forces, such as pipetting, that would break the DNA.

When considering methods to quantify DSBs, there are alternative assays that may be better applications depending on the situation. Constant-field gel electrophoresis (CFGE) is a more cost effective alternative to PFGE (that is, the CFGE apparatus is less expensive than the PFGE apparatus) (Saleh et al., 2012), and it has been suggested that it is comparable in sensitivity (Wlodek et al., 1991); however, it has not yet been fully embraced by the scientific community. The neutral comet assay (Olive and Banath, 2006) has the capacity to measure the levels of DSBs in mammalian culture in individual cells. The method avoids a 50 ^{0}C incubation step used in the processing of embedded cells for PFGE, which can cause excess DNA breakage after radiation (Rydberg, 2000). The neutral comet assay does not

require a large number of cells and does not require the purchase of an expensive PFGE apparatus, but it requires expertise in the image analysis, and the method does not have the capacity to define the range of lengths of broken DNA fragments. Quantification of DNA repair proteins, such as measurement of the levels of phosphorylated H2AX, which is the substrate for activated ATR, ATM, and DNA-PK protein kinases, has been widely used as a readout for the levels of DNA damage (Bonner et al., 2008); however, due to the fact that exposure of both ssDNA and dsDNA results in phosphorylation of H2AX, it is not possible to determine the type of DNA damage that has been induced when using this method. Recently, RNA transcripts have been shown to be mediate DSB repair under certain circumstances, and assays have been developed which can quantify RNA-dependent DSBs (Keskin et al., 2014; Keskin and Storici, 2018). Small double stranded RNAs have also been recently implicated in DSB repair (Michelini et al., 2017). However, assays to detect these specific repair RNAs to quantify DSB levels have not yet been developed.

We describe here a PFGE protocol that consolidates fragments of DNA of lengths ranging from 500 kb to approximately 2 Mb into a single band for easier quantification (Hanada et al., 2007). DNA fragments from 200 kb to greater than 6 Mb are also visible in the lane (Ouyang et al., 2009). The PFGE protocol allows for a population-based analysis of DSBs without laborious image analysis. Importantly, additional steps can be added to this protocol, such as Southern or immunoblot analysis, in order to quantify the amount of DSBs associated with the replication fork (Kawashima et al., 2017).

2. Materials

2.1 Tissue Culture and Tissues

1. For culturing cells in vitro, a sterile environment is critical. Investigators should use a standard tissue culture hood, incubator, media, and growth conditions optimized for

mammalian cell culture in which assays are to be run. Mammalian cells should be incubated in a water-jacketed incubator at 37 °C and 5% CO_2. Manipulations of cells outside the incubator should be done in a Class II (HEPA-filtered) laminar flow bio-safety cabinet.

2. Tissue samples from animals and humans can also be used for PFGE analysis. The main requirement for the method is to obtain a single-cell suspension. Hence, nucleated cells from blood or disaggregated cells from solid tissues are also a source of material.

2.2 Buffers and Solutions

1. Agarose insert buffer: 10 mM Tris-HCl pH 7.5, 20 mM NaCl, 50 mM EDTA, diluted in ultrapure water. 50 ml can be made and stored at room temperature indefinitely.

2. Lysis Buffer (prepared fresh for each use): 100 mM EDTA pH 8.0, 0.2% (wt/vol) sodium deoxycholate, 1% (wt/vol) sodium lauryl sarcosine, and 1 mg/ml proteinase K. 500 µl of lysis buffer is required for each plug (see below).

3. Tris-Acetate-EDTA (TAE) running buffer for gel electrophoresis: Prepare 1800 ml of 1x running buffer from 50x stock (2M Tris, 1M acetate, 50 mM EDTA) in ultrapure water. This reagent can re-used once after first use.

4. Pulsed-Field Certified Agarose. Prepare fresh for each gel run 1% (wt/vol) agarose in TAE buffer.

5. Tris-EDTA (TE) buffer: 10 mM Tris-HCl (adjusted to pH 8.0), 1 mM EDTA pH 8.0 (prepared and sterilized by filtration through 0.2 µm filter). A 500 ml stock of TE buffer can be made and kept at room temperature indefinitely.

6. CHEF DNA size marker agarose blocks (*S. cerevisiae).*

7. DNA staining solution optimized for agarose gel imaging.

8. Low Melting Point Agarose. Add 0.8 grams of low-melt agarose to 40 ml of ultrapure water. Equilibrate the 2% solution at 50 °C until the agarose is entirely dissolved and prepare

4-ml aliquots using 15-ml round bottom tubes. Store at 4 °C. Round bottom tubes should be closed tightly to prevent evaporation.

9. 302 nm UV illuminator and gel imaging system.

2.3 Gel System and Hardware

1. PFGE Gel system: Electrophoresis chamber, power module, variable speed pump, cooling module, casting stand, comb, and disposable sample plug molds. The instructions that we give in this protocol for gel set up are based on this system. Other PFGE systems can be used, and the experimenter should refer to the manufacturer's instructions for gel set up in their system.

3. Methods

3.1 Cell culture, treatment, and harvest

1. The overall procedure depends on the DNA damage or cell stress protocol. For chemical treatments or ultraviolet irradiation, cells are seeded into dishes or flasks, treated or not with chemical agent or irradiation, allowed to recover and repair, and then prepared for analysis by embedding the cells in low-melt agarose plugs (see Note 1 and 2.2.8). The protocol that we describe here generates 3 plugs for each sample. A typical scheme for monitoring damage and repair in tissue culture cells is shown in Figure 1.

2. The PFGE method can be used on both attached and suspension cell cultures. Calculate the number of cells needed at the beginning of the experiment so that 1 million cells are obtained at harvest, taking into account the cell proliferation expected over the course of the experiment.

3. Seed cells into dishes so that cells are sub-confluent and growing at the maximal rate throughout the experiment.

4. Allow at least 12 hours recovery after seeding, expose cells to agent and harvest cells at different times following the accrual of DSBs and repair at each time point (Figure 2; see Note 2).

5. If the cells grown in suspension, disaggregate the cells, centrifuge them to make a pellet (our standard condition is 300 x g for 5 min). Attached cells must be dislodged from the substrate and a single-cell suspension of cells obtained for an accurate cell count. Wash cells with PBS (see Note 4), expose the cells to the agent used to detach the cells (typically trypsin-EDTA) until they are easily detached and disaggregated, and re-suspend the cells in media, ensuring a thoroughly homogeneous single-cell suspension. Wash the cells twice in PBS, and then count the cells using a hemocytometer. Ensuring an accurate count of cell numbers across conditions is critical. Keep cells on ice until ready to embed the cells in plugs (see Note 3).

3.2 Preparing Low-melting Point Agarose Plugs

1. Place the 4-ml aliquot of 2% low-melt agarose in a 100-ml beaker with 40 ml of water and microwave the aliquot for 10-30 seconds until agarose is melted. Make sure the cap to the round bottom tube is loose and avoid boiling the agarose. Use the minimum amount of time required for melting and ensure the agarose is thoroughly melted by checking for opacities in the solution.

2. Place the round bottom tube in a beaker of 42 ^{o}C water and allowed several minutes to equilibrate.

3. Centrifuge 7.5 x 10^5 cells at 300 x g for 5 minutes at 4 °C (see Note 5). Aspirate PBS and re-suspend the cells (entire pellet) in 150 µl of agarose insert buffer.

4. Add 150 µl of the low-melt agarose for each ml of cell suspension and mix the solution well using a large diameter pipette tip (see Note 6).

5. Molds are purchased with the bottom side covered, but they can be reused (after cleaning in soapy water, rinsing, and drying) by covering the bottom side with standard adhesive laboratory tape. Fill three wells of the disposable sample plug mold with 90 µl of the low-melt agarose-cell suspension (see Note 7). Avoid introducing bubbles by filling from one corner of the mold. The mold should not be over-filled.

6. After filling, place the molds at 4 °C for 10-15 min, but not longer, to allow the agarose to solidify.

7. Extrude the plugs from each sample into a 15-ml round bottom tube containing 1.5 mls of lysis buffer and incubate in a stationary water bath at 50 °C overnight (see Note 8).

3.3 Preparing DNA samples and Loading the Gel

1. Wash the plugs with 1.5 ml of TE buffer for at least 30 min three times (gentle rocking or nutation can be used). Use a disposable inoculating loop to prevent loss of plugs while decanting during washing steps. Decant into a small beaker to allow for recovery of lost plugs. Plugs can be kept at 4 °C in TE buffer for up to 1 year. During the lysis and protein digestion steps, the plugs should have gone from cloudy-looking to clear and are more difficult to see while in the TE buffer.

2. To prepare the agarose gel for running, assemble the casting stand (see Figure 2B). The gel will sit on the black platform (see Figure 2A) that holds the gel in place in the gel running tank. Place the platform in the casting stand and attach the white casting stand end gates so

that the platform slides into the end gate grooves. Ensure that the screws are tight and the platform is firmly fitted into the grooves of the end gates. Adjust the casting stand so that the space between the platform and the casting stand is minimal to minimize liquid agarose leaking under the platform. Adjust the comb to at least 2 mm above the platform. Before pouring the gel, ensure the casting stand is placed on a level surface.

3. Prepare 100 ml of 1% pulsed-field certified agarose gel solution using microwave or a hot plate. Combine 1.0 g agarose and 100 ml water in a clean 250-ml Erlenmeyer flask, cover the flask tightly with plastic wrap to minimize evaporation, and microwave at medium intensity. Ensure all the agarose is melted and avoid excess boiling. Cool the agarose solution to < 60 ^{o}C. Carefully pour the solution into the prepared casting stand. Avoid bubbles and make sure to allow the gel to cool and solidify fully before loading. Any persistent bubbles can be swept to the periphery with an inoculating loop or Pasteur pipet.

3. Gently pull the comb from the gel and ensure the wells are fully intact.

5. Place one of the *S. cerevisiae* DNA size standard plugs on a 10 cm x 10 cm square of parafilm laid on the bench. Cut a small square of the size standard and load it with an empty well between the standard and the first sample to avoid contamination of signal (see Note 9).

6. To prepare the plugs for loading on the gel, use a plastic inoculating loop to gently remove one of the plugs from the tube and place on the 10 cm x 10 cm square of parafilm on the bench and (Note 10). To ensure a standard size of plug to run in each experiment, plugs should be cut in half (see Figure 2C and Note 11). Next, slide the plug fragment onto a razor, and gently load each plug fragment into each well (see Figure 2E). Take care not to break the plugs as they are fragile at this step.

3.4 Preparing the Gel Box

1. Add 1.8-2 L of 1 x TAE buffer to the gel box and cool the buffer to 14 °C by engaging the cooler and pump. Set the pump speed to 0.8 to 1 L per min.

2. The black platform frame (see Figure 2A) is a black metal sheet with a 20 cm x 20 cm square cut out and holds the platform in place in the gel box. Place the platform barrier in the center of the gel box and ensure the white plastic fastener pegs are engaged in the bottom of the gel box to prevent the black gel platform from moving.

3.5 Running the Gel

1. After the buffer is cooled, slide the platform from the casting stand and carefully remove any solidified gel from the bottom of the platform using a wipe. Do not remove the gel from the platform. Gently place the platform into the black platform frame (see Figure 2A and Note 12). Ensure the gel is completely submerged in buffer (see Note 13).

2. Perform the electrophoresis for 21 h at 14 °C using the following protocol: block I: 9 h, 120° included angle, 5.5 V/cm, 30 to 18-s switch; block II: 6 h, 117° included angle, 4.5 V/cm, 18 to 9-s switch; block III: 6 h, 112° included angle, 4.0 V/cm, 9 to 5-s switch.

3.6 DNA and Double-Strand Break Detection

1. Prepare 100 ml of 1 x SYBR gold detection solution in a dish slightly larger than the gel. Remove the gel from the gel box and gently slide the gel off of the platform and into the container. Cover the container with plastic wrap and gently rock for 10-15 min at room temperature.

2. Image the gel using UV illumination and acquire high resolution images adjusted for the exposure of the DSB bands. Ensure that the bands in image are captured in the linear range of exposure.

3.7 Gel Quantification

1. Quantify the gel images using Image J densitometry measurements with background correction. Use the rectangle tool to draw a region of interest around the single band that contains the consolidated DNA fragments. Measure the intensity of each band in the column (see Note 14). Subtract the background from an empty lane and represent data as either fold change compared to untreated samples or in arbitrary units.

4. Notes

1. If a baseline measurement of DSBs is to be quantified after gamma- or X-irradiation, then a different procedure for cell preparation is followed because the repair process for DSBs in response to gamma- or X-irradiation exposure is very rapid. Here, the cells are embedded in plugs prior to exposure, bathed in growth medium, and exposed to irradiation on ice. A set of plugs can be incubated at 37 °C in medium for varying times to follow the repair process. This method can also be adapted to calibrate the number of DSBs an experimenter achieves in their DNA damaging system by exposing the plugs in ice to increasing doses of irradiation (e.g., 2, 4, 8, 12 Gray).

2. The levels of DSBs are determined by the rate at which breaks are generated by the treatment and the rate at which they are repaired. In order to determine the rate at which DSBs are generated by an agent, it is necessary to inhibit the repair process. This can be accomplished by using pharmacological agents to inhibit specific repair proteins (e.g., inhibition of DNA-PK) or by testing isogenic cell lines in which mutations have been introduced into specific repair pathways.

3. Counting the cells is the longest active step (up to an hour for 12 samples). Keeping cells on ice during sample accrual, subsequent processing, and the counting process is essential to prevent DNA repair during the preparation of the samples.

4. DSBs can occur during apoptosis and cell death, apoptotic or dead cells will usually float or become loosely attached. Thorough washing will allow for greater accuracy of apoptosis-independent DSBs quantification. Repeating the experiment using an inhibitor of apoptosis or a parallel apoptosis assay can be used to ensure that apoptosis-independent DSBs are being observed. In general, it is best to avoid conditions in which more than 10% of the cells are apoptotic.

5. Rotating the tubes 180^0 and spinning down for 1 minute can even out the shape of the pellet, resulting in less cell loss during the aspiration steps.

6. A P200 tip can be cut at an angle with a razor blade for gentler pipetting to avoid exposing the cells to excess shear force.

7. Remove the samples in agarose insert buffer from ice and place at room temperature for at least one minute before mixing with the low-melt agarose to avoid sample solidification prior to being placed into the mold. Do not add low-melt agarose to the cell samples in batches. Add the low-melt agarose to each sample one at a time and immediately fill the plug mold with the sample. This procedure will avoid sample solidification during processing.

8. DNA preparation in plugs can be processed in batches. Alternatively, plugs can be extruded into TE buffer and processed for DNA preparation at a later time. During protein digestion and for storage of plugs after processing, use of an air-tight tube will allow for less loss of buffer through evaporation. Use printed labels or avoid labeling areas of the tubes that will be in contact to the water bath.

9. The plug used for the ladder can be significantly smaller than the well because the signal intensity is usually very high.

10. Take care not to crush or split the plugs as they are removed from the tube.

11. Use a ruler to cut the plug in half. Cutting the plugs exactly in half allows for duplicate runs. To insert the plug into the well in the gel, add the plugs first at an angle then turn them upright to avoid air bubbles; you can also use a small syringe to extract a bubble that gets trapped under the plug. Top up the well with 1% agarose solution and allow time to solidify before placing the gel in the gel box. This prevents plugs from floating out of the wells.

12. The platform should be flush against the bottom of the tank and the frame should prevent the gel from moving during the run. Make sure that none of the plugs floated out of the wells during this step.

13. Ensure that the buffer lines running in to the pump are circulating properly and devoid of air bubbles. Run bubbles through the tubing and into the tank. Air bubbles can accumulate during the run, so the tank should be monitored several times after starting the run. A large air bubble can prevent proper buffer circulation.

14. Make sure to use the same region of interest for each measurement and that the region of interest is wide enough to encompass the entire width of all the bands.

CHAPTER IV: Resection and Dynamics of Collapsed Replication Forks in NSMCE2-Deficient Cells

Introduction

The limited degradation of nascent DNA by nucleases is an essential step in the process of HR. ssDNA is required for damaged DNA to search out a homologous sequence. Nucleases also help to process the complex DNA structures which occur as a result of replication stress. The ssDNA produced by nuclease resection is thought to be downstream of replicative helicase uncoupling and recruitment of ATR. Resection by nucleases is tightly regulated by competition with other repair factors, post translational modifications, and DNA structure selectivity. For example, the endonuclease MUS81 is considered responsible for the formation of DSBs after fork reversal based on substrate specificity (Dehe and Gaillard, 2017). This would create the DSB which would then become resected to allow for fork repair by break induced replication (BIR) or a stable structure which could be rescued by newly fired replication forks to prevent genome instability (Figure 1-1 and 4-3). However, biochemical studies have shown that MUS81 has a preference for 4-way structures which contain a 3' flap (Pepe and West, 2014), which resemble reversed forks, and cannot cleave bona fide holliday junctions (HJs) (Holliday, 2007). In yeast, replication associated DSBs are resected by carboxy-terminal binding protein (CtBP)-interacting protein (CtIP), which promotes the 5' to 3' resection carried out by other nucleases Mre11 and Exo1 (Cotta-Ramusino et al., 2005). Recently, in human BRCA2 defective cells, a similar role for the CtIP/MRE11/Exo1 resection axis, where these proteins were prerequisite for reversed fork cleavage by MUS81 (Lemacon et al., 2017). In human cells with functional BRCA2, reversed fork resection to expose a 3' flap is thought to be dependent on DNA replication helicase/nuclease 2 (DNA2) and werner syndrome RecQ like helicase (WRN), and is

independent of CtIP/MRE11/EXO1 (Thangavel et al., 2015). These resection-dependent 3' overhangs are essential to promote DSBs and the downstream HR repair process. Importantly, resection during replication stress is also is promoted by BLM helicase (Gravel et al., 2008; Pond et al., 2019). The activity of any or all of these nucleases could mediate the exposure of a 3' sequence which would then invade ahead of the replicating DNA at a homologous sequence. (Figure 5-3; top).

NSMCE2-deficient cells have: 1) excessive RAD51, which is required for fork reversal, 2) defective production of the normal repair-associated DSBs, and 3) reduction in RPA accumulation and ssDNA accumulation during fork collapse. It is possible that NSMCE2-deficient cells are defective in the activity of one or more nucleases in addition to being defective in the recruitment or retention of BLM (Pond et al., 2019). This would explain why BLM deficient cells do not phenocopy NSMCE2 deficient cells. For these reasons, we hypothesized that resection is required for processing of collapsed forks to enable collapsed-fork rescue. To test our hypothesis, we measured resection during fork collapse and rescue in NSMCE2-deficient cells.

Results

Normal or NSMCE2-null HEK293T cells were pulsed with 20 μM EdU for 30 minutes followed by 2 mM HU for 24 hours. Cells were then harvested and analyzed by flow cytometry (Figure 4-1A and B). EdU signal was reduced by ~40% in normal cells after treatment with HU for 24 hours compared to untreated controls. This indicates that resection had occurred in these cells during fork collapse. Upon release from HU, EdU signal increased indicating that some resected EdU was then re-incorporated into new origins after resumption of DNA synthesis, returning to ~75% of normal. After cells were released for 6 hours, a second resection event was observed resulting in a loss of EdU signal

by ~50% indicating resection occurring during rescue of collapsed replication forks. Interestingly, cell heterozygous to NSMCE2 displayed a defect in this process and NSMCE2-null cells showed a lack of normal resection events.

In order to quantify the amount of free EdU returning to the nucleotide pool as a result of resection of collapsed forks, we measured the nuclear pool of free EdU in cells using mass spectrometry (Xing et al., 2004). After treatment with 2 mM HU for 24 hours, normal cells displayed a 6-fold increase in the amount of free EdU label within the nucleotide pool, indicative of a resection event (Figure 4-1C). In contrast, NSMCE2-null cells displayed a defect in this process, resulting in a 2.5-fold increase in EdU signal after HU treatment. These data demonstrate a correlation between a reduction of incorporated EdU and an increase in EdU in the nuclear pool during fork collapse. These data suggest that there is a resection defect in NSMCE2-deficient cells during fork collapse. This could either be due to a defect in nuclease activity or an overprotected repair intermediate.

In order to directly measure the amount of resection occurring at collapsed forks at single replication sites, we used replication track analysis (RTA) to determine the speed and resection of NSMCE2-null 293T cells. Because of the effect on incorporated EdU by flow cytometry and mass spectrometry, we expected significant resection in normal cells after HU-induced fork collapse. To assess resection at the replication fork, we pulsed the cells with 50 μM CldU for 30 minutes followed by PBS washing and a second pulse using 50 μM IdU. After the initial pulses, cells were then incubated in 2 mM HU for 24 hours prior to harvesting and analysis. We then measured the length of the IdU label in order to observe any abnormal resection, such as that seen in cells without BRCA2 (Schlacher et al., 2011). However, to our surprise, we found that there was no effect on resection of nascent DNA in normal cells and NSMCE2-null cells showed similar responses compared to controls after

fork collapse (Figure 4-2A). Also unexpectedly, we found that replication fork speed was significantly faster in NSMCE2 deficient cells displaying a mean speed of 1.12 kb/min compared to 0.89kb/min in normal HEK293T cells (Figure 4-2B).

Discussion

These data have important implications for normal cells. (1) The loss of incorporated nucleotide observed after fork collapse is distinct from a fork protection defect and (2) normal cells do not undergo extensive resection during fork collapse. NSMCE2-null cells showed a defect in loss of incorporated nucleotide during fork collapse, and maintained normal lengths of nascent DNA by molecular combing. Combined with our previous results showing loss of exposed ssDNA and RPA accumulation in NSMCE2-deficient cells, I maintain that NSMCE2 promotes resection during fork collapse. The resection could be occurring at gaps behind the replication fork. This model is also supported by hyper-accumulated RAD51 in NSMCE2-null cells, which directly opposes transient and post-replicative resection events (Hashimoto et al., 2011; Hashimoto et al., 2010). A defect in fork resection behind the replication fork would result in loss of the overall signal of incorporated nucleotide but maintain the overall pulse length analyzed by molecular combing. Unfortunately, the intensity of the labeled segment of DNA cannot be quantified by our current tools. Green tracks were overall longer in length in NSMCE2-null cells which could be due to faster replication speed or technical errors. The RTA experiment (n=1) will need to be repeated in order to conclude the relative fork speed in NSMCE2-deficient cells. It is tempting to claim that because the NSCME2-null cells grow slower but have longer tracks by RTA, they may have fewer but faster replication forks, as this is a new and interesting mechanism of DNA damage (Quinet and Vindigni, 2018). However, more experiments will need to be conducted to ensure that the RTA result is reproducible.

It is difficult to determine the cause of the defective resection in NSMCE2 cells. A defect in sumoylation of various substrates could lead to resection defects. For example, Sae2, which is similar to CtIP in human cells, is sumoylated to become soluble and promote Mre11-dependent resection (Sarangi et al., 2015). Transient and post-replicative resection during replication stress is carried out by MRE11, so the next obvious stage of this project would be interrogation of those nucleases to see if normal cells will phenocopy the defects seen in NSMCE2-null cells. A more compelling approach would be to restore resection in NSMCE2-null cells. 53BP1 and Rif1 are both potential targets which block MRN/CtIP resection pathways during repair pathway choice (Escribano-Diaz et al., 2013). Depletion of 52BP1 or Rif1 could potentially restore resection and downstream HR as has been shown in BRCA mutant cells (Bunting et al., 2010). In BRCA mutant cells, 53BP1 loss is also associated with resistance to PARP inhibitors. It is also possible that a repair intermediate is resistant to resection. If this is the case the NEMCE2-deficient phenotype should be rescued if RAD51 can be destabilized in NSMCE2-deficent cells after a recombination intermediate is formed. BODL1 is also an intriguing target and it acts within the BLM/RAD51 axis to stabilize RAD51 at replication forks and prevent resection (Higgs et al., 2015). Removal of BODL1 could destabilize the accumulated RAD51 in NSMCE2-deficient cells and complement one or more phenotypes.

CHAPTER V: Sensitization of Mammalian Cells to Topoisomerase Poison Using a Potential NSMCE2 Inhibitor

Introduction

During normal DNA replication, cells rely on topoisomerases to contend with the entangled DNA which naturally occurs during genome duplication. Topoisomerases perform this function through the introduction of transient DNA breaks which allow for relaxation or disentanglement of various DNA structures. For example, topoisomerase 2 can untangle catenated parental DNA strands during the convergence of replication forks to allow for successful replication termination (Baxter and Diffley, 2008; Fachinetti et al., 2010; Lucas et al., 2001; Sundin and Varshavsky, 1980) and topoisomerase 1 also acts to relax supercoils that preced the replication fork (Strumberg et al., 2000). NSMCE2 is required for the completion of DNA synthesis after replication stress, MMS21 mutant cells accumulate x-shaped DNA molecules after replication stress (Branzei et al., 2006), and topoisomerase proteins are involved in segregation of entangled DNA (Pommier et al., 2016). It is possible that a hyper-stable, collapsed replication fork would require topoisomerase activity to allow successful rescue by a converging fork (Figure 5-2). We therefore hypothesized that cells deficient in NSMCE2 would be more dependent on topoisomerase proteins.

Results

To test the hypothesis that NSMCE2-deficient cells would be more reliant on topoisomerase proteins, we used an in-silico method using molecular modeling approaches and the yeast MMS21 crystal structure (Duan et al., 2009). We generated a 3D model of human NSMCE2 and identified a pocket close to the Zn^{2+} binding motif of NSMCE2 (Figure 5-1 A). Residues immediately proximal to and within a 3-Å sphere of the identified surface were marked and used to generate protomols. Individual protomols were merged

into a single 'global' protomol, encompassing ~80% (3-Å sphere definition) of the surface area. Utilizing the protomol as a guide, adjacent amino acid residues were used to create pharmacophores with SYBYL Suite software. These pharmacophores were used to screen the ZINC database 'CLEAN-DRUGLIKE' (Irwin et al., 2012) for compounds, yielding approximately 2000 hits. The hits were docked into the binding pocket and scored using Surflex-Dock software. Hits were sorted from highest to lowest docking scores, and 12 compounds were selected based on visual inspection of the optimal binding interactions. This work was done in collaboration with Larry Cooke and Dr. Daruka Mahadevan at the Arizona Cancer Center.

In order to screen for our hypothesized phenotype, we ordered 12 compounds and tested for potential synergistic effects when compounds were combined with topoisomerase poisons. We reasoned that, if one of the compounds inhibited NSMCE2, then we would expect a synergistic effect with camptothecin (CPT), an inhibitor of topoisomerase I that generates DSBs during DNA replication (Ryan et al., 1991). With the help of Hanen Alassady, we measured the metabolism of cells after treatment using MTT assay (Mosmann, 1983), none of the compounds limited cell growth of U2OS cells when treated at 10 μM for 48 hours (Figure 5-1B; right). Four of the 12 compounds exerted an effect on CPT-induced cell inhibition by MTT; compound 3 (Figure 5-1 A; upper right) demonstrated the strongest effect, inhibiting cell proliferation by nearly one log (Figure 5-1 B; left). In addition, using NSMCE2-null 293t cells we also showed a mild sensitization of HEK293t cells to the less toxic catalytic inhibitor of topoisomerase 2α, ICRF-187 (Figure 5-1 C). Previous reports using human cells have also demonstrated a sensitivity of NSMCE2 knockout cells to topoisomerase poisons (Verver et al., 2016). Together, these data suggest that indeed NSMCE2-deficient cells are more reliant on topoisomerase proteins.

Discussion

We showed that cells without NSMCE2 are sensitive to the inhibition of topoisomerase 2α. However, we do not know at what stage Top2 is utilized most in NSMCE2-null cells. Our current hypothesis is that NSMCE2-null cells rely on Top2 to disentangle catenated DNA during the convergence of a newly fired fork on a collapsed fork (Figure 5-2). In yeast, Sgs1 promotes Top2-mediated decatenation so it is possible that the two work in concert to decatenate sister chromatids (model not shown). In MMS21/NSMCE2-deficient cells, X-shaped structures form and ultra-fine bridge structures are increased, which is similar to situations where Top2 is depleted (Fachinetti et al., 2010; Liu et al., 2014). Moreover, because we showed that NSMCE2 is dispensable for the recruitment of BLM to UFBs, it makes sense that without Top2, BLM would be less effective at disentangling UFBs in NSMCE2-null cells during mitosis. In order to test this hypothesis NSMCE2-null cells would need to be put into a collapsed-fork rescue state, then released into topoisomerase inhibitor and analyzed for UFB abundance. The increased reliance on BLM/Top2 to repair UFBs in NSMCE2-null cells is also supported by previous reports of synthetic lethality between NSMCE2 and BLM (Jacome et al., 2015). Due to the failure of forks to converge in NSMCE2-null cells, it is tempting to speculate that runoff associated with camptothecin treatment (stabilized topo-cleavage complex) would result in high levels of DSB, whereas NSMCE2-null cells would be protected in such an environment.

Our results for the topoisomerase 2α inhibitor ICRF-187 in NSMCE2-null cells is not surprising because NSMCE2-null cells have shown sensitivity to topoisomerase 2 poison previously (Verver et al., 2016). However, this finding does indicate that the NSMCE2-null cells rely on the enzymatic activity of topoisomerase 2 rather than simply being more sensitive to a topoisomerase 2-induced DNA lesion. The result we observed using

camptothecin in U2OS cells was more surprising because our data using 293T cells (not shown) and previous reports have shown no differences in toxicity induced by cisplatin in NSMCE2-null cells (Payne et al., 2014; Verver et al., 2016). Off-target effects have been controlled for using the potential NSMCE2 compounds via lack of toxicity in NSMCE2-null cells (Alassady, 2018), however direct binding of the compounds has yet to be shown. Assuming the compounds are specific to NSMCE2, the only explanation left for a lack of toxicity in NSMCE2-null cells compared to synergy observed from compounds is that the protein itself is required for the toxicity of the inhibitor. This is very similar to the mechanism of PARP inhibitor toxicity (Murai et al., 2012), where the protein must be trapped onto the DNA for toxicity to occur. This "trapping" requirement for toxicity is also the mechanism of other classic repair protein inhibitors such as topisomerase 1 and 2 (Khan et al., 2003; Pourquier et al., 2001). A model which explains why trapped NSMCE2 would be dominant to lack of NSMCE2 has yet to be tested. FRAP of GFP-tagged NSMCE2 in the presence of the potential NSMCE2 inhibitors would be the best way to test this idea along with chromatin fractionation experiments. The finding that NSMCE2-null cells or NSMCE2 inhibited cells rely more on topoisomerases has a clear impact. As an adjuvant therapy, NSMCE2 inhibition could significantly lower the effective dose of clinically approved, but highly toxic chemotherapies.

CHAPTER VI: Discussion and Conclusions

In order to study the rescue of the collapsed replication forks we have used a system which collapses ~90% of the replication forks and therefore allows for enrichment of the repair-deficient phenotype. Prolonged replication fork stalling leads to dissociation of the replisome components, the consequence of which is that replication forks are unable to restart. This process is known as fork collapse. In order for replication to be completed after fork collapse, cells must fire dormant origins, then new replication forks converge upon the collapsed forks. During normal replication termination, the converging DNA polymerases move past one another to complete replication (Dewar et al., 2015). In contrast, when a new fork converges upon a collapsed fork, it encounters a stabilized nucleoprotein structure (Mijic et al., 2017). This specialized convergence event, called collapsed-fork rescue, is associated with a double strand break (DSB) (Petermann et al., 2010) and repair by homologous recombination (HR) (Ouyang et al., 2009). Defective collapsed-fork rescue results in under-replicated DNA, mitotic damage, and genomic instability. There is a major gap in knowledge regarding the mechanisms that control collapsed-fork rescue to complete DNA replication. There is an urgent need to fill this gap because the mechanisms that enable the rescue of collapsed forks are prime targets for pharmacologic manipulation in cancer therapeutics.

We are still unsure which targets of NSMCE2-mediated sumoylation are causing the defects we have observed in the absence of NSMCE2. We have identified BLM sumoylation as being dependent on the presence of NSMCE2 and have shown that NSMCE2 recruits or retains BLM at collapsed replication forks. However, because NSMCE2 loss does not

phenocopy BLM loss and is in fact epistatic during collapsed-fork rescue, other factors are clearly involved in the NSMCE2-mediated repair pathway.

RAD51 is an attractive next target, because its defective accumulation is associated with the prevention of normal DSBs during collapsed-fork rescue. It is tempting to hypothesize that if RAD51 were effectively removed from the collapsed fork structure in NSMCE2 cells, then we could restore DSBs and prevent mitotic DNA damage. However, cells rely on HR for repair after endonucleolytic induction of the DSB during collapsed-fork rescue to complete repair of the DSB. We utilized an inhibitor of RAD51 which prevents ssDNA binding as well as siRNA mediated knockdown of RAD51 and were unable to rescue the NSMCE2 phenotype. Because RAD51 is required for fork reversal (Zellweger et al., 2015), our data suggests that if replication forks cannot become reversed, collapsed-fork rescue cannot occur. Therefore, if we are to test the hypothesis that RAD51 removal from the collapsed fork will rescue the NSMCE2-deficient phenotype, a separation of function allele of RAD51 must be used.

Fortunately, such an allele exists and was identified from a patient with Fanconi anemia like symptoms (Wang et al., 2015). RAD51 T131P expressing cells are HR proficient but sensitive to the replication-dependent DNA damaging agent MMS. These cells, however, are not sensitive to ionizing radiation. The RAD51 T131P allele was also recently shown to be capable of performing fork reversal, but is unable to prevent resection by MRE11(Mijic et al., 2017). If this allele were expressed in NSMCE2-null cells, one would expect a restoration of the resection phenotype during collapsed-fork rescue. If resection were restored it is possible that the 3' flap that is required for nucleolytic cleavage by MUS81 would then be exposed, leading to DSB formation. These cells could then perform canonical HR similar to that needed after exposure to a radiation-induced DSB. Alternatively, interrogation of an

effector of RAD51, such as BOD1L, could be used to destabilize the fork-associated RAD51. BOD1L is a particularly attractive target as it has already been described as a stabilizer of RAD51 via to prevent resection (Higgs et al., 2015).

We have shown that the E3 SUMO ligase is an essential component of a previously uncharacterized DNA repair process in human cells. Fork collapse occurs in normal human cells as a result of unavoidable obstacles such as difficult to replicate DNA and collision with other DNA-associated proteins. The repair pathways that deal with normal fork collapse are just one component of the multiple mechanisms that the cell used to protect the integrity of the human genome. Our work is particularly important in the context of human cancers as cells have high levels of replication stress and consequent fork collapse. Our work suggests that cancer cells rely more heavily on NSMCE2 because of higher levels of replication stress and genomic instability and would therefore be more sensitive to the inhibition of the collapsed-fork rescue pathway. To support this hypothesis, in our attempts to build a system to study NSMCE2 we were unable to derive homozygous null clones of NSMCE2 in HeLa cancer cells, but did succeed in making several clones using normal HEK293T cells, suggesting that NSMCE2 may be essential in some tumor cells. Further evidence for this was provided by our experiments in which we inhibited NSMCE2 using experimental compounds. Potential inhibition of NSMCE2 had almost no cytotoxic effects on the cells at relatively high doses for 72 hours but conferred a log increase in the cytotoxicity of the replication damaging agent camptothecin, suggesting that replication stress could be required for NSMCE2 to become essential.

As with any project, the assessment of novel questions breeds more questions rather than answers. We have created a new model for the rescue of collapsed replication forks in the wake of many destroyed models and disproven hypothesis. Most of our expectations

proved to be incorrect, which is what led us to a unique model. This provides more confidence that our model is partially correct. More experiments are needed to disprove our current model for the role of NSMCE2 during collapsed-fork repair.

Materials and Methods

Antibodies and siRNAs

Antibodies for immunofluorescence and western blots were obtained as follows: anti-RPA2 (Abcam; mouse monoclonal ab2175), anti-RAD51 (Abcam; rabbit monoclonal ab133534), anti-NSMCE2 (OriGene; mouse monoclonal TA501632), anti-BLM (Beresten et al., 1999), anti-RANGAP (Thermo Fisher Scientific; rabbit polyclonal PA1-5866), anti-histone H3 (Cell Signaling Technology; rabbit polyclonal 9715), anti-PCNA (OriGene; mouse monoclonal TA800875), anti-SMC5 (Bethyl; rabbit polyclonal A300-236A), anti-HSP90 (OriGene; mouse monoclonal TA500494), γ-H2AX (BioLegend; 613406; or Upstate; mouse monoclonal 05-636), anti-bromodeoxyuridine (BrdU) (Bio-Rad; mouse monoclonal OBT0030), RPA32 (Abcam; mouse monoclonal ab2175), RPA70 (Santa Cruz; mouse monoclonal SC-53497), PML (Santa Cruz; mouse monoclonal SC-966), and Phalloidin-546 (Thermo Fisher Scientific; Alexa Fluor A22283), and phospho-histone H3 (serine 10; Cell Signaling; mouse monoclonal 9706). siRNAs for NSMCE2, BLM, and RAD51 were as follows:

siNSMCE2-2: 5'-rUrUrArCrArUrArArUrGrGrUrUrUrArGrUrUrGrCrCrGrArUrCrCrA-3'

5'-rGrArUrCrGrGrCrArArCrUrArArArCrCrArUrUrArUrGrUdAdA-3'

siNSMCE2-6: 5'-rUrArUrArUrUrCrArCrUrArCrUrCrArCrUrUrCrArGrUrCrUrGrArC-3'

5'-rCrArGrArCrUrGrArArGrUrGrArGrUrArGrUrGrArArUrAdTdA-3'

siBLM: 5’-rArUrUrCrUrUrGrArGrArGrCrArGrUrArUrCrCrCrGrGrGrArUrU-3’

5’-rUrCrCrCrGrGrGrArUrArCrUrGrCrUrCrUrCrArArGrAdAdAdT3’

siRAD51: 5’-rGrArGrCrUrUrGrArCrArArArCrUrArCrUrU-3’

5’-rCrArCrCrUrUrGrArArGrUrArGrUrUrUrGrU-3’

Genome editing for NSMCE2

Genome editing was carried out with Integrated DNA Technologies (IDT) ALT-R CRISPR-Cas9 system with crRNA guide (GTCCATACCAGAGTTGATAC) targeting the first coding exon. Ribonucleoprotein particles were introduced into HEK293T cells using FuGENE HD (Promega). After 48 h, single cells were deposited in a 96-well plate by flow cytometry. After four to six weeks, clones were analyzed by the T7 endonuclease assay (New England Biolabs), and clones that scored positively were PCR sequenced. >50 clones were analyzed in the first screen and a single heterozygous NSMCE2-null mutant was obtained. This clone was genome edited again to obtain two NSMCE2-null mutants.

Western blot analysis

Cells were lysed in RIPA buffer supplemented with 5 mM EDTA, 1 mM EGTA, 25 mM sodium fluoride, 1 mM sodium orthovanadate, 1 mM phenylmethane sulfonyl fluoride (PMSF) in 1x EDTA-free Halt protease inhibitor (Thermo Scientific). Protein concentration was measured using Pierce BCA Protein Assay. 30-50 μg of total protein from cell lysates was separated by electrophoresis through 4-20% gradient polyacrylamide gels and transferred onto Hybond nitrocellulose membranes by semi-dry transfer. Before addition of primary antibodies, membranes were probed with Ponceau S (Sigma) for 7 min, imaged, and washed with 1% glacial acetic acid in water. Membranes were blocked for 1 h in Tris-buffered saline with 0.1% polysorbate 20 (TBST) containing 5% Bio-Rad Blotting-Grade Blocker, then incubated with primary antibody in 3% BSA in TBST overnight at 4°C.

SUMO2 pull-down

U2OS cells that were stably transfected with a His-tagged SUMO2 were kindly provided by Dr. Michael Matunis at Johns Hopkins University, who obtained them from Dr. Mary Dasso's lab at NIH. The cells were reverse-transfected with siRNAs using LifeTechnologies' Lipofectamine RNAiMAX. Cells were treated with 2 mM HU for 16 h. His-SUMO2 conjugates were purified as described by Tatham et al. (Tatham et al., 2009). Briefly, cells were washed with ice-cold phosphate-buffered saline (PBS) and directly lysed in 4 ml lysis buffer (6 M guanidine-HCl, 100 mM NaCl, 10 mM Tris-HCl pH7.4, 3 mM imidazole and 2 mM β-mercaptoethanol) and sonicated to reduce viscosity. Lysates were incubated with 50 ml Talon Metal Affinity Resin (Clontech Laboratories, Inc.) overnight at 4°C with gentle mixing, and then washed 2 times with 4 ml guanidine wash buffer (6 M guanidine-HCl, 100 mM NaCl, 10 mM Tris-HCl pH 7.4, 0.1% Triton X-100, 2 mM β-mercaptoethanol) followed by 3 washes in 4 ml urea wash buffer (8 M urea, 100 mM NaCl, 10 mM Tris-HCl pH 7.4, 0.1% Triton X-100, 2 mM β-mercaptoethanol). The beads were transferred to 1.5 ml microfuge tubes for one more wash with urea wash buffer and proteins eluted for 1 h at room temperature with elution buffer (63 mM Tris-HCl pH 6.8, 2% SDS, 200 mM imidazole, 1.5% β-mercaptoethanol, 10% glycerol, with bromophenol blue). The eluates were boiled for 5 min and cleared by centrifugation prior to loading on a 10% polyacrylamide gel. The whole cell lysates were lysed in RIPA buffer (150 mM NaCl, 1% Triton X-100, 0.25% sodium deoxycholate, and 50 mM Tris-HCl, pH 8.0). Laemmli buffer was added to 1X in aliquots representing 10% of the eluate, then boiled for 5 min prior to gel loading.

Analysis of chromatin-bound RPA

The protocol from Mendez and Stillman for chromatin isolation by small-scale fractionation was followed (Mendez and Stillman, 2000). HEK293T normal and NSMCE2-null cells treated or not with 2 mM HU for 16 h were harvested by scraping, centrifuging, and washing twice with PBS. The cells were resuspended such that there were 1 x 10^7 cells per 200 µl of Buffer A (10 mM HEPES pH7.9, 10 mM KCl, 1.5 mM $MgCl_2$, 0.34 M sucrose, 10% glycerol, 1 mM DTT, 0.1 mM PMSF, and 1x Protease Inhibitor Cocktail). Triton X-100 was added to a concentration of 0.05%, and the cells were incubated for 5 min on ice. Nuclei were collected by low-speed centrifugation (4 min, 1300 x g at 4°C) and the supernatant was reserved as the cytoplasmic fraction. The nuclei were washed once in Buffer A, and then lysed in 100 µl Buffer B (3 mM EDTA, 0.2 mM EGTA, 1 mM DTT, 1x Protease Inhibitor Cocktail). Nucleoplasmic proteins were separated from chromatin-bound proteins by centrifugation (5 min, 1700 x g at 4 °C). Nucleoplasmic fractions were collected in the supernatant. The chromatin pellet was resuspended in 250 µl Laemmli buffer and the material was sonicated. The cytoplasmic and nucleoplasmic fractions were clarified by high-speed centrifugation (5 min, 20,000 x g at 4°C). The proteins in the fractions were analyzed by Western blot. Initially, cytoplasmic and nucleoplasmic fractions were analyzed separately; however, because the cytoplasmic fraction contained varying amounts of different RPA components, for comparisons of the amounts of RPA70 we combined equal parts of the cytoplasmic and nucleoplasmic fractions.

Immunofluorescence and image analysis

The protocol was adapted from Dimitrova and Gilbert (Dimitrova and Gilbert, 2000). Cells were grown on coverslips overnight and washed with cold CSK buffer (10 mM HEPES pH7.4, 300 mM sucrose, 100 mM NaCl, 3 mM $MgCl_2$) and nucleoplasm was extracted for 90 s with cold extraction buffer (0.5% Triton X-100 in CSK buffer with 1 mM PMSF, 50 mM sodium fluoride, 0.1 mM sodium orthovanadate and 1x EDTA free Halt protease inhibitor) prior to 30-min fixation in 4% formaldehyde at room temperature. Cells were washed twice with cold PBS then treated with 0.5% Triton X-100 at room temperature before staining. Cells were blocked at room temperature for 1 h using sterile filtered 3% BSA in PBS, then probed using primary antibodies for 1 h at room temperature. Secondary antibodies (Alexa Fluor 488 and 546) were used at 1:1000 for 45 min and nuclei were stained using Molecular Probes NucBlue reagent (R37606). For 5-ethynyl-2´-deoxyuridine (EdU) labeling cells were incubated in 10 μM EdU for 20 min. EdU labeling and detection was performed using Life technologies Click-iT EdU Alexa Fluor 647 imaging kit according to manufacturer's instructions. Cells were mounted in Molecular Probes ProLong Gold Antifade Reagent. Fixed and stained cells were imaged using the Leica SP5-II spectral confocal microscope using the 63x/1.4 NA PL Apo objective. Using the nuclear signal to screen the region of interest enabled accurate measurement of the number and intensity of nuclear foci and the percent of nucleus occupied by signal for each antibody target. No less than 10,000 foci were analyzed per experimental group. Box and whisker plots were used to visualize distribution of foci. For analysis of EdU labeled forks and ultra-fine bridges (UFBs), z-stacks were created using 100x objective and deconvolved using the GE DeltaVision Elite High Resolution Microscope. Images were analyzed and 3D representations were created using the NIS Elements software.

Flow cytometry

Cells were harvested with trypsin/EDTA, resuspended in ice cold PBS, and fixed and stained using BioLegend True-Nuclear Transcription Factor Buffer. Cells were then stained for γ-H2AX using directly conjugated antibody and counterstained using 7AAD to monitor cell DNA content. For cell cycle assays, analysis was performed using the BD Pharmingen FITC BrdU Flow Kit. A minimum of 30,000 events was recorded for each group using the BD FACSCanto II or BD LSR II flow cytometer. Apoptosis analysis was carried out using the BioLegend FITC Annexin V Apoptosis Detection Kit with propidium iodide (PI).

Cytogenetic analysis

For SCE analyses, cells were cultured with 10 μM BrdU (Sigma-Aldrich). After 60 h, the cells were incubated with 0.02 μg per ml colcemid (Invitrogen) for up to 2 h, harvested and processed as described earlier [14]. For the epistasis experiments using HEK293T cells, the cells were incubated in 0.6 μg per ml colcemid for 16 h prior to harvest. The slides were examined under the microscope at 100×, and SCEs were counted from metaphases with an acceptable quality of sister-chromatid discrimination. For measurements of HU-induced SCEs, cells were cultured in 10 μM BrdU for 30 h, washed one time with 1× PBS, and treated with 2 mM HU for 24 h. Cells were then released into medium containing 10 μM BrdU for an additional 20 h. Metaphases were collected in colcemid and processed as described above.

For analysis of micronuclei, normal or NSCME2-depleted HeLa cells were seeded onto coverslips, treated or not with 2 mM HU for 24 h, and fixed with 4% formaldehyde. The cells were stained with Nuc-Blue (Thermo Fisher) at 2 drops per ml in PBS for 30 m,

washed briefly, mounted, and imaged using the GE DeltaVision Elite High Resolution Micro.

For analysis of chromosomes at metaphase, normal and NSMCE2-null HEK293T cells were seeded into 60 mm dishes and incubated overnight. For analysis of γ-H2AX labeled chromosomes, cells were treated with 2 mM HU for 24 h, then washed and incubated in medium with 7.5 μM RO-3306 for 10 h for HEK 293T control or 20 h for NSMCE2-null cells. Cells were then released into normal medium and harvested at the indicated time points. Cells were fixed with 4% formaldehyde and stained with anti-phospho-histone H3 (serine 10). For analysis of chromosome spreads, cells were treated with 0.02 μg per ml colcemid for 45 m or with 0.6 μg per ml colcemid for 16 h prior to harvest. Cells from both experiments were harvested and metaphases prepared as described [14]. Metaphase chromosomes were stained with Nuc-Blue. Cells or chromosomes were imaged using the GE DeltaVision Elite High-Resolution Microscope.

DSB detection by pulsed-field gel electrophoresis

The procedure was performed as previously described (Hanada et al., 2007; Ouyang et al., 2009). Sub-confluent cultures of HeLa cells or HEK293T cells untreated, treated with 2 mM HU for 24 h, or treated with HU for 24 h and released for different times were harvested by trypsinization, and agarose plugs of 2.5 x 10^5 cells were prepared in disposable plug molds (Bio-Rad Laboratories). In some experiments, cells were released into medium containing 10 μM aphidicolin. Plugs were then incubated in lysis buffer (100 mM EDTA, 1% wt/vol sodium lauroyl sarcosinate, 0.2% wt/vol sodium deoxycholate, and 1 mg/ml proteinase K) at 37°C for 16 h. Plugs were then washed four times in 20 mM Tris-HCl, pH 8.0, and 50

mM EDTA before loading onto an agarose gel. Electrophoresis was performed for 21 h at 14°C in 0.9% (wt/vol) agarose containing Tris-borate/EDTA buffer in a PFGE apparatus (CHEF DR III; Bio-Rad Laboratories), according to the following protocol: block I: 9 h, 120° included angle, 5.5 V/cm, 30 to 18-s switch; block II: 6 h, 117° included angle, 4.5 V/cm, 18 to 9-s switch; block III: 6 h, 112° included angle, 4.0 V/cm, 9 to 5-s switch. The gel was then stained with SYBR Gold (1 part in 10,000 in water; Invitrogen) and analyzed by the AlphaImager system (ProteinSimple). Relative DSB levels were assessed by comparing DSB signals for each treatment to the background levels observed in untreated conditions using Image J. Data were analyzed with GraphPad Prism software.

Microfluidic-assisted replication track analysis

maRTA was performed as previously described with some modifications (Sidorova et al., 2009). Briefly, 36 h after siRNA transfection, HeLa cells were pulse-labeled with 50 μM iododeoxyuridine (IdU) for 40 min. Cells were then treated or not with 2 mM HU for 5 or 16 h. The cells were released in fresh medium containing 50 μM of chlorodeoxyuridine (CldU) for 40 min. Cells were then harvested and embedded into agarose plugs containing 20,000 cells/plug. After proteinase K digestion and agarose digestion by beta-agarase, DNA fibers were stretched on 3-aminopropyltriethoxysilane coated slides (LabScientific) using polydimethylsiloxane molds fashioned with micro-capillary channels prepared as described (Sidorova et al., 2009). DNA fibers were then denatured in 2.5 M HCl, and probed with the following antibodies: mouse IgG_1 anti-BrdU/IdU (clone BD44, Becton Dickinson), rat anti-BrdU/CldU (clone B1/75, Bio-Rad OBT0030), and mouse IgG_{2a} anti-ssDNA (clone 16-19, Millipore). Secondary antibodies included Alexa Fluor 488 anti-mouse IgG_1, Alexa Fluor 594

anti-rat, and Alexa Fluor 647 anti-mouse IgG_{2a}, respectively (Life Technologies). Images were acquired on Leica DMI6000 epifluorescence microscope using Leica LAS-AF software. Signals were measured using NIH ImageJ software with custom-made modifications and the data analyzed with GraphPad Prism software.

Statistics

Statistical evaluations of experiments with continuous variables (e.g., quantitation of SUMO-BLM and DSBs) or discrete variables in which the data was normal were carried out by paired Students t-test. Evaluations of experiments with non-normal discrete variables (e.g., focal counts) were analyzed by Mann-Whitney test. All p-values were two-sided.

Appendix A: FIGURES & FIGURE LEGENDS

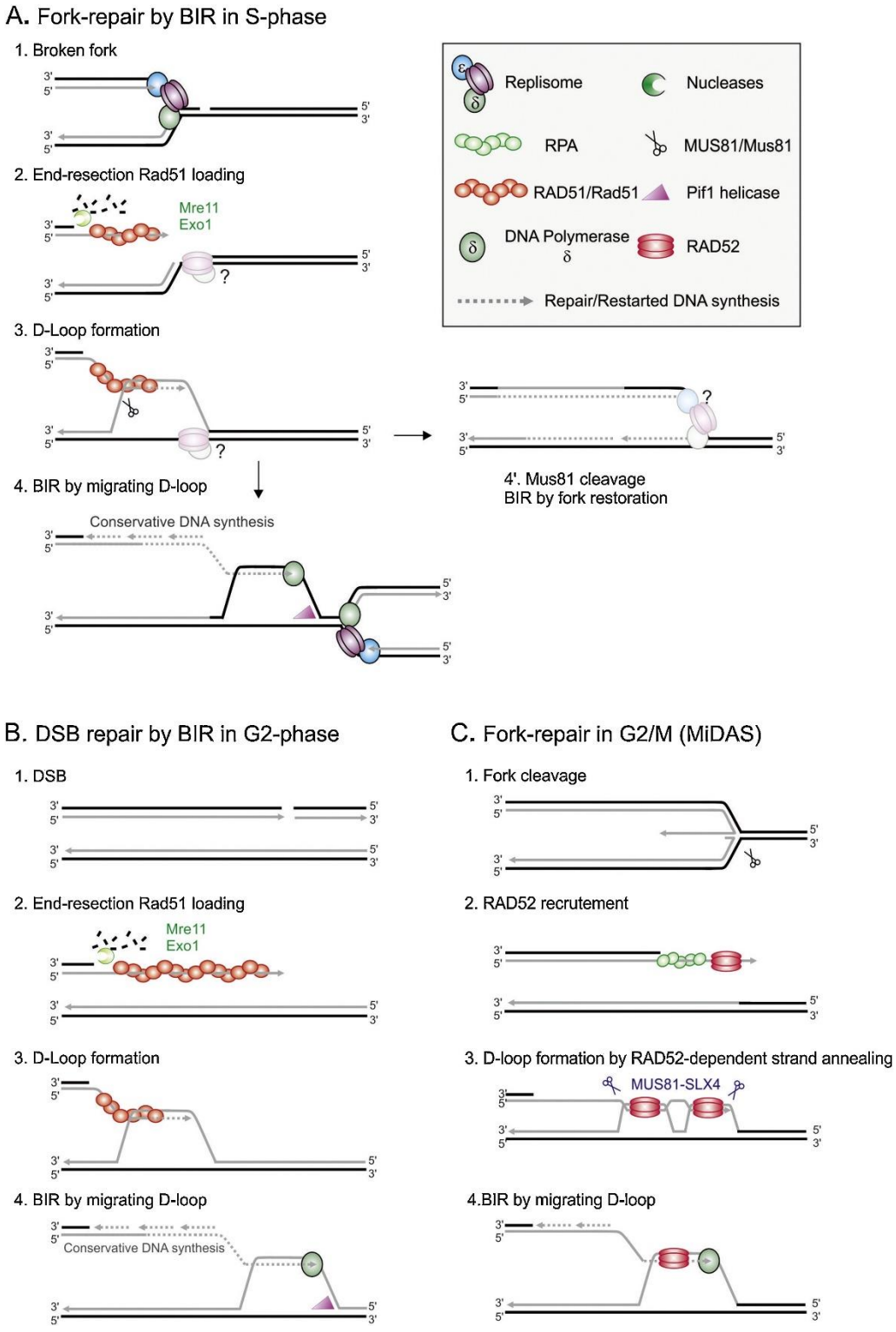

Figure 1-1.
Schematic for the introduction of readers to the roles of DNA repair proteins during the stalling/collapse of replication forks. This image was taken from an excellent review from Saada and Carr, DNA Repair, 2018. PMID: 30220600. The figure legend is as follows, "Models of DSB-initiated recombination-dependent replication. A. Replication forks encountering a DNA nick are converted into broken fork, which may be accompanied by the loss of replisome components (1). The DNA end-resection machinery (i.e. Mre11 and Exo1) generates a single-stranded 3' overhang that is coated by the RAD51 recombinase (2) which promotes strand invasion into the sister chromatid to form a D-loop structure from which DNA synthesis can be primed (3). In budding yeast, break induced replication (BIR) proceeds by conservative DNA synthesis using a migrating D-loop that is mediated by Pif1 helicase. The non-essential Pol32 sub-unit of the DNA polymerase delta is required for BIR, which is highly error-prone and limited by an incoming converging fork (4). Alternatively, Mus81 endonuclease can cleave the D-loop structure allowing the restoration of semi-conservative DNA synthesis (4'). It is not known if the replisome associated with such a re-set fork is canonical or not. B. BIR can be initiated by the breakage of a single chromatid in G2 (1,2). The migrating D-loop and its associated conservative DNA synthesis can proceed until the end of the chromosome (3). In the example shown, the sister chromatid provides the donor template, but BIR can employ ectopic homologous sequence during repair of a DSB. BIR in G2 generates long stretches of ssDNA (4) which is highly sensitive to mutation and formation of secondary recombination intermediates. C. Unresolved replication forks in mammalian cells are cleaved by MUS81 in late G2 and mitosis (1). The strand annealing activity of RAD52 (2) promotes the formation of joint molecules (3) the nature of which remains elusive. Mitotic DNA synthesis (MiDAS) requires POLD3, a component of the DNA polymerase delta homologous to yeast Pol32."

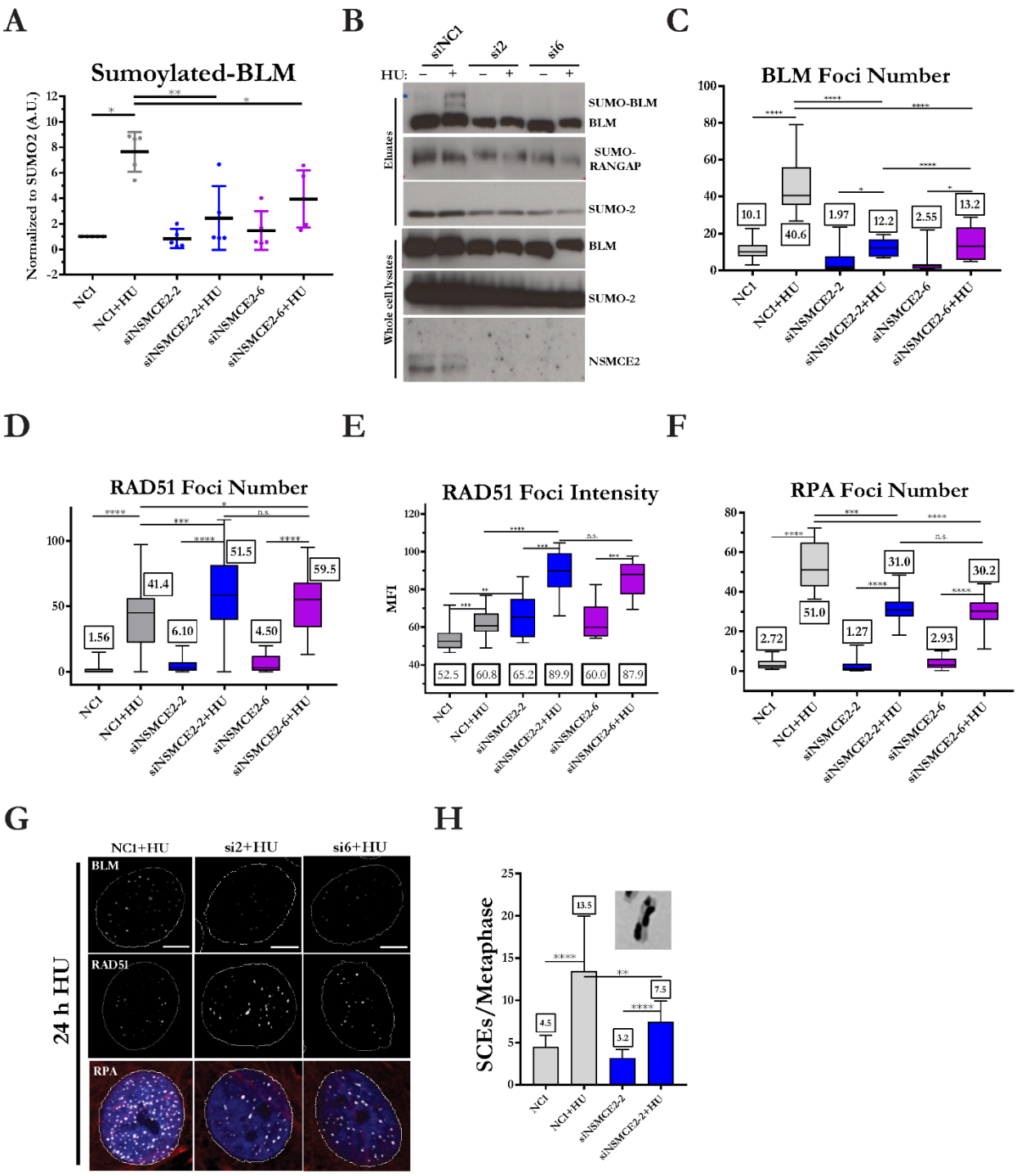
A
Sumoylated-BLM
Normalized to SUMO2 (A.U.)
NC1
NC1+HU
siNSMCE2-2
siNSMCE2-2+HU
siNSMCE2-6
siNSMCE2-6+HU
B
siNC1
si2
si6
HU:
SUMO-BLM
BLM
SUMO-RANGAP
SUMO-2
BLM
SUMO-2
NSMCE2
Eluates
Whole cell lysates
C
BLM Foci Number
10.1
40.6
1.97
12.2
2.55
13.2
D
RAD51 Foci Number
1.56
41.4
6.10
51.5
4.50
59.5
E
RAD51 Foci Intensity
MFI
52.5
60.8
65.2
89.9
60.0
87.9
F
RPA Foci Number
2.72
51.0
1.27
31.0
2.93
30.2
G
NC1+HU
si2+HU
si6+HU
BLM
RAD51
RPA
24 h HU
H
SCEs/Metaphase
4.5
13.5
3.2
7.5

Figure 2-1. NSMCE2 is required for normal accumulations of BLM, RAD51, and RPA at stalled replication forks. (A) Depletion of NSMCE2 is associated with a reduction in SUMO2-BLM. Quantitation of SUMO2-BLM in U2OS cells normalized to controls (NC1). SUMO2-conjugates were pulled down from U2OS cells that stably overexpress His-tagged SUMO2 protein. NSMCE2 was depleted with two different siRNAs, and cells were treated or not with 2 mM HU for 16 hours. The levels of SUMO2-BLM pulled down were normalized to the amounts of SUMO2. Shown are the mean and standard deviation of five independent experiments. (B) Representative images of western blots quantitated in (A). (C) Quantitative analysis of the number of BLM foci in HeLa cells. NSMCE2 was depleted in HeLa cells with two different siRNAs, and cells were treated or not with 2 mM HU for 24 hours. Box and whisker plots represent cell distributions of BLM foci per cell. Numerical labels represent the median value of at least 10,000 BLM foci in each experimental condition. Three independent experiments were performed. (D) Quantitative analysis of the number of RAD51 foci per cell. Plots and analysis performed as in panel C. RAD51 and RPA staining were performed in the same experiment. Three independent experiments were performed. (E) Quantitative analysis of the median fluorescence intensity of RAD51 per cell. (F) Quantitative analysis of the number of RPA foci per cell. (G) Representative immunofluorescence images of RAD51 and RPA foci in cells analyzed in (D-F), showing colocalization of RAD51 and RPA. Scale bars represent 10 microns. (H) SCEs in HeLa cells exposed to control or NSMCE2 siRNA and treated or not with 2 mM HU for 24 hours. Mean and standard deviation of the number of SCEs/metaphase is shown. Three independent experiments were performed. Asterisks represent statistical analysis by paired t-test (A) or Mann-Whitney test (C) (*=$p<0.05$, **=$p<0.01$, ***=$p<0.001$, ****=$p<0.0001$).

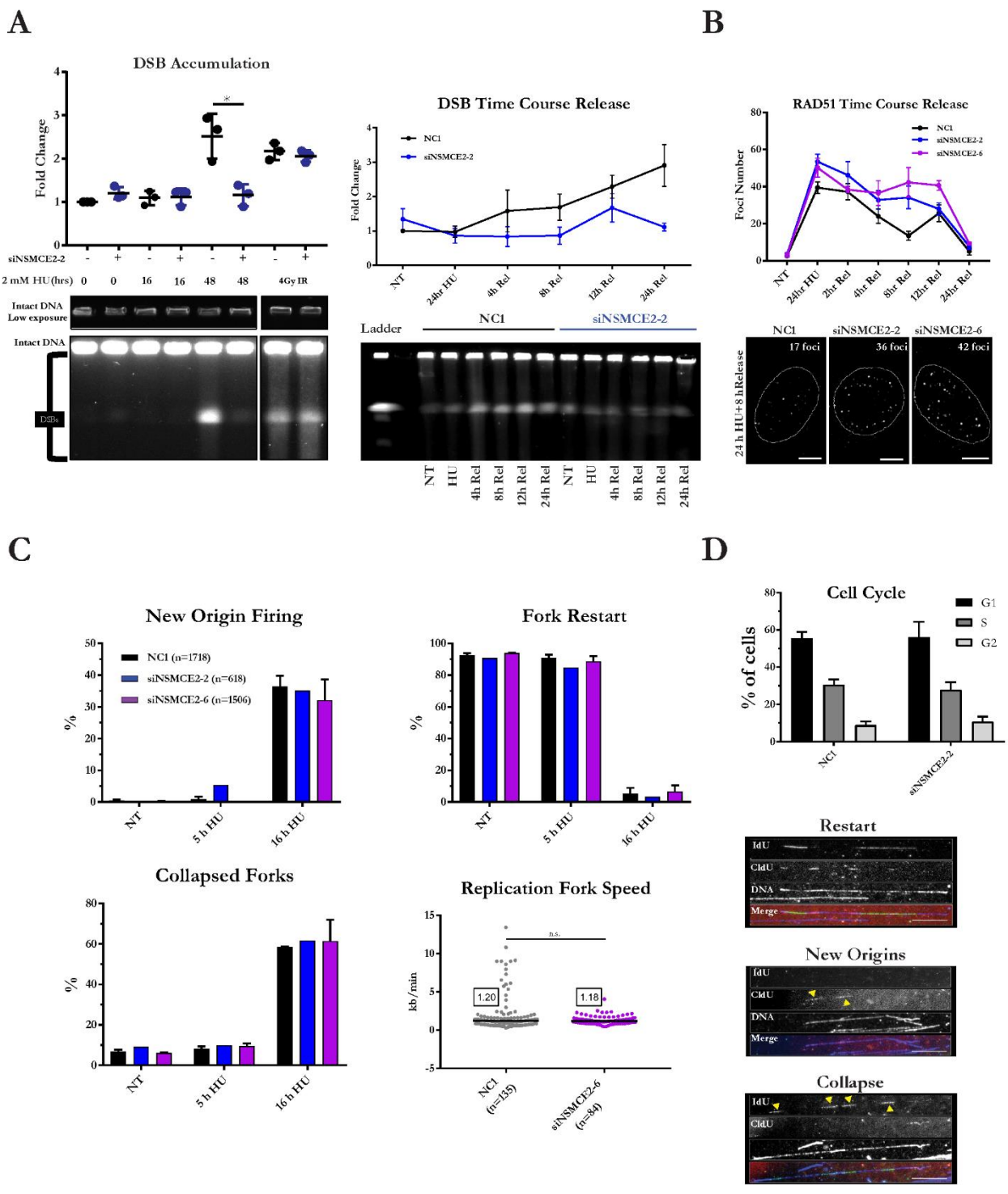
A
DSB Accumulation
Fold Change
siNSMCE2-2
2 mM HU (hrs)
4Gy IR
Intact DNA
Low exposure
Intact DNA
DSBs
DSB Time Course Release
NC1
siNSMCE2-2
Ladder
NT
24hr HU
4h Rel
8h Rel
12h Rel
24h Rel
B
RAD51 Time Course Release
Foci Number
NC1
siNSMCE2-2
siNSMCE2-6
24 h HU+8 hRelease
17 foci
36 foci
42 foci
C
New Origin Firing
NC1 (n=1718)
siNSMCE2-2 (n=618)
siNSMCE2-6 (n=1506)
%
NT
5 h HU
16 h HU
Fork Restart
Collapsed Forks
Replication Fork Speed
kb/min
n.s.
1.20
1.18
NC1 (n=135)
siNSMCE2-6 (n=84)
D
Cell Cycle
% of cells
G1
S
G2
Restart
IdU
CldU
DNA
Merge
New Origins
Collapse

Figure 2-2. DSB formation and resolution of RAD51 foci at collapsed forks is dependent on NSMCE2. (A) Cleavage of collapsed forks is dependent on NSMCE2. Quantitative analysis (top, left) and representative image (bottom, left) of DSBs in NSMCE2-deficient HeLa cells treated or not with HU for 24 h then released for 16 or 48 h or cells irradiated with 4 Gy. DSBs were visualized by PFGE. (top, right) Quantitative analysis of DSBs at different times after release from HU block. Mean and standard deviation is shown. Different time courses were performed, including release times of 4 h and 8 h; 12 h and 24 h; and 4 h, 8 h, 12 h, and 24 h. In each time course, the no-treatment sample was used to normalize the data. A minimum of two independent experiments were analyzed for 4 h and 8 h and the 12 h and 24 h time courses. (bottom, right) Image of a representative PFGE experiment. (B) (top) Quantitative analysis of number of RAD51 foci per cell at different times after release from HU block. Mean and standard error are shown. At least 10,000 RAD51 foci were analyzed in each experimental condition. Three independent experiments were performed. (bottom) Three representative images from the experiment. Scale bars represent 10 microns. (C) DNA combing analysis by maRTA of HeLa cells exposed to control and NSMCE2 siRNAs and treated or not with 2 mM HU for 5 h or 16 h. Two independent experiments were performed. Panels at right show quantitative analysis of new origin firing, replication fork re-start, fork collapse, and replication fork speed. Panels at left show representative images from the maRTA. (D) Cell cycle analysis by flow cytometry of untreated HeLa cells pulsed with 20 μM BrdU for 40 min. Mean and standard deviation is shown. Three independent experiments were performed. See Figure 1 for definition of asterisks.

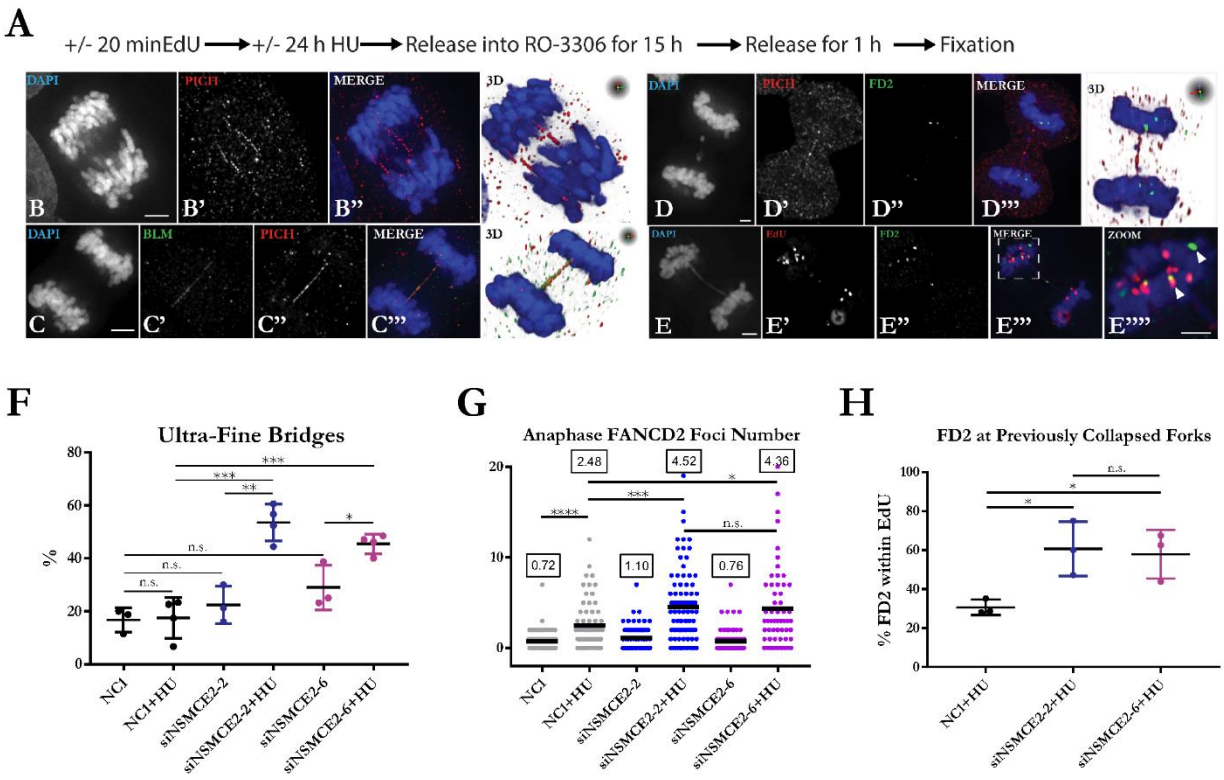
A
+/- 20 minEdU
+/- 24 h HU
Release into RO-3306 for 15 h
Release for 1 h
Fixation
DAPI
PICH
MERGE
3D
B
B'
B''
DAPI
BLM
PICH
MERGE
3D
C
C'
C''
C'''
DAPI
PICH
FD2
MERGE
3D
D
D'
D''
D'''
DAPI
EdU
FD2
MERGE
ZOOM
E
E'
E''
E'''
E''''
F
Ultra-Fine Bridges
%
NCI
NCI+HU
siNSMCE2-2
siNSMCE2-2+HU
siNSMCE2-6
siNSMCE2-6+HU
G
Anaphase FANCD2 Foci Number
2.48
4.52
4.36
0.72
1.10
0.76
H
FD2 at Previously Collapsed Forks
% FD2 within EdU

Figure 2-3. NSMCE2 prevents mitotic dependent DNA damage. (A) Schematic for treatment and enrichment of anaphase cells for analysis of UFBs and FANCD2 foci. (B) Representative deconvoluted, maximum intensity projection images of z-stacks showing multiple PICH positive UFBs, (C) BLM/PICH colocalization, (D) FANCD2 foci flanking UFBs, and (E) EdU/FANCD2 co-localization in anaphase cells. Scale bars represent 5 microns. (F) Quantitative analysis of PICH-stained UFBs in NSMCE2-deficient and control cells, processed as in A. 30-50 anaphase z-stacks were analyzed in each experimental condition. At least three independent experiments were performed. (G) Quantitation of number of FANCD2 foci per cell in anaphase cells independent of UFBs. 30-50 anaphase z-stacks were analyzed in each experimental condition. (H) Quantitation of EdU positive anaphase cells represented as the percent of FANCD2 foci localized in regions with EdU signal. At least 100 FANCD2 foci were analyzed in each experiment in cells positive for EdU signal only. Mean and standard deviation is shown. Three independent experiments were performed. See Figure 1 for definition of asterisks.

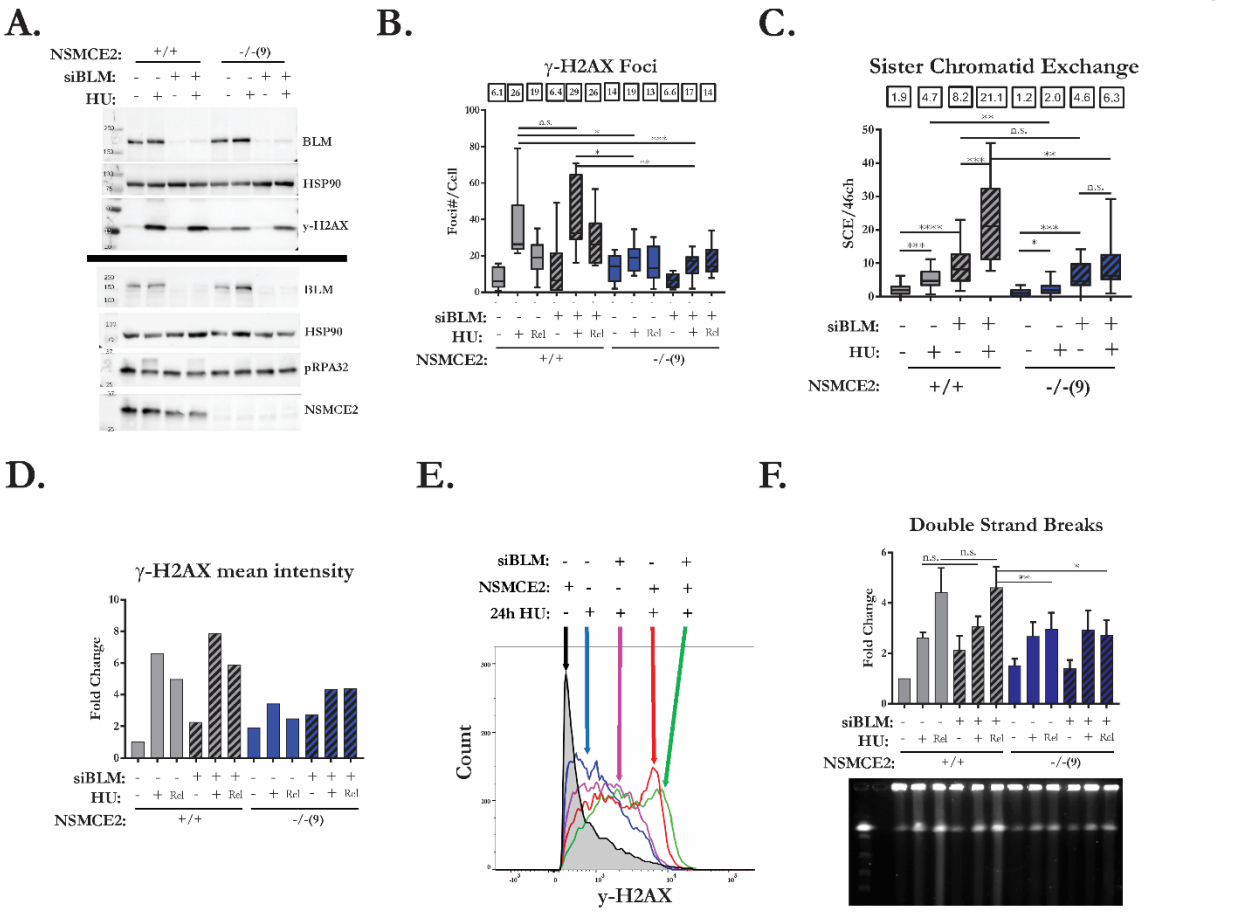
A.
NSMCE2: +/+ -/-(9)
siBLM: - - + + - - + +
HU: - + - + - + - +
BLM
HSP90
γ-H2AX
BLM
HSP90
pRPA32
NSMCE2
B.
γ-H2AX Foci
6.1 26 19 6.4 29 26 14 19 13 6.6 17 14
Foci#/Cell
siBLM: - - - + + + - - - + + +
HU: - + Rel - + Rel - + Rel - + Rel
NSMCE2: +/+ -/-(9)
C.
Sister Chromatid Exchange
1.9 4.7 8.2 21.1 1.2 2.0 4.6 6.3
SCE/46ch
n.s.
siBLM: - - + + - - + +
HU: - + - + - + - +
NSMCE2: +/+ -/-(9)
D.
γ-H2AX mean intensity
Fold Change
siBLM: - - - + + + - - - + + +
HU: - + Rel - + Rel - + Rel - + Rel
NSMCE2: +/+ -/-(9)
E.
siBLM: - - + - +
NSMCE2: + - - + +
24h HU: - + + + +
Count
γ-H2AX
F.
Double Strand Breaks
Fold Change
n.s.
siBLM: - - - + + + - - - + + +
HU: - + Rel - + Rel - + Rel - + Rel
NSMCE2: +/+ -/-(9)

Figure 2-4. *NSMCE2* is epistatic to *BLM* for HU-induced phenotypes. Analysis of HU-induced phenotypes in normal HEK293T and NSMCE2-null cells in which BLM levels were reduced or not by siRNA-mediated depletion. (A) Western blot analysis of levels of phosphorylation of H2AX and RPA. Black line indicates separate blots using lysates from the same experiment. Experiment was performed two times. (B) Analysis of focal concentrations of γ-H2AX after treatment with HU for 24 h and after release into normal medium for 6 h. Box and whisker plots representing at least 10,000 γH2AX foci in two independent experiments. Medians are shown above the graph. (C) Levels of HU-induced SCEs. Medians of the combined data are shown above the graph. Two independent experiments were performed. Unpaired t-test was performed to analyze the distributions. (D) Analysis by flow cytometry of fluorescence intensity of γ-H2AX after treatment with HU for 24 h and after release into normal medium for 6 h. Median florescence intensity was measured from a minimum of 10,000 events. The bar graph represents the fold change in median fluorescent intensity normalized to untreated normal HEK293T cells exposed to control siRNA. Two independent experiments were performed. (E) Representative distributions of fluorescence intensity of cells in selected conditions from the flow cytometry data. (F) Analysis by PFGE of DSBs after treatment with HU for 24 h and after release into medium for 6 h. The bar graph represents fold change in DSBs detected by PFGE normalized to untreated normal NSMCE2 cells exposed to control siRNA. The error bars represent the SEM of three independent experiments. The gel below the bar graph contains the results from one experiment. See Figure 1 for definition of asterisks.

K.Pond_Figure5

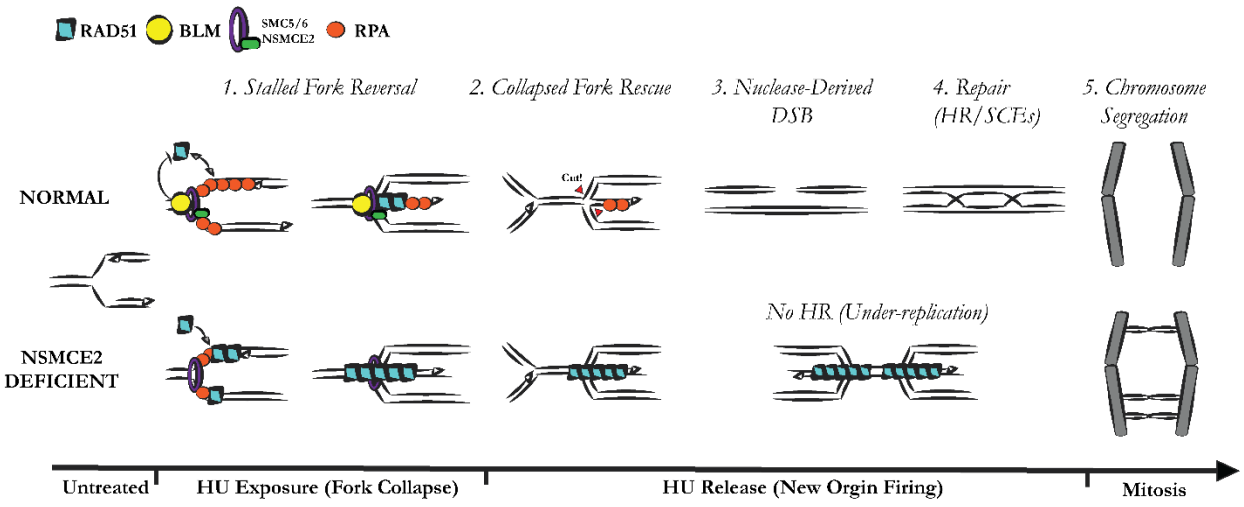

Figure 2-5. Model for collapsed-fork rescue by NSMCE2. Normally (top part of model), after exposure to HU, uncoupling of the replicative helicase from the replicative DNA polymerase at the fork leads to production of ssDNA, which is immediately bound by ssDNA binding protein RPA (red circle). BLM (yellow circle) is one of the first factors to be recruited to the stalled replication fork and this accumulation of BLM is dependent on the NSMCE2 protein (green rectangle) on the SMC5/6 complex (purple ring). The localization of BLM at the stalled fork assists in maintaining functional RAD51 (teal rhombus) exchange during fork reversal. Given enough time in the reversed configuration, the fork is unable to restart (fork collapse). After resumption of DNA synthesis at dormant origins, an active fork converges upon the collapsed fork. The convergence is associated with DSBs at the collapsed fork, followed by DSB repair by HR via the canonical RAD51-mediated pathway. In NSMCE2-deficient cells (bottom part of model), BLM is no longer recruited to the stalled fork, and there is a failure in the regulation of RAD51 loading at the fork, shown here as a loss of dynamic exchange of RAD51 and RPA resulting in excess, hyper-stable RAD51. After resumption of DNA synthesis at dormant origins, the aberrant RAD51 structure prevents convergence of the active fork with the collapsed fork, resulting in a double fork stall instead of a DSB. The double fork stall persists into mitosis where it results in an ultra-fine DNA bridge and mitotic DNA damage.

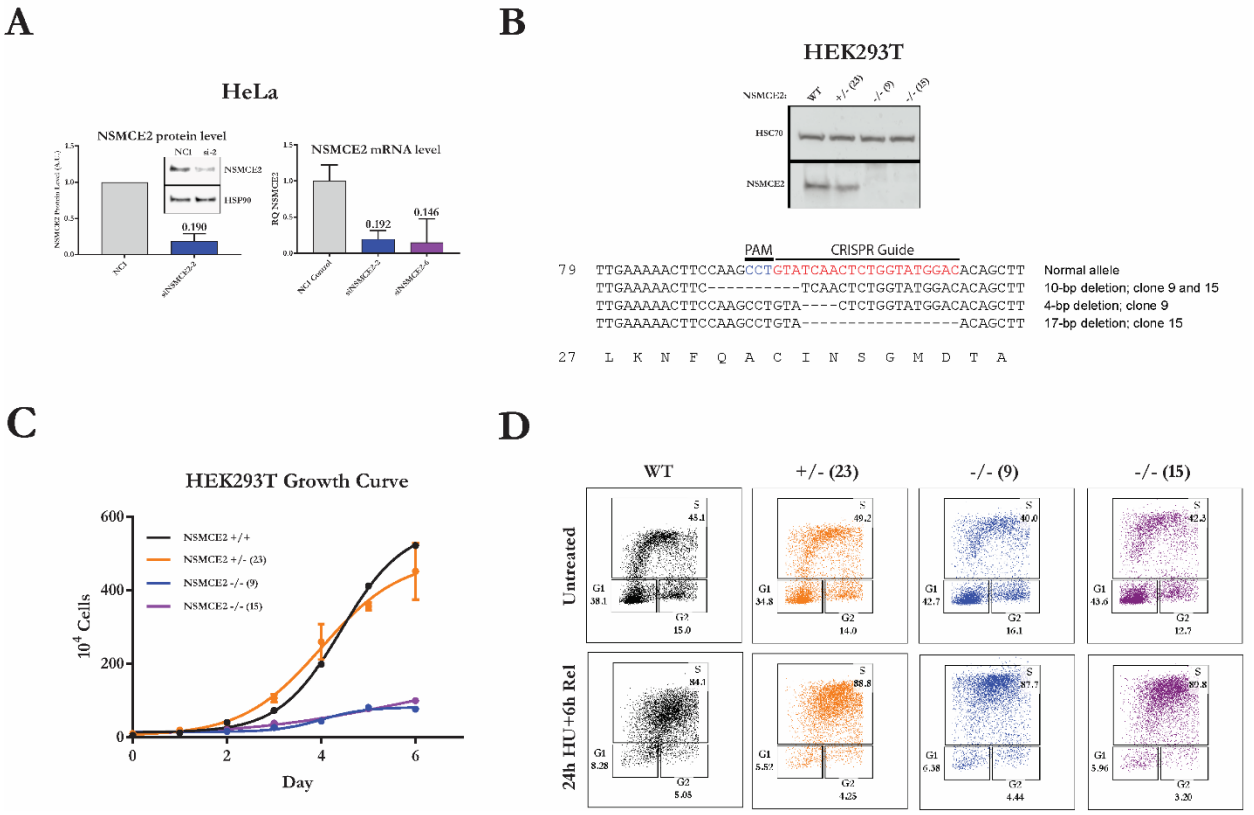
A
HeLa
NSMCE2 protein level
NC1
si-2
NSMCE2
HSP90
0.190
NC1
siNSMCE2-2
NSMCE2 mRNA level
0.192
0.146
NC1 Control
siNSMCE2-5
siNSMCE2-6
B
HEK293T
NSMCE2:
WT
+/- (23)
-/- (9)
-/- (15)
HSC70
NSMCE2
PAM
CRISPR Guide
79 TTGAAAAACTTCCAAGCCTGTATCAACTCTGGTATGGACACAGCTT Normal allele
TTGAAAAACTTC----------TCAACTCTGGTATGGACACAGCTT 10-bp deletion; clone 9 and 15
TTGAAAAACTTCCAAGCCTGTA----CTCTGGTATGGACACAGCTT 4-bp deletion; clone 9
TTGAAAAACTTCCAAGCCTGTA----------ACAGCTT 17-bp deletion; clone 15
27 L K N F Q A C I N S G M D T A
C
HEK293T Growth Curve
NSMCE2 +/+
NSMCE2 +/- (23)
NSMCE2 -/- (9)
NSMCE2 -/- (15)
10^4 Cells
Day
D
WT
+/- (23)
-/- (9)
-/- (15)
Untreated
24h HU+6h Rel
S
G1
G2

Supplementary Figure 2-1. (A) 80% reduction of the levels of NSMCE2 after depletion with siRNA in HeLa cells as measured by Western blot and qPCR analysis. (B-D) Analysis of the construction of NSMCE2-null cells in the HEK293T cell line. (B) Western blot analysis of normal, heterozygous, and two cell clones (clone 9 and clone 15) that are null for NSMCE2. The homozygous null cell clones were both derived from the heterozygous mutant of *NSCME2* that carried a 10-bp deletion in exon 2 of *NSMCE2*. Analysis by PCR and sequencing showed that clone 9 and clone 15 each contain the 10-bp deletion and a second clone-specific frameshift mutation. The sequence of the PAM site is denoted in blue and the sequence of the guide RNA is denoted in red. (C) Analysis of cell proliferation of normal, heterozygous, and null cell clones of NSMCE2. The cell counting experiments indicated that the rate of proliferation of *NSMC2*+/+ cells is approximately 20 hours per division and of *NSMC2*-/- cells 40 hours per division. (D) Flow cytometric analysis of the cell cycle. Cells were treated or not with 2 mM HU and then released (Rel) into normal medium for 6 hours. Cells were pulsed with 10 μM EdU prior to harvest and processing for flow cytometry. The NSCME2-null cells exhibit a mild G1 delay. Normal cells were pulsed with EdU for 20 min and NSMCE2-null cells were pulsed for 40 min to account for the slower cell cycle.

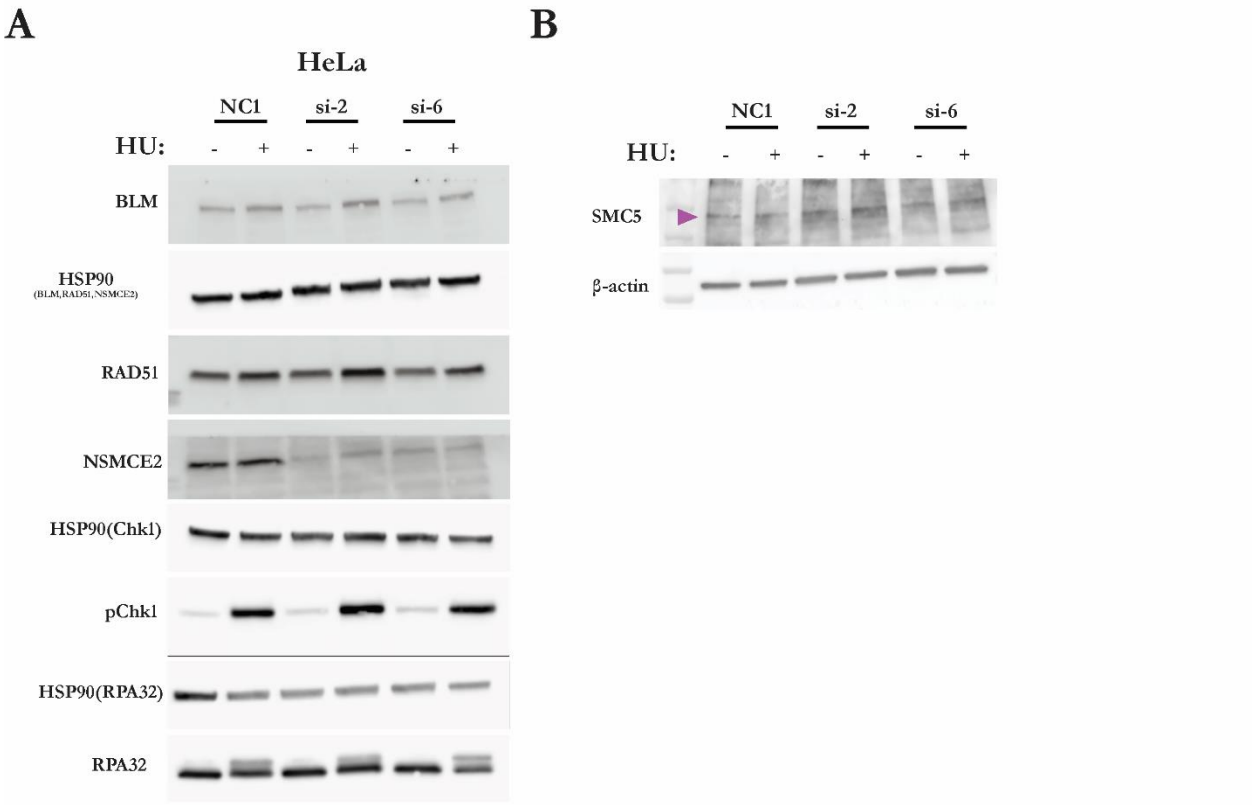
A
HeLa
NC1
si-2
si-6
HU: - + - + - +
BLM
HSP90
(BLM,RAD51,NSMCE2)
RAD51
NSMCE2
HSP90(Chk1)
pChk1
HSP90(RPA32)
RPA32
B
NC1
si-2
si-6
HU: - + - + - +
SMC5
β-actin

Supplementary Figure 2-2. (A) Representative Western blots of HeLa cells transfected with control or two different siRNAs against NSMCE2 and treated or not with 2 mM HU for 24 hours. Multiple loading controls (HSP90) are shown for separate gel runs and Westerns of the same cell lysate. (B) Western blot analysis of SMC5.

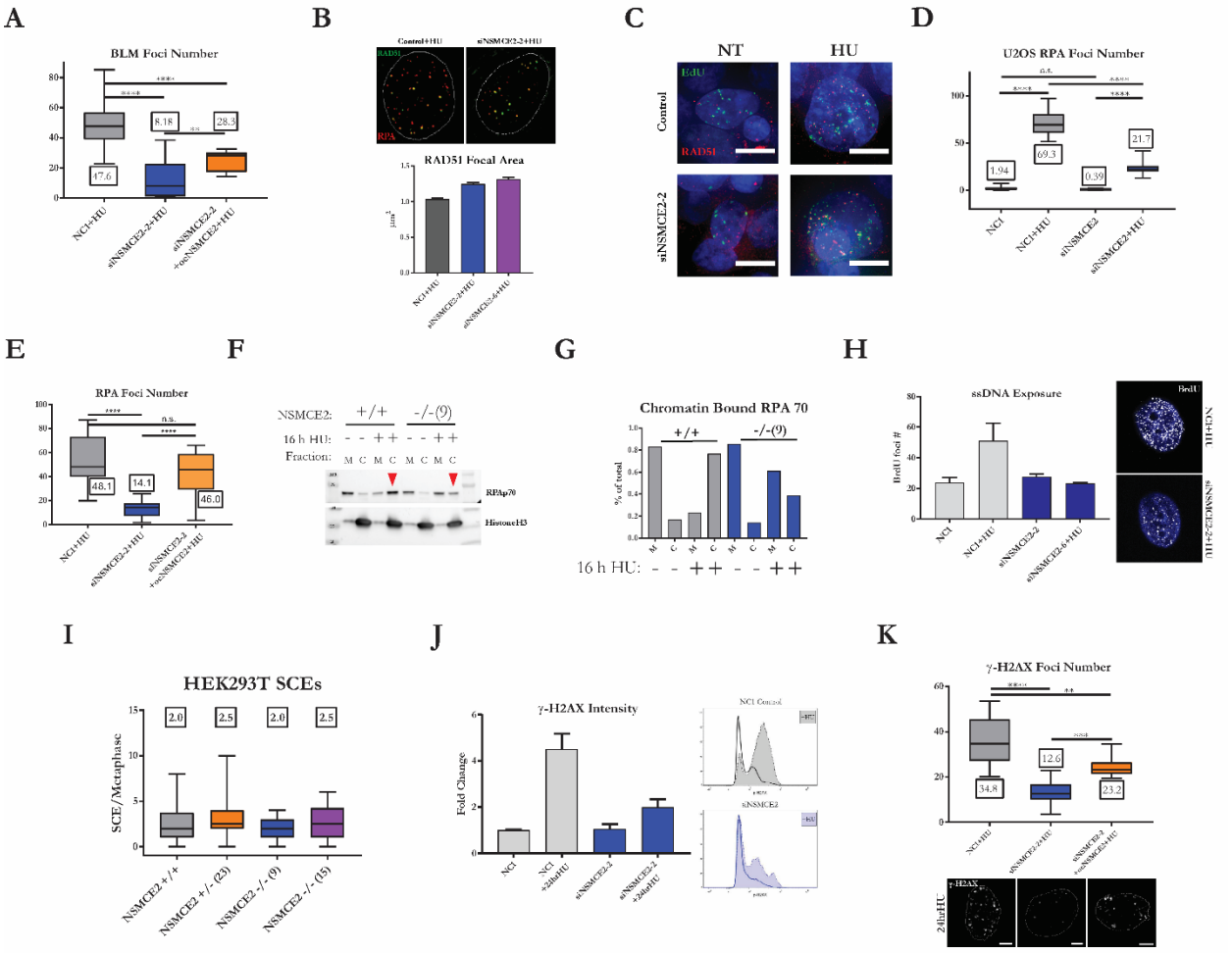
A
BLM Foci Number
47.6
8.18
28.3
NC1+HU
siNSMCE2-2+HU
siNSMCE2-2 +ocNSMCE2+HU
B
Control+HU
siNSMCE2-2+HU
RAD51
RPA
RAD51 Focal Area
NC1+HU
siNSMCE2-2+HU
siNSMCE2-4+HU
C
NT
HU
Control
siNSMCE2-2
EdU
RAD51
D
U2OS RPA Foci Number
1.94
69.3
0.39
21.7
NC1
NC1+HU
siNSMCE2
siNSMCE2+HU
E
RPA Foci Number
48.1
14.1
46.0
NC1+HU
siNSMCE2-2+HU
siNSMCE2-2 +ocNSMCE2+HU
F
NSMCE2: +/+ -/-(9)
16 h HU: - - + + - - + +
Fraction: M C M C M C M C
RPAp70
HistoneH3
G
Chromatin Bound RPA 70
+/+
-/-(9)
% of total
M C M C M C M C
16 h HU: - - + + - - + +
H
ssDNA Exposure
BrdU foci #
NC1
NC1+HU
siNSMCE2-2
siNSMCE2-4+HU
BrdU
NC1+HU
siNSMCE2-2+HU
I
HEK293T SCEs
SCE/Metaphase
2.0
2.5
2.0
2.5
NSMCE2 +/+
NSMCE2 +/- (23)
NSMCE2 -/- (9)
NSMCE2 -/- (15)
J
γ-H2AX Intensity
Fold Change
NC1
NC1 +24hrHU
siNSMCE2-2
siNSMCE2-2 +24hrHU
NC1 Control
siNSMCE2
K
γ-H2AX Foci Number
34.8
12.6
23.2
NC1+HU
siNSMCE2-2+HU
siNSMCE2 +ocNSMCE2+HU
γ-H2AX
24hrHU

Supplementary Figure 2-3. (A) Complementation of accumulation of BLM foci by transfection of siRNA-resistant NSMCE2 cDNA construct. HeLa cells were exposed to control or NSMCE2 siRNAs and were treated or not with 2 mM HU for 24 hours. Box and whisker plots represent distributions of the number of BLM foci per cell. The median values are shown in boxes. At least 10,000 BLM foci were analyzed in each experimental condition. Three independent experiments were performed. (B) Quantitation of the area of RAD51 foci. Mean and standard error are shown. At least 10,000 RAD51 foci were analyzed in each experimental condition. Three independent experiments were performed. (C) Colocalization of RAD51 and EdU in HU-treated cells. Representative images of control and NSMCE2-depleted HeLa cells exposed to 2 mM HU for 24 hours. EdU was incorporated for 12 min prior to HU treatment. After HU, cells were fixed and stained with RAD51. Images show the merge of EdU (green) and RAD51 (red) channels. (D) Reduced accumulation of RPA foci in HU-treated U2OS cells. Box and whiskers plot represent distribution of the number of RPA foci in cells exposed to control or NSMCE2 siRNA and treated or not with 2 mM HU for 24 hours. The median values are shown in boxes. Three independent experiments were performed. (E) Complementation of accumulation of RPA foci by transfection of siRNA-resistant NSMCE2 cDNA construct. HeLa cells were exposed to control or NSMCE2 siRNA and treated or not with 2 mM HU for 24 hours. Box and whiskers plot represent the distributions of number of RPA foci per cell. The median values are shown in boxes. Three independent experiments were performed. (F) Reduced accumulation of chromatin-bound RPA in HU-treated NSMCE2-nulls cells compared to HU-treated normal HEK293T cells. Western blot analysis of levels of chromatin-bound RPA (RPA p70 subunit). Cells were treated or not with 2 mM HU for 16 hours. The M fraction contains equal parts of the cytoplasmic and nucleoplasmic fractions. The C fraction contains the

chromatin-bound material. The red carets point to the HU-induced chromatin-bound RPA. Four independent experiments were performed. (G) Quantitation of experiment in F. (H) Reduced levels of ssDNA in HU-treated NSMCE2-deficient cells. Quantitation of immunofluorescence analysis of BrdU to measure exposed ssDNA. HeLa cells were exposed to control or NSMCE2 siRNAs and treated or not with 2 mM HU for 24 hours. The bar represents median values of numbers of BrdU foci and the error bar represent the SEM values from three independent experiments. Representative images of BrdU foci are shown. (I) Similar levels of SCEs in normal HEK293T cells and NSMCE2-null cells. Box and whiskers plot represent the numbers of SCEs per metaphase in cells treated or not with 2 mM HU for 24 hours. Two independent experiments were performed. (J) Reduced levels of γ-H2AX in HU-treated treated NSMCE2-deficient cells. Flow cytometric analysis of γ-H2AX response in HeLa cells. Mean and standard deviation is shown. To the right of the bar graph are representative histograms showing γ-H2AX induction. Shaded histograms represent the treated cell populations. Three independent experiments were performed. (K) Complementation of accumulation of γ-H2AX foci by transfection of siRNA-resistant NSMCE2 cDNA construct. Quantitative analysis of γ-H2AX foci. Box and whisker plots represent distributions of the number of γ-H2AX foci per cell. The median values are shown in boxes. At least 10,000 γ-H2AX foci were analyzed in each experimental condition. Below the bar graph are representative immunofluorescence images. Three independent experiments were performed.

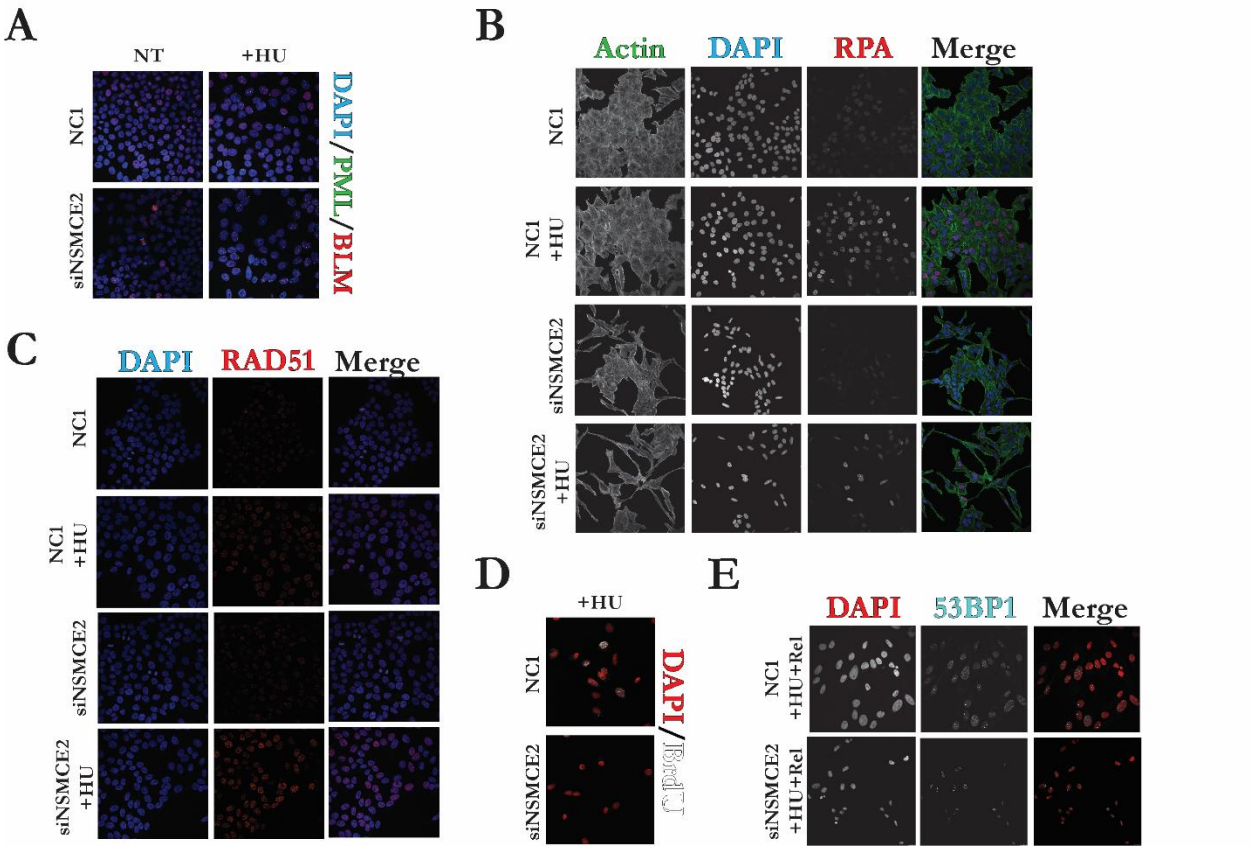
A
NT
+HU
NC1
siNSMCE2
DAPI/PML/BLM
B
Actin
DAPI
RPA
Merge
NC1
NC1 +HU
siNSMCE2
siNSMCE2 +HU
C
DAPI
RAD51
Merge
NC1
NC1 +HU
siNSMCE2
siNSMCE2 +HU
D
+HU
NC1
siNSMCE2
DAPI/BrdU
E
DAPI
53BP1
Merge
NC1 +HU+Rel
siNSMCE2 +HU+Rel

Supplementary Figure 2-4. Low power image of cells analyzed for the indirect immunofluorescence experiments. (A) Merged images of untreated or HU-treated control- and NSMCE2-depleted HeLa cells stained with antibodies to BLM (red) and PML (green) and countered with DAPI. Depletion of NSMCE2 is associated with increased numbers of PML nuclear bodies. In HU-treated control-depleted cells, BLM moves to stalled replication fork. In HU-treated NSMCE2-depleted cells, BLM remains associated with PML. (B) Images of HeLa cells stained with phalloidin, DAPI, anti-RPA p32 antibodies. (C) Images of HeLa cells stained with DAPI and anti-RAD51 antiboides. (D) Images of HeLa cells and stained with DAPI and anti-BrdU antibodies. Cells were incubated with 10 μM BrdU for 48 h, treated with HU for 24 h, then processed for immunofluorescence. (E) Images of HeLa cells treated with HU for 24 h then released for 12 h and stained with DAPI and anti-53BP1 antibodies.

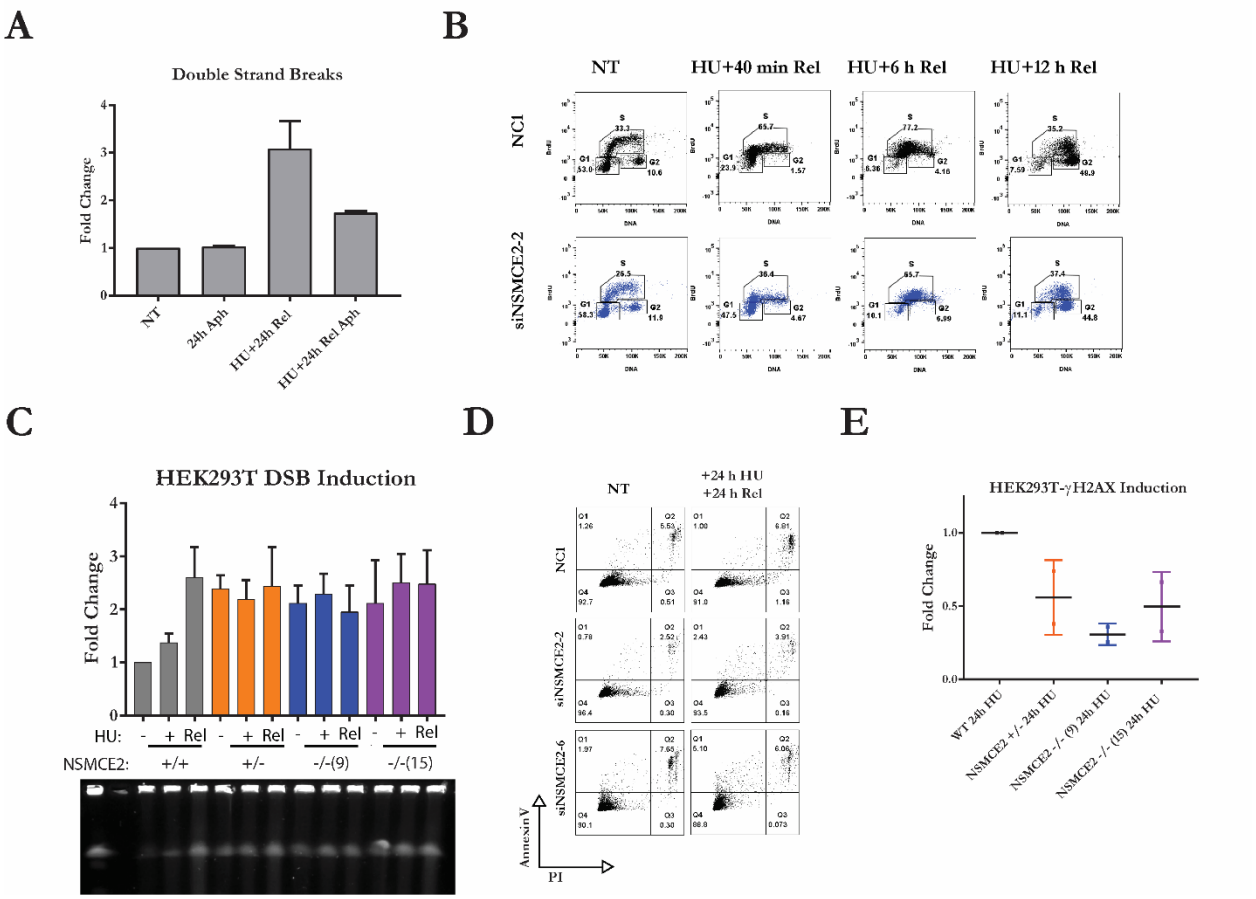
A
Double Strand Breaks
Fold Change
NT
24h Aph
HU+24h Rel
HU+24h Rel Aph
B
NT
HU+40 min Rel
HU+6 h Rel
HU+12 h Rel
NC1
siNSMCE2-2
C
HEK293T DSB Induction
Fold Change
HU:
NSMCE2:
+/+
+/-
-/-(9)
-/-(15)
D
NT
+24 h HU
+24 h Rel
NC1
siNSMCE2-2
siNSMCE2-6
Annexin V
PI
E
HEK293T-γH2AX Induction
Fold Change
WT 24h HU
NSMCE2 +/- 24h HU
NSMCE2 -/- (9) 24h HU
NSMCE2 -/- (15) 24h HU

Supplementary Figure 2-5. (A) (B) Flow cytometric analysis of cell cycle after HU treatment and release. HeLa cells were transfected with siRNA for NSMCE2 or control. After 24 h, they were treated or not with 2 mM HU for 24 h prior to release for 40 min, 6 h, or 12 h. The cells were then pulsed with 20 μM EdU for 20 min prior to harvest and staining with click reagents. A minimum of 10,000 events were recorded in each experimental condition. (C) PFGE analysis of HEK293T cells treated or not with 2 mM HU for 24 h prior to release for 12 h before harvest for DSB quantitation. The bar graph shows the mean fold change values, normalized to the untreated normal HEK293T mean, and SEM values from three independent experiments. A representative gel image of one experiment is shown below the graph. We note that the fold induction with HU in these experiments is lower than the fold induction with HU in experiments in which an siRNA-mediated depletion protocol was used, as shown in Figure 7. (D) Analysis of apoptosis in Hela cells after HU treatment and released as described above using PI and antibodies against AnnexinV. A minimum of 10,000 events were recorded in each experimental condition. (E) Graph showing fold change in median levels of HU-induced γ-H2AX in normal HEK293T cells, the heterozygous NSMCE2+/- cells, and the two NSMCE2-/- clones.

A

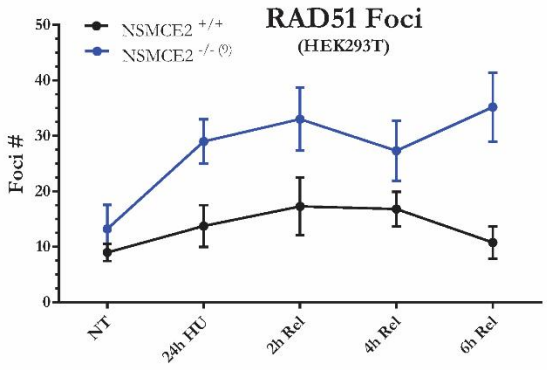
RAD51 Foci
(HEK293T)
NSMCE2 +/+
NSMCE2 -/-(9)
Foci #
0
10
20
30
40
50
NT
24h HU
2h Rel
4h Rel
6h Rel

B

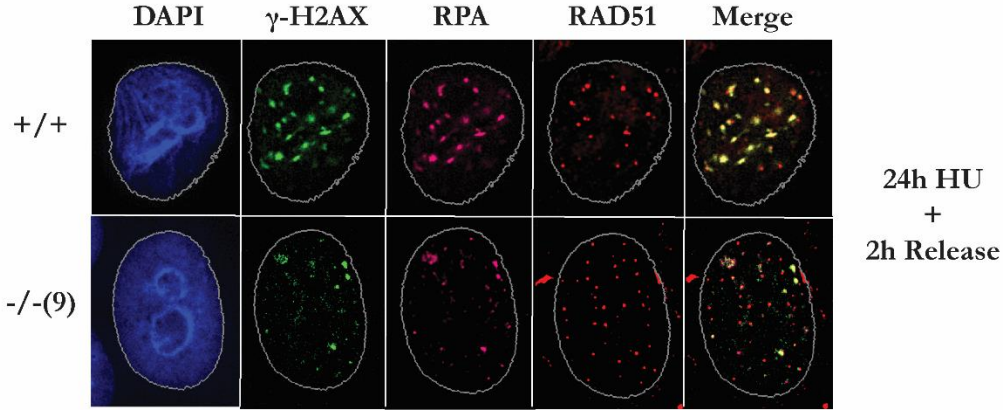
DAPI
γ-H2AX
RPA
RAD51
Merge
+/+
-/-(9)
24h HU
+
2h Release

Supplementary Figure 2-6. (A) Immunofluorescence analysis of HEK293T cells treated or not 2 mM HU for 24 h prior to release for 2 h, 4 h, or 6 h before staining, imaging, and quantitation. Each point on the graph represents the median value and the error bar represent SEM values from randomly binned averages of 10 cells from at least 50 cells in each experimental condition. Two independent experiments were performed. (B) Representative images of data shown in (A) showing co-localization of γ-H2AX, RPA, and RAD51 in HEK293T cells after 24 h treatment with HU and 2h release.

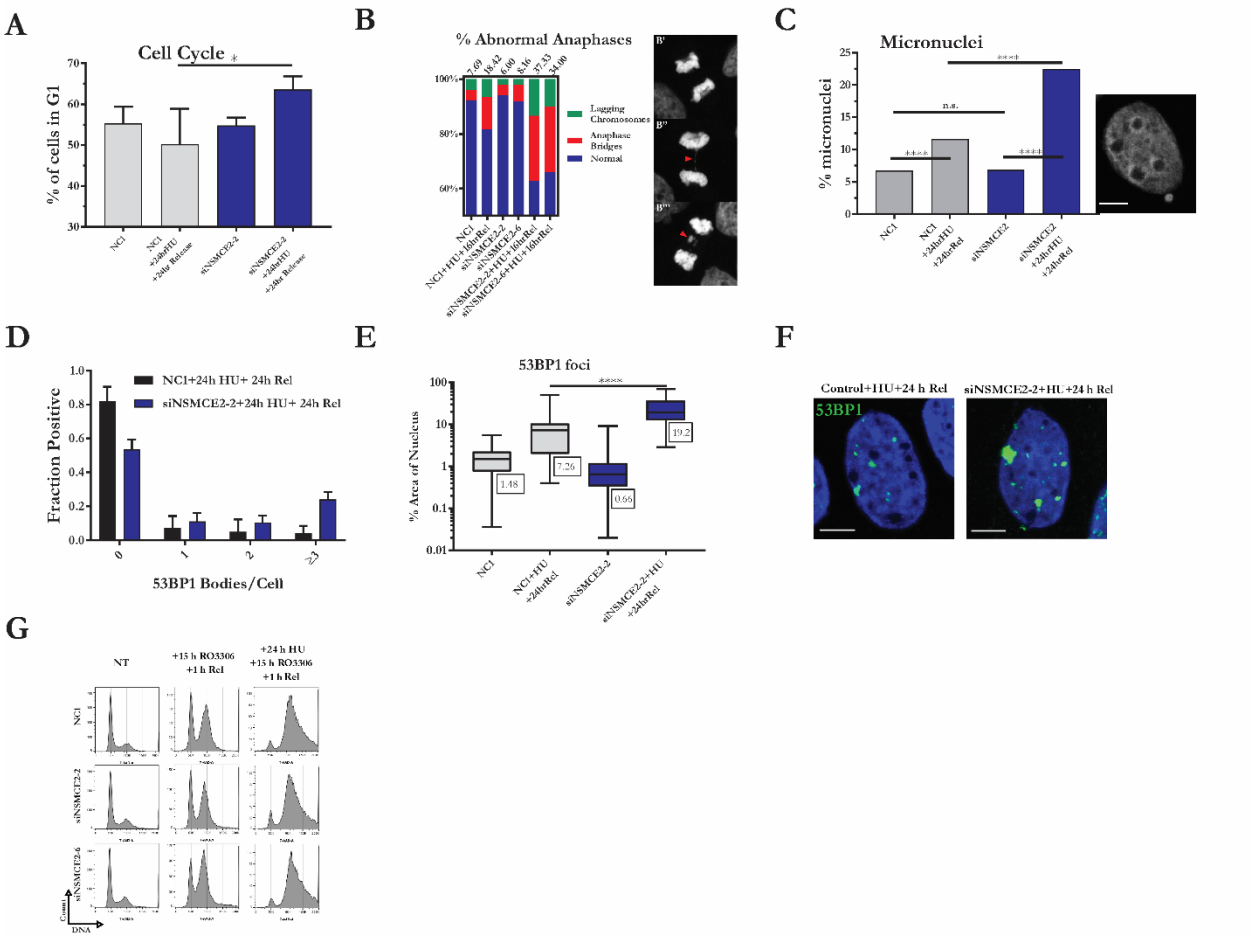
A
Cell Cycle
% of cells in G1
NC1
NC1 +24hrHU +24hr Release
siNSMCE2-2
siNSMCE2-2 +24hrHU +24hr Release
B
% Abnormal Anaphases
7.69
18.42
6.00
8.16
37.33
34.00
Lagging Chromosomes
Anaphase Bridges
Normal
NC1
NC1+HU+16hrRel
siNSMCE2-2
siNSMCE2-2+HU+16hrRel
siNSMCE2-6
siNSMCE2-6+HU+16hrRel
C
Micronuclei
% micronuclei
n.s.
NC1
NC1 +24hrHU +24hrRel
siNSMCE2
siNSMCE2 +24hrHU +24hrRel
D
NC1+24h HU+ 24h Rel
siNSMCE2-2+24h HU+ 24h Rel
Fraction Positive
53BP1 Bodies/Cell
E
53BP1 foci
% Area of Nucleus
1.48
7.26
0.66
19.2
NC1
NC1+HU +24hrRel
siNSMCE2-2
siNSMCE2-2+HU +24hrRel
F
Control+HU+24 h Rel
siNSMCE2-2+HU +24 h Rel
53BP1
G
NT
+15 h RO3306 +1 h Rel
+24 h HU +15 h RO3306 +1 h Rel
NC1
siNSMCE2-2
siNSMCE2-6
Count
DNA

Supplementary Figure 2-7. (A) Quantitative analysis of G1 arrest after release of control and NSMCE2-depleted HeLa cells from HU block into normal medium for 24 h. (B) Quantitative analysis of abnormal anaphases encountered after release from HU block. The graph plots % values of normal (blue), anaphase bridges (red), and lagging chromosomes (green). The value shown above the graph is the % of normal mitosis scored. Representative images of normal mitosis (B'), mitosis with an anaphase bridge (red caret in B"), and mitosis with a lagging chromosome (red caret in B"') are shown. At least 100 anaphase cells were analyzed in each experimental condition. Three independent experiments were performed. (C) Quantitative analysis of micronuclei formation after release from HU block and a representative image to the right of the graph. Scale bars represent 10 microns. (D) Quantitation of 53BP nuclear bodies/cell. HeLa cells were treated with 2 mM HU for 24 h, then released into fresh media for 24 h before fixation and staining. Each bar represents the mean percent of total cells observed in each class and the error bar represent the SEM values. Flow cytometric analysis showed that the majority of cells in G1 (see panel A). Cells with large nuclei indicative of being in the G2 phase were excluded from the quantitation. Three independent experiments were performed. (E) Quantitative analysis of area of the nucleus inhabited by 53BP1 signal after release from HU block. Box and whisker plot represents area distribution per cell in at least 250 cells in each experimental condition. Three independent experiments were performed. (F) Representative images of cells stained for 53BP1 analyzed in panels D and E. (G) Flow cytometric analysis of the effect of the treatment schedule to enrich for mitotic cells used in the experiments shown in Figure 3. HeLa cells were transfected with siRNA for NSMCE2 or control. After 24 h, they were treated or not with 2 mM HU for 24 h prior to release into medium with 7.5 μM RO-3306

for 15 h, followed by release into fresh media for 1 h. Cells were harvested, fixed, and stained with 7-AAD. 10,000 events were analyzed in each experimental condition.

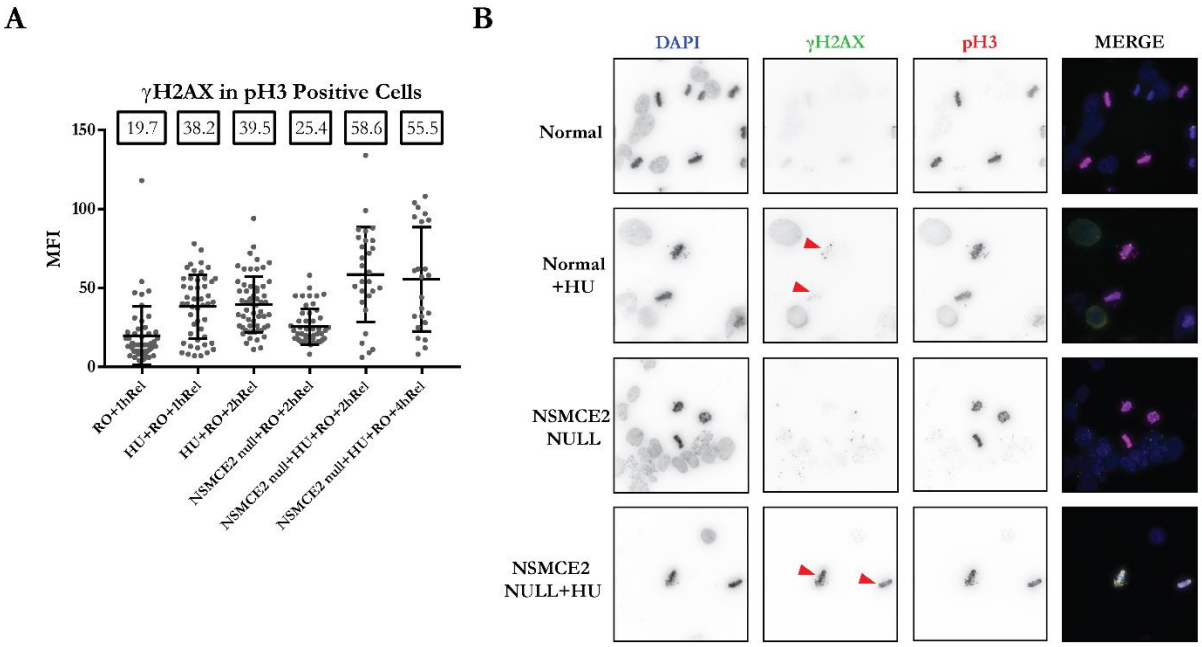
A
γH2AX in pH3 Positive Cells
MFI
150
100
50
0
19.7
38.2
39.5
25.4
58.6
55.5
RO+1hRel
HU+RO+1hRel
HU+RO+2hRel
NSMCE2 null+RO+2hRel
NSMCE2 null+HU+RO+2hRel
NSMCE2 null+HU+RO+4hRel
B
DAPI
γH2AX
pH3
MERGE
Normal
Normal +HU
NSMCE2 NULL
NSMCE2 NULL+HU

Supplementary Figure 2-8. (A) Quantitation of median fluorescence intensity of γ-H2AX on phospho-histone H3-positive chromosomes. Cells were treated with 2 mM HU for 24, released into medium containing 7.5 μM RO-3306 for 10 h (HEK 293T) or 20 h (NSMCE2-null) to block cells at the G2/M boundary, and then released into normal medium and harvested at the indicated times for analysis of metaphase chromosomes. Two independent experiments were performed. (B) Representative images of metaphase chromosomes stained with γ-H2AX, anti-phospho-histone H3 (serine 10), and DAPI.

A

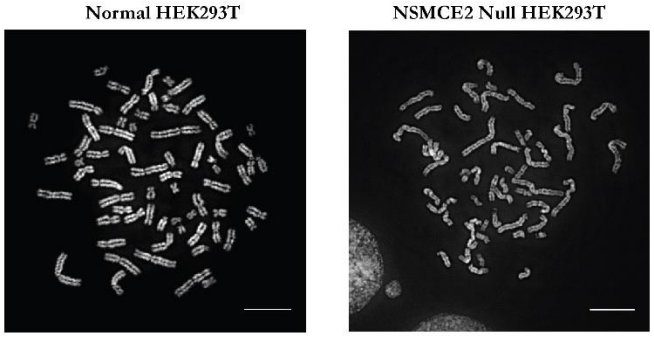

B

	Total (n)	Chromatid Breaks	Chromosome Breaks	Gaps	Telomere Fusions	Triradials	Quadriradials	Secondary Constrictions	Abbs/46ch
Normal	2651	2	1	0	2	1	0	4	**0.17**
Normal+HU	1874	11	2	1	1	2	1	5	**0.56**
NSMCE2 Null	2882	10	0	1	12	5	0	13	**0.65**
NSMCE2 Null+HU	2723	36	1	3	14	7	3	22	**1.45**

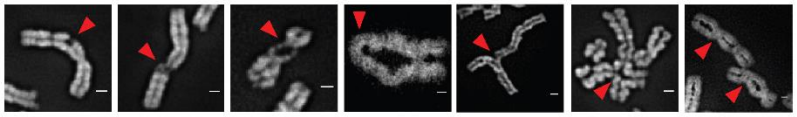

Supplementary Figure 2-9. (A) Representative images of metaphases prepared from normal HEK293T and NSMCE-/- cells clone 9. (B) Analysis of chromosome aberrations identified in untreated and HU-treated normal and mutant HEK293T cells. Representative chromosome image are shown below the grid of counts of chromosome aberrations. Approximately 25 metaphases were analyzed from each of two experiments. Total indicates the number of chromosomes scored. 1, chromatid break. 2, chromosome break. 3, chromosome gap. 4, telomere fusion. 5, tri-radial. 6, quadriradial. 7, secondary constriction.

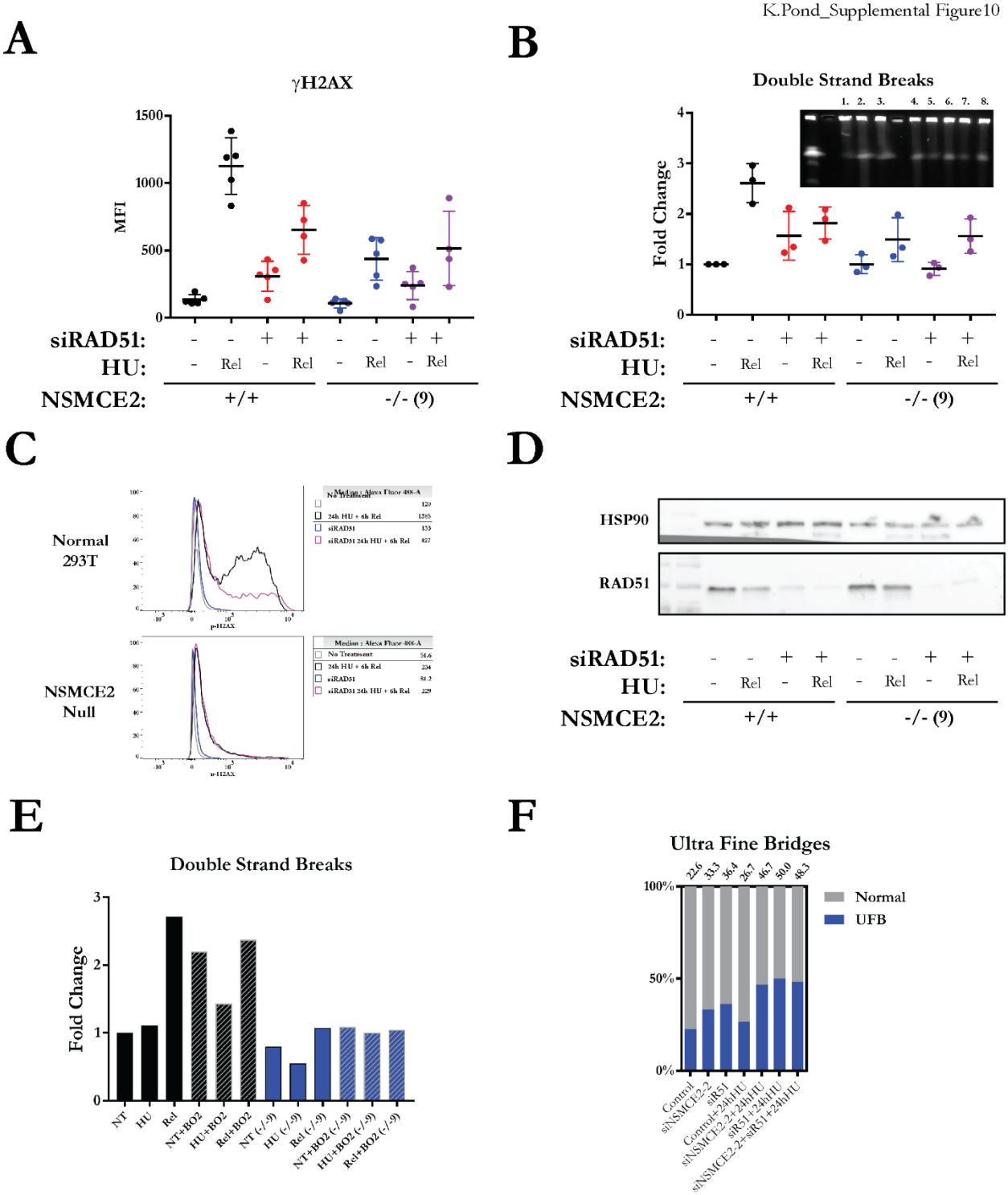
A
γH2AX
MFI
1500
1000
500
0
siRAD51: - - + + - - + +
HU: - Rel - Rel - Rel - Rel
NSMCE2: +/+ -/- (9)
B
Double Strand Breaks
Fold Change
4
3
2
1
0
1. 2. 3. 4. 5. 6. 7. 8.
siRAD51: - - + + - - + +
HU: - Rel - Rel - Rel - Rel
NSMCE2: +/+ -/- (9)
C
Normal 293T
NSMCE2 Null
No Treatment
24h HU + 6h Rel
siRAD51
siRAD51 24h HU + 6h Rel
D
HSP90
RAD51
siRAD51: - - + + - - + +
HU: - Rel - Rel - Rel - Rel
NSMCE2: +/+ -/- (9)
E
Double Strand Breaks
Fold Change
3
2
1
0
NT
HU
Rel
NT+BO2
HU+BO2
Rel+BO2
NT (-/-9)
HU (-/-9)
Rel (-/-9)
NT+BO2 (-/-9)
HU+BO2 (-/-9)
Rel+BO2 (-/-9)
F
Ultra Fine Bridges
22.6
33.3
36.4
26.7
46.7
50.0
48.3
100%
50%
0%
Normal
UFB
Control siNSMCE2-2
siR51
Control+24hHU siNSMCE2-2+24hHU
siR51+24hHU siNSMCE2-2+siR51+24hHU

Supplementary Figure 2-10. *RAD51* and *NSMCE2* are epistatic with respect to HU-induced phenotypes. Analysis of HU-induced phenotypes in normal HEK293T and NSMCE2-null cells in which RAD51 levels were reduced or not by siRNA-mediated depletion. (A) Analysis by flow cytometry of fluorescence intensity of γ-H2AX after treatment with HU for 24 h followed by release into normal medium for 6 h (Rel). The error bars represent the SD of median fluorescence intensity from a minimum of 10,000 events in five independent experiments. (B) Analysis by PFGE of DSBs after treatment with HU for 24 h followed by release into medium for 6 h (Rel). The bar graph represents the mean fold change in DSBs detected by PFGE normalized to untreated normal NSMCE2 cells exposed to control siRNA. The error bars represent the SD of three independent experiments. The inset gel shows the results from one experiment. (C) Representative distributions of fluorescence intensity of cells from the flow cytometry data. (D) Western analysis of RAD51 levels from samples prepared for the PFGE experiment shown in (B). (E)

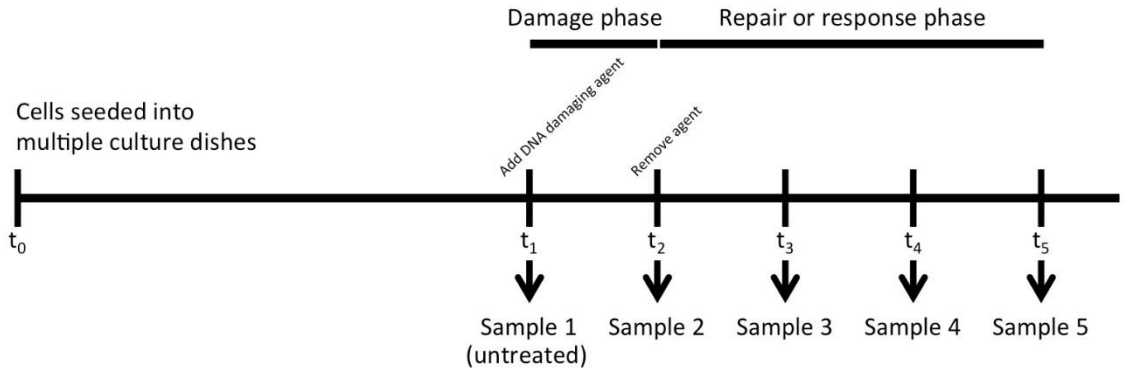
Damage phase
Repair or response phase
Cells seeded into
multiple culture dishes
Add DNA damaging agent
Remove agent
t_0
t_1
t_2
t_3
t_4
t_5
Sample 1
(untreated)
Sample 2
Sample 3
Sample 4
Sample 5

Figure 3-1. Schema for a typical experiment with a treatment phase followed by a response or repair phase. Cells are seeded into dishes at the beginning of the experiment. The cell density is chosen so that the cells are growing at their maximal rate and so that there are at least 1 million cells at the point of harvest. A dish of cells is prepared as an untreated control to be collected at the end of the experiment. At least 12 hours is allowed for the cells to recover from culturing (t_0). Cells at treated with agent at t_1. The treatment runs from t_1 to t_2. Dishes of cells are harvested immediately after treatment (t_2) and then and times after treatment (t_3, t_4, t_5, etc.) to monitor accrual of additional DSBs, repair of DSBs, or both.

A.

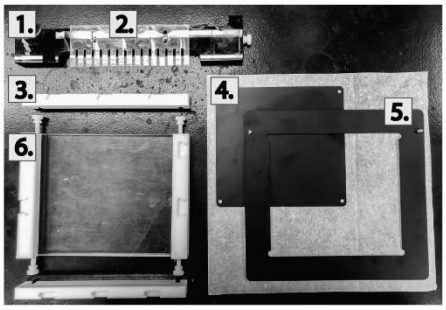
1.
2.
3.
4.
5.
6.

B.

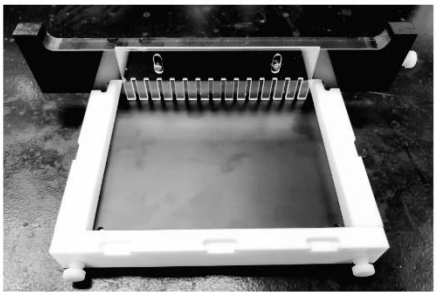

C.

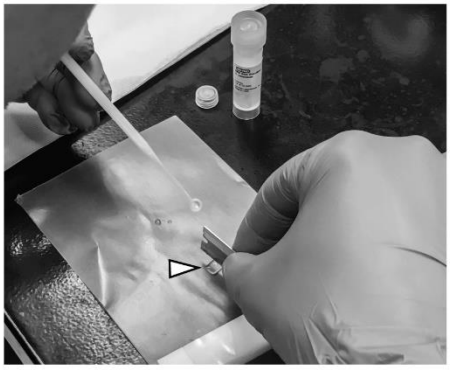

D.

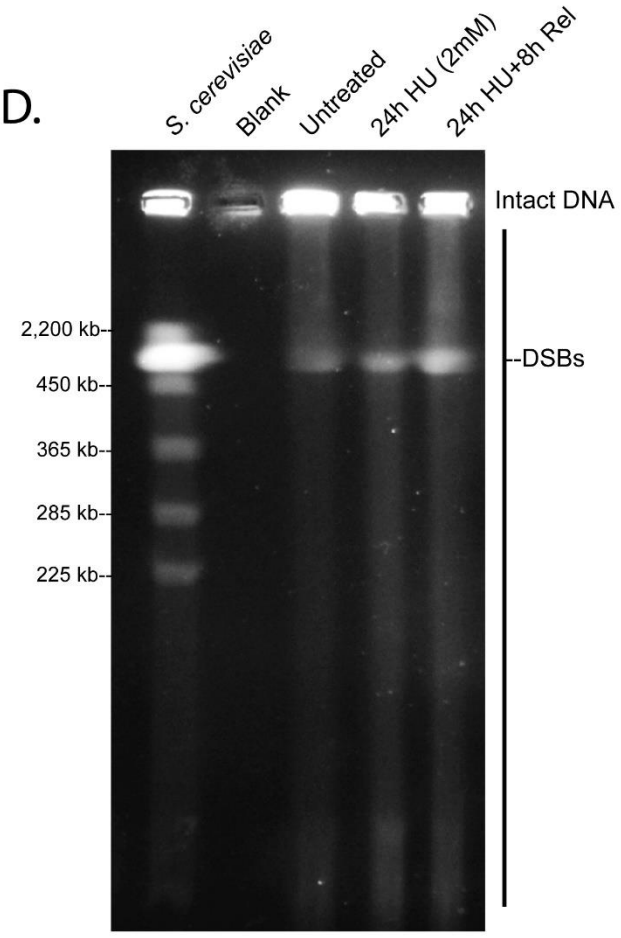
S. cerevisiae
Blank
Untreated
24h HU (2mM)
24h HU+8h Rel
Intact DNA
2,200 kb--
450 kb--
365 kb--
285 kb--
225 kb--
--DSBs

E.

Figure 3-2. **A.** Components of the casting stand and comb holder: 1) comb holder, 2) comb, 3) casting stand end gate, 4) platform, 5) platform frame, 6) casting stand. **B.** Assembled casting stand and comb holder prior to casting the gel. **C.** Cutting of a marker plug prior to gel loading. **D.** Representative gel of HeLa cells treated under the following conditions: cells were untreated, treated with 2 mM HU for 24 hours, or treated for 24 hours prior to HU washout and release for 8 hours. **E.** Gentle sliding of the cut plugs from the razor into the gel prior to running.

A

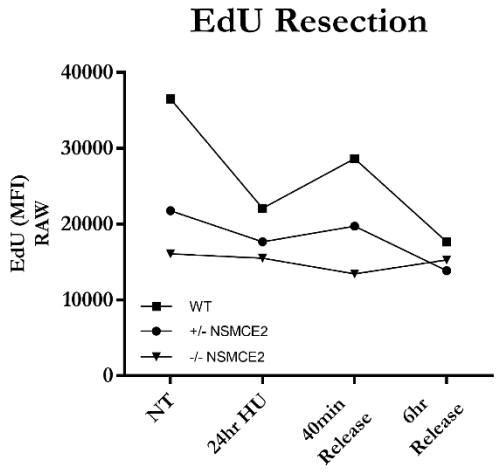
EdU Resection
EdU (MFI) RAW
40000
30000
20000
10000
0
WT
+/- NSMCE2
-/- NSMCE2
NT
24hr HU
40min Release
6hr Release

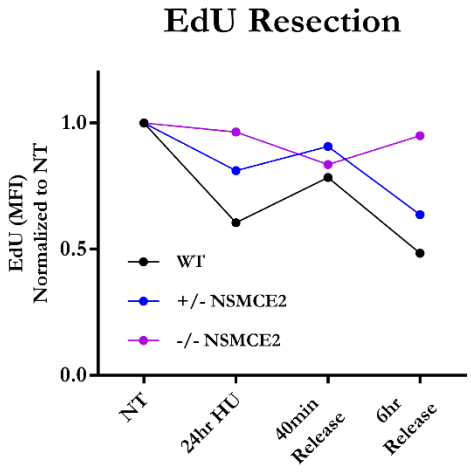
EdU Resection
EdU (MFI) Normalized to NT
1.0
0.5
0.0
WT
+/- NSMCE2
-/- NSMCE2
NT
24hr HU
40min Release
6hr Release

B

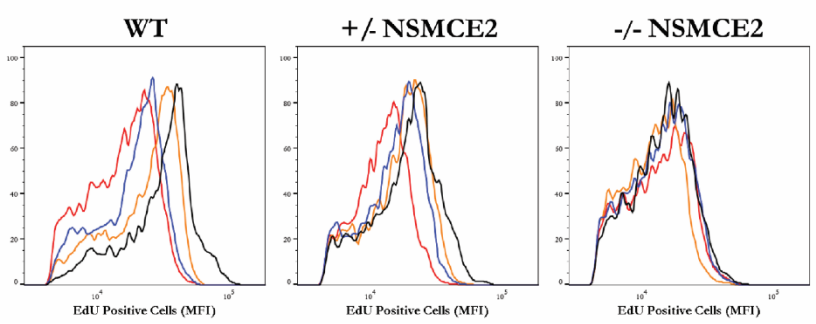
WT
+/- NSMCE2
-/- NSMCE2
EdU Positive Cells (MFI)
EdU Positive Cells (MFI)
EdU Positive Cells (MFI)

C

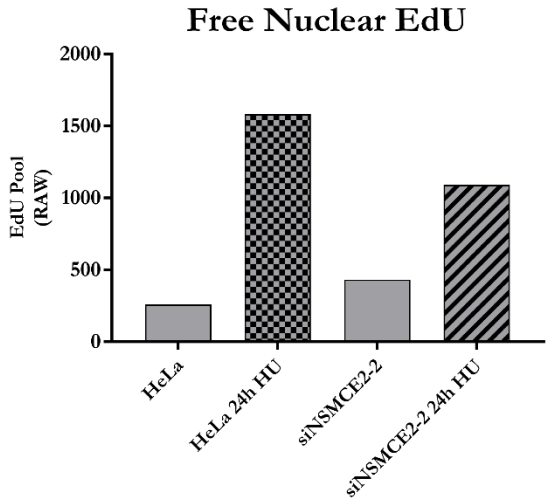
Free Nuclear EdU
EdU Pool (RAW)
2000
1500
1000
500
0
HeLa
HeLa 24h HU
siNSMCE2-2
siNSMCE2-2 24h HU

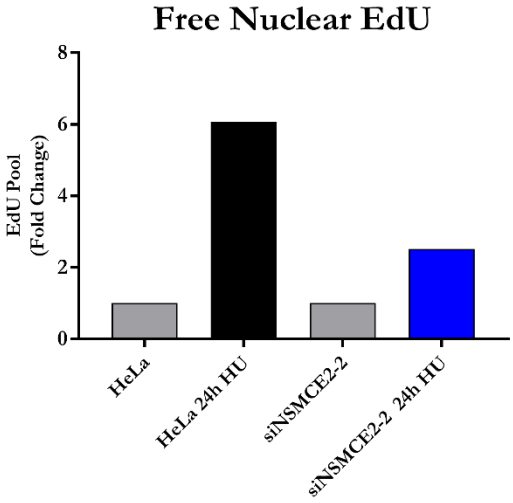
Free Nuclear EdU
EdU Pool (Fold Change)
8
6
4
2
0
HeLa
HeLa 24h HU
siNSMCE2-2
siNSMCE2-2 24h HU

Figure 4-1- A. Left-Raw data from flow cytometric analysis of median fluorescence intensity of EdU-labeled normal and NSMCE2-null HEK293T cells. Cells were pulsed with 20 μM EdU for 30 minutes prior to harvest or treatment with HU. Cells were washed twice with PBS prior to HU treatment and before release into fresh media. After 24h of 2mM HU treatment, ~40% of the EdU label is lost from DNA in normal cells. 40m after release from HU, some EdU label is reincorporated into DNA. After 6 hours, cells lose ~50% of their EdU labelling. Cells heterozygous for NSMCE2 displayed similar pattern with a reduced intensity. For NSMCE-null cells, EdU label is retained during HU treatment and after release. Right-To control for incorporation differences, the data was normalized to the untreated controls of each cell strain. **B.** Representative histograms from the flow cytometry data shown in A. Untreated cells are shown in black, HU treated in blue, 40 minute release in orange, and 6 hour release in red. **C.** Left-Raw data from mass spectrometry analysis of EdU levels within the nuclear pool using normal and NSMCE2-null HEK293T cells. The levels of EdU in the pool increased after treatment with HU in normal cells. Right-Normalized data from the left experiment, a 6-fold increase is seen in normal cells after HU treatment compared to a 2.5-fold increase in NSMCE2-null cells.

A.

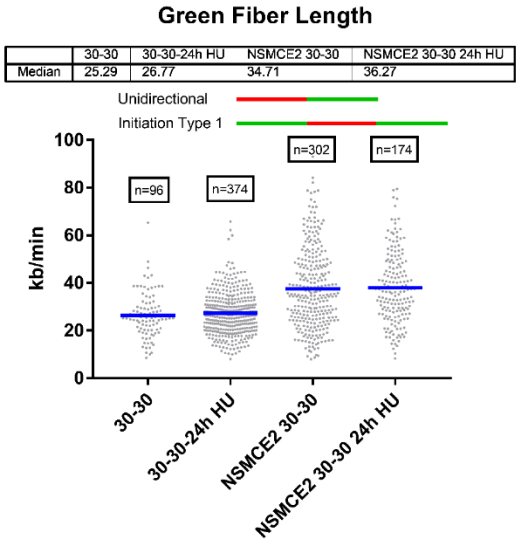
Green Fiber Length
30-30
30-30-24h HU
NSMCE2 30-30
NSMCE2 30-30 24h HU
Median
25.29
26.77
34.71
36.27
Unidirectional
Initiation Type 1
kb/min
n=96
n=374
n=302
n=174
30-30
30-30-24h HU
NSMCE2 30-30
NSMCE2 30-30 24h HU

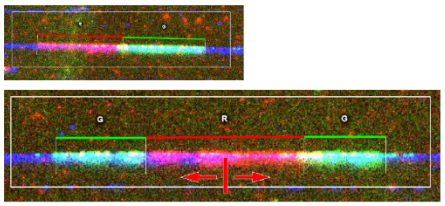
G
R
G

B.

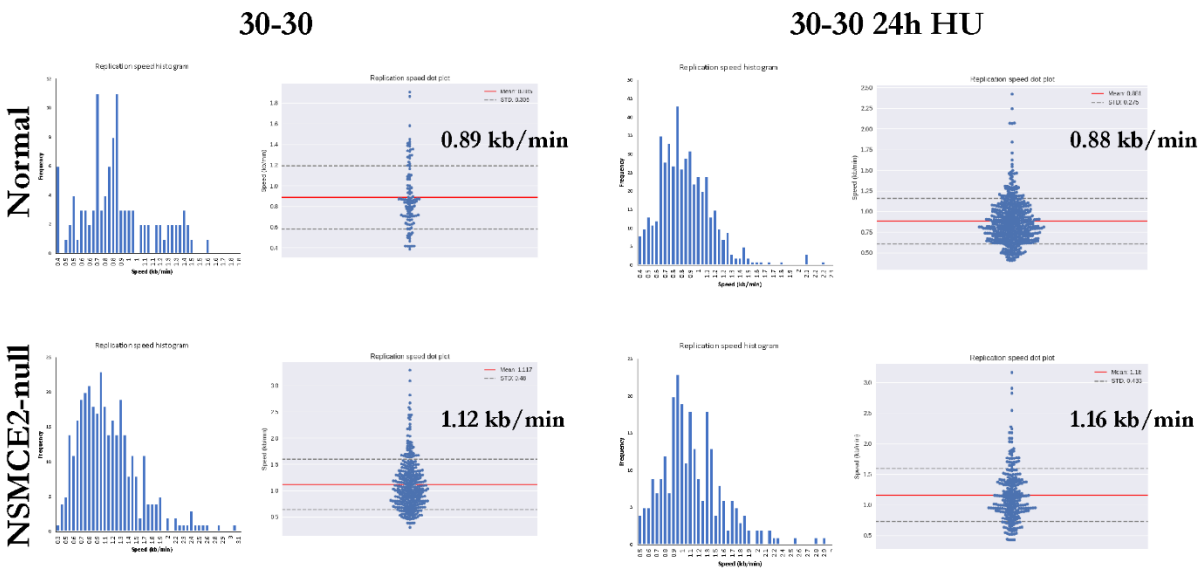
30-30
30-30 24h HU
Normal
NSMCE2-null
0.89 kb/min
0.88 kb/min
1.12 kb/min
1.16 kb/min

Figure 4-2. Replication fork speed and resection is unchanged in NSMCE2 cells by molecular combing. **A.** Resection analysis by molecular combing. Normal or NSMCE2-null HEK293T cells were pulsed with 50 μM CldU for 30 minutes, washed twice with warm PBS, pulsed with 50 μM IdU for 30 minutes. HU treated samples were treated the same with an additional treatment of 2 mM HU for 24 hours prior to harvest. Cells were then washed with cold PBS, harvested, and analyzed by genomic vision. Stitched DNA fiber images were then quantified using fiber studio software. Dot plots represent the distribution of green label lengths. Median values are shown above the graph and mean values are represented by the blue bars. Representative images for unidirectional and initiation type 1 signal are shown to the right of the figure. **B.** Replication fork speed by molecular combing. Normal or NSMCE2-null HEK293T cells were treated as in A. Data is represented as histogram and dot plot of both red and green tracks. The kb/min value is an average of the mean from both red and green track averages. A minimum of 100 track measurements were analyzed in each condition. These data are representative of a single experiment.

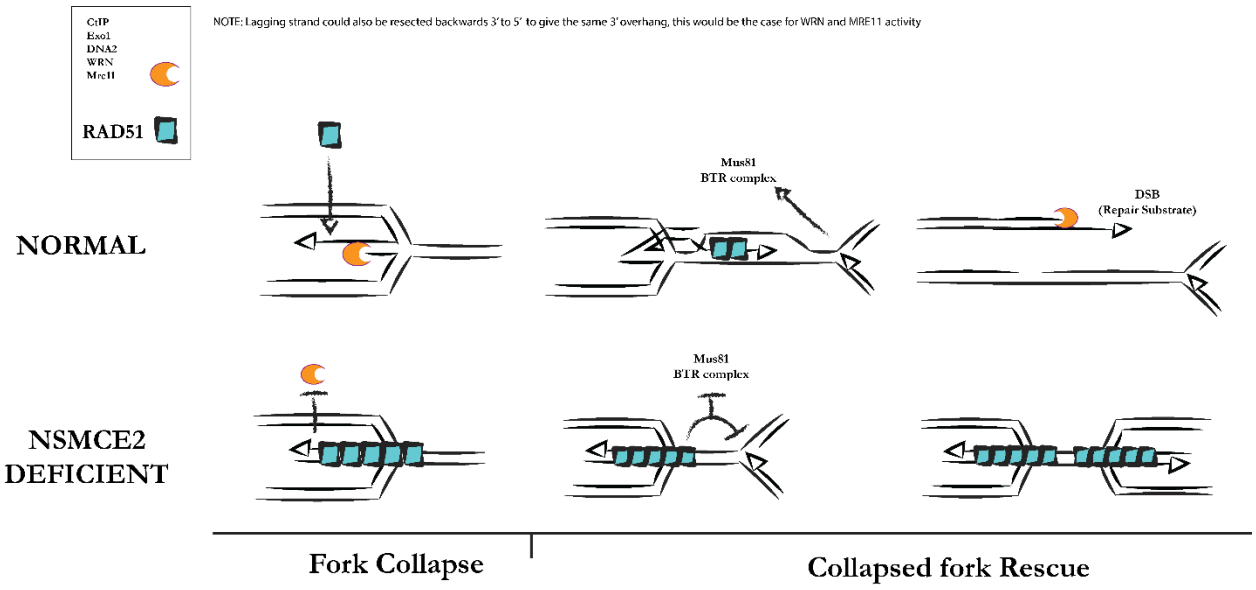
CtIP
Exo1
DNA2
WRN
Mre11
RAD51
NOTE: Lagging strand could also be resected backwards 3' to 5' to give the same 3' overhang, this would be the case for WRN and MRE11 activity
NORMAL
Mus81
BTR complex
DSB
(Repair Substrate)
NSMCE2
DEFICIENT
Mus81
BTR complex
Fork Collapse
Collapsed fork Rescue

Figure 4-3 Model for defective resection in NSMCE2-deficient cells. Normally at replication associated DSBs, CtIP promotes resection by MRE11. This process is then continued by Exo1 or DNA2 which performs extensive resection. The resulting 3' overhangs are essential to promote the HR repair process. This resection process is also dependent on BLM helicase, which unwinds DNA at the DSB prior to resection. At the replication fork, reversed fork resection at the 5' end of the exposed single-ended DSB is dependent on freeing the 5' end by helicase activity. This mediates the exposure of a 3' sequence which is then resected and can invade ahead of the replicating DNA at a homologous sequence (top middle). Upon fork rescue, the BTR complex could unwind the d-loop formed after the initial resection even which would produce the ideal substrate for MUS81 cleavage and DSB production (top right). This newly formed DSB would result in an additional process of resection prior to merging with the incoming replication fork. In NSMCE2 cells, because the hyper-stable fork is bound by RAD51, the initial resection event would be blocked, and therefore all subsequent resection events would also be prevented, leading to repair failure and under replication (bottom). This model does not take into account the potential for resection behind the collapsed fork to be defective in NSMCE2 cells. It is also possible that double HJ structures which result from post replicative gaps are not resected properly or resolved, most likely due to the lack of recruitment of BLM helicase, which is required for this process. Defects in resection behind the replication fork could also lead to unresolved DNA and damage in mitosis. At this time it is not possible to differentiate between resection at or behind the replication fork in human cells.

A

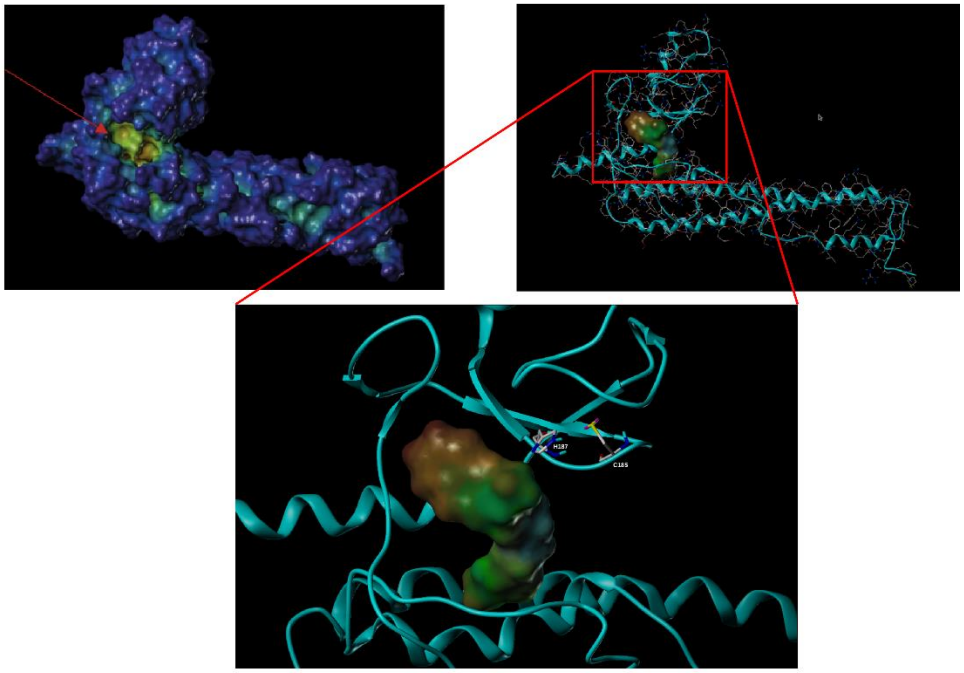

B

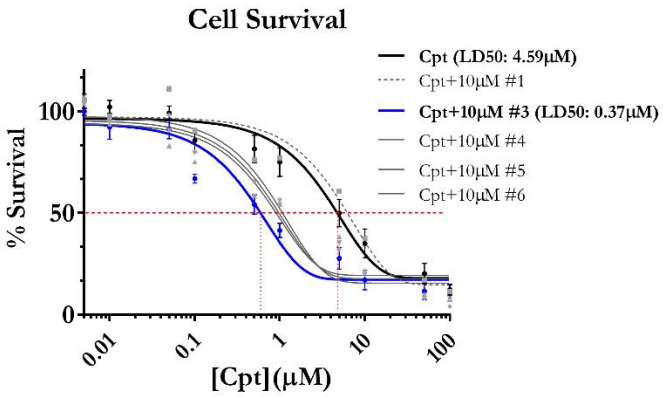
Cell Survival
Cpt (LD50: 4.59μM)
Cpt+10μM #1
Cpt+10μM #3 (LD50: 0.37μM)
Cpt+10μM #4
Cpt+10μM #5
Cpt+10μM #6
% Survival
100
50
0
0.01
0.1
1
10
100
[Cpt](μM)

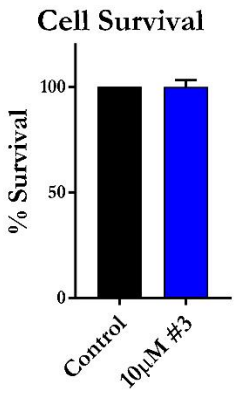
Cell Survival
% Survival
100
50
0
Control
10μM #3

C

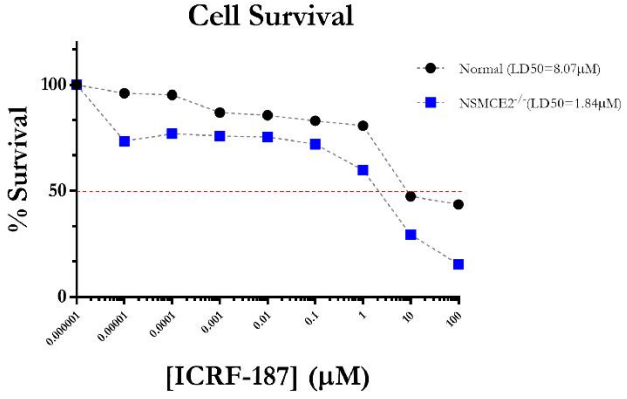
Cell Survival
Normal (LD50=8.07μM)
NSMCE2-/- (LD50=1.84μM)
% Survival
100
50
0
0.000001
0.00001
0.0001
0.001
0.01
0.1
1
10
100
[ICRF-187] (μM)

Figure 5-1. A. Left-3D surface filling model of human NSMCE2 generated by threading the human amino acid sequence into the yeast crystal structure. The yellow pocket shown using the red arrow was fitted pharmacophores using SYBYL software. Right and bottom inset- The pocket corresponds to the zinc binding domain, which is in close proximity with the SP-RING active site containing cysteine at residue 215 and histidine 187. Both of these sites have been shown previously to prevent NSMCE2 SUMO ligase activity when mutated. **B**. Left-Graph of cell viability by MTT assay. U2OS cells were treated with a concentration gradient of CPT for 72 hours in the presence of a fixed amount of each compound tested [10 μM] 24 hours prior to and during CPT treatment. Data were normalized to untreated control. Compounds 3, 4, 5, and 6 synergize with CPT. Compound 1 is an example of results from the remaining 8 compounds tested, where no combinatorial effect was observed. Right-Compound 3 has no effect on cell viability after treatment for 96 hours. **C.** Graph of cell viability by MTT assay. Normal or NSMCE2-null HEK293T cells were treated with the topoisomerase 2α inhibitor ICRF-187. To account for the 2-fold increase in doubling time, normal cells were treated for 48 hours and NSMCE2 cells were treated for 96 hours. Sensitization was observed in NSMCE2-null cells. LD50 calculations were done using an online LD50 calculator at http://www.ic50.tk.

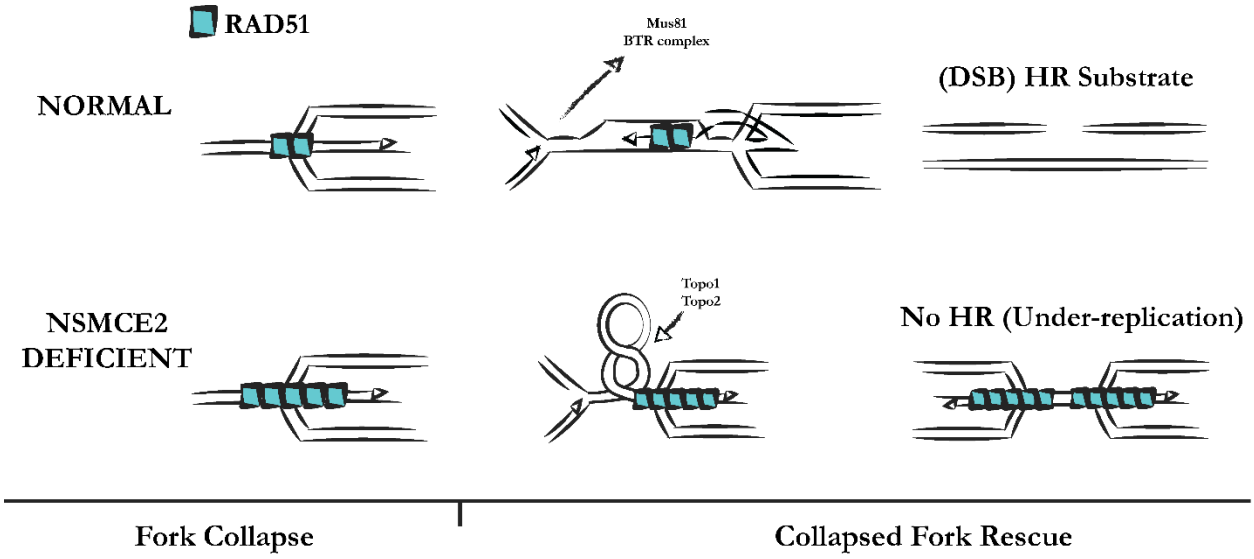
RAD51
NORMAL
Mus81
BTR complex
(DSB) HR Substrate
NSMCE2
DEFICIENT
Topo1
Topo2
No HR (Under-replication)
Fork Collapse
Collapsed Fork Rescue

Figure 5-2 Model for the increase in sensitivity of NSMCE2-deficient cells to Topoisomerase poisons. Normal cells are able to rescue collapsed forks by induction of a double strand break in order to prepare for DSB repair by HR (upper pathway). The hyper stable collapsed fork which is bound by unproductive RAD51 in NSMCE2-deficient cells (bottom left) could lead to the inability to relax DNA as incoming replication forks attempt rescue. Because Topo 1 is known to relax supercoils in front of replication forks and because Topo2α can unwind catenated DS-DNA, this would result in an increased reliance on topoisomerase proteins in NSMCE2-deficient cells. In the case of CPT, the increased sensitivity is likely due to most rescuing forks failing due to DSB induced by runoff when the replication fork encounter nicked DNA.

References

1. Aggarwal, M., Sommers, J.A., Morris, C., and Brosh, R.M., Jr. (2010). Delineation of WRN helicase function with EXO1 in the replicational stress response. DNA repair *9*, 765-776.

2. Ampatzidou, E., Irmisch, A., O'Connell, M.J., and Murray, J.M. (2006). Smc5/6 is required for repair at collapsed replication forks. Mol Cell Biol *26*, 9387-9401.

3. Andor, N., Maley, C.C., and Ji, H.P. (2017). Genomic Instability in Cancer: Teetering on the Limit of Tolerance. Cancer Res *77*, 2179-2185.

4. Ashour, M.E., Atteya, R., and El-Khamisy, S.F. (2015). Topoisomerase-mediated chromosomal break repair: an emerging player in many games. Nat Rev Cancer *15*, 137-151.

5. Baxter, J., and Diffley, J.F. (2008). Topoisomerase II inactivation prevents the completion of DNA replication in budding yeast. Mol Cell *30*, 790-802.

6. Ben-David, U., Beroukhim, R., and Golub, T.R. (2019). Genomic evolution of cancer models: perils and opportunities. Nat Rev Cancer *19*, 97-109.

7. Bennett, C.B., Lewis, A.L., Baldwin, K.K., and Resnick, M.A. (1993). Lethality induced by a single site-specific double-strand break in a dispensable yeast plasmid. Proc Natl Acad Sci U S A *90*, 5613-5617.

8. Benson, F.E., Stasiak, A., and West, S.C. (1994). Purification and characterization of the human Rad51 protein, an analogue of E. coli RecA. EMBO J *13*, 5764-5771.

9. Beresten, S.F., Stan, R., van Brabant, A.J., Ye, T., Naureckiene, S., and Ellis, N.A. (1999). Purification of overexpressed hexahistidine-tagged BLM N431 as oligomeric complexes. Protein Expr Purif *17*, 239-248.

10. Bermudez-Lopez, M., and Aragon, L. (2016). Smc5/6 complex regulates Sgs1 recombination functions. Curr Genet.

11. Bermudez-Lopez, M., Villoria, M.T., Esteras, M., Jarmuz, A., Torres-Rosell, J., Clemente-Blanco, A., and Aragon, L. (2016). Sgs1's roles in DNA end resection, HJ dissolution, and crossover suppression require a two-step SUMO regulation dependent on Smc5/6. Genes Dev *30*, 1339-1356.

12. Blocher, D. (1988). DNA double-strand break repair determines the RBE of alpha-particles. Int J Radiat Biol *54*, 761-771.

13. Boddy, M.N., Gaillard, P.H., McDonald, W.H., Shanahan, P., Yates, J.R., 3rd, and Russell, P. (2001). Mus81-Eme1 are essential components of a Holliday junction resolvase. Cell *107*, 537-548.

14. Bohren, K.M., Nadkarni, V., Song, J.H., Gabbay, K.H., and Owerbach, D. (2004). A M55V polymorphism in a novel SUMO gene (SUMO-4) differentially activates heat shock transcription factors and is associated with susceptibility to type I diabetes mellitus. J Biol Chem *279*, 27233-27238.

15. Bonner, J.N., Choi, K., Xue, X., Torres, N.P., Szakal, B., Wei, L., Wan, B., Arter, M., Matos, J., Sung, P.*, et al.* (2016a). Smc5/6 Mediated Sumoylation of the Sgs1-Top3-Rmi1 Complex Promotes Removal of Recombination Intermediates. Cell reports *16*, 368-378.

16. Bonner, J.N., Choi, K., Xue, X., Torres, N.P., Szakal, B., Wei, L., Wan, B., Arter, M., Matos, J., Sung, P.*, et al.* (2016b). Smc5/6 Mediated Sumoylation of the Sgs1-Top3-Rmi1 Complex Promotes Removal of Recombination Intermediates. Cell reports *16*, 368-378.

17. Bonner, W.M., Redon, C.E., Dickey, J.S., Nakamura, A.J., Sedelnikova, O.A., Solier, S., and Pommier, Y. (2008). GammaH2AX and cancer. Nat Rev Cancer *8*, 957-967.

18. Branzei, D., Sollier, J., Liberi, G., Zhao, X., Maeda, D., Seki, M., Enomoto, T., Ohta, K., and Foiani, M. (2006). Ubc9- and mms21-mediated sumoylation counteracts recombinogenic events at damaged replication forks. Cell *127*, 509-522.

19. Bugreev, D.V., Mazina, O.M., and Mazin, A.V. (2009). Bloom syndrome helicase stimulates RAD51 DNA strand exchange activity through a novel mechanism. J Biol Chem *284*, 26349-26359.

20. Bugreev, D.V., Yu, X., Egelman, E.H., and Mazin, A.V. (2007). Novel pro- and anti-recombination activities of the Bloom's syndrome helicase. Genes Dev *21*, 3085-3094.

21. Bunting, S.F., Callen, E., Wong, N., Chen, H.T., Polato, F., Gunn, A., Bothmer, A., Feldhahn, N., Fernandez-Capetillo, O., Cao, L.*, et al.* (2010). 53BP1 inhibits homologous recombination in Brca1-deficient cells by blocking resection of DNA breaks. Cell *141*, 243-254.

22. Byun, T.S., Pacek, M., Yee, M.C., Walter, J.C., and Cimprich, K.A. (2005). Functional uncoupling of MCM helicase and DNA polymerase activities activates the ATR-dependent checkpoint. Genes Dev *19*, 1040-1052.

23. Calderon, I.L., Contopoulou, C.R., and Mortimer, R.K. (1983). Isolation and characterization of yeast DNA repair genes : II. Isolation of plasmids that complement the mutations rad50-1, rad51-1, rad54-3, and rad55-3. Curr Genet *7*, 93-100.

24. Carlborg, K.K., Kanno, T., Carter, S.D., and Sjogren, C. (2015). Mec1-dependent phosphorylation of Mms21 modulates its SUMO ligase activity. DNA repair *28*, 83-92.

25. Carreira, A., Hilario, J., Amitani, I., Baskin, R.J., Shivji, M.K., Venkitaraman, A.R., and Kowalczykowski, S.C. (2009). The BRC repeats of BRCA2 modulate the DNA-binding selectivity of RAD51. Cell *136*, 1032-1043.

26. Chaganti, R.S., Schonberg, S., and German, J. (1974). A manyfold increase in sister chromatid exchanges in Bloom's syndrome lymphocytes. Proc Natl Acad Sci U S A *71*, 4508-4512.

27. Chan, K.L., Palmai-Pallag, T., Ying, S., and Hickson, I.D. (2009). Replication stress induces sister-chromatid bridging at fragile site loci in mitosis. Nat Cell Biol *11*, 753-760.

28. Chen, Z., Yang, H., and Pavletich, N.P. (2008). Mechanism of homologous recombination from the RecA-ssDNA/dsDNA structures. Nature *453*, 489-484.

29. Copsey, A., Tang, S., Jordan, P.W., Blitzblau, H.G., Newcombe, S., Chan, A.C., Newnham, L., Li, Z., Gray, S., Herbert, A.D.*, et al.* (2013). Smc5/6 coordinates formation

and resolution of joint molecules with chromosome morphology to ensure meiotic divisions. PLoS genetics *9*, e1004071.

30. Cotta-Ramusino, C., Fachinetti, D., Lucca, C., Doksani, Y., Lopes, M., Sogo, J., and Foiani, M. (2005). Exo1 processes stalled replication forks and counteracts fork reversal in checkpoint-defective cells. Mol Cell *17*, 153-159.

31. Cunniff, C., Bassetti, J.A., and Ellis, N.A. (2017). Bloom's Syndrome: Clinical Spectrum, Molecular Pathogenesis, and Cancer Predisposition. Mol Syndromol *8*, 4-23.

32. Davies, S.L., North, P.S., and Hickson, I.D. (2007). Role for BLM in replication-fork restart and suppression of origin firing after replicative stress. Nat Struct Mol Biol *14*, 677-679.

33. De Piccoli, G., Cortes-Ledesma, F., Ira, G., Torres-Rosell, J., Uhle, S., Farmer, S., Hwang, J.Y., Machin, F., Ceschia, A., McAleenan, A.*, et al.* (2006). Smc5-Smc6 mediate DNA double-strand-break repair by promoting sister-chromatid recombination. Nat Cell Biol *8*, 1032-1034.

34. de Renty, C., and Ellis, N.A. (2017). Bloom's syndrome: Why not premature aging?: A comparison of the BLM and WRN helicases. Ageing research reviews *33*, 36-51.

35. Dehe, P.M., and Gaillard, P.H. (2017). Control of structure-specific endonucleases to maintain genome stability. Nat Rev Mol Cell Biol *18*, 315-330.

36. Delgado, J.L., Hsieh, C.M., Chan, N.L., and Hiasa, H. (2018). Topoisomerases as anticancer targets. Biochem J *475*, 373-398.

37. Dewar, J.M., Budzowska, M., and Walter, J.C. (2015). The mechanism of DNA replication termination in vertebrates. Nature *525*, 345-350.

38. Dimitrova, D.S., and Gilbert, D.M. (2000). Stability and nuclear distribution of mammalian replication protein A heterotrimeric complex. Exp Cell Res *254*, 321-327.

39. Duan, X., Sarangi, P., Liu, X., Rangi, G.K., Zhao, X., and Ye, H. (2009). Structural and functional insights into the roles of the Mms21 subunit of the Smc5/6 complex. Mol Cell *35*, 657-668.

40. Duda, H., Arter, M., Gloggnitzer, J., Teloni, F., Wild, P., Blanco, M.G., Altmeyer, M., and Matos, J. (2016). A Mechanism for Controlled Breakage of Under-replicated Chromosomes during Mitosis. Dev Cell *39*, 740-755.

41. Dungrawala, H., Bhat, K.P., Le Meur, R., Chazin, W.J., Ding, X., Sharan, S.K., Wessel, S.R., Sathe, A.A., Zhao, R., and Cortez, D. (2017). RADX Promotes Genome Stability and Modulates Chemosensitivity by Regulating RAD51 at Replication Forks. Mol Cell *67*, 374-386.e375.

42. Dungrawala, H., Rose, K.L., Bhat, K.P., Mohni, K.N., Glick, G.G., Couch, F.B., and Cortez, D. (2015). The Replication Checkpoint Prevents Two Types of Fork Collapse without Regulating Replisome Stability. Mol Cell *59*, 998-1010.

43. Eladad, S., Ye, T.Z., Hu, P., Leversha, M., Beresten, S., Matunis, M.J., and Ellis, N.A. (2005). Intra-nuclear trafficking of the BLM helicase to DNA damage-induced foci is regulated by SUMO modification. Hum Mol Genet *14*, 1351-1365.

44. Elia, M.C., DeLuca, J.G., and Bradley, M.O. (1991). Significance and measurement of DNA double strand breaks in mammalian cells. Pharmacol Ther *51*, 291-327.

45. Escribano-Diaz, C., Orthwein, A., Fradet-Turcotte, A., Xing, M., Young, J.T., Tkac, J., Cook, M.A., Rosebrock, A.P., Munro, M., Canny, M.D.*, et al.* (2013). A cell cycle-dependent regulatory circuit composed of 53BP1-RIF1 and BRCA1-CtIP controls DNA repair pathway choice. Mol Cell *49*, 872-883.

46. Fachinetti, D., Bermejo, R., Cocito, A., Minardi, S., Katou, Y., Kanoh, Y., Shirahige, K., Azvolinsky, A., Zakian, V.A., and Foiani, M. (2010). Replication termination at eukaryotic chromosomes is mediated by Top2 and occurs at genomic loci containing pausing elements. Mol Cell *39*, 595-605.

47. Fernandez-Capetillo, O. (2016). The (elusive) role of the SMC5/6 complex. Cell Cycle, 0.

48. Forget, A.L., Loftus, M.S., McGrew, D.A., Bennett, B.T., and Knight, K.L. (2007). The human Rad51 K133A mutant is functional for DNA double-strand break repair in human cells. Biochemistry *46*, 3566-3575.

49. Froget, B., Blaisonneau, J., Lambert, S., and Baldacci, G. (2008). Cleavage of stalled forks by fission yeast Mus81/Eme1 in absence of DNA replication checkpoint. Mol Biol Cell *19*, 445-456.

50. Fugger, K., Chu, W.K., Haahr, P., Kousholt, A.N., Beck, H., Payne, M.J., Hanada, K., Hickson, I.D., and Sorensen, C.S. (2013). FBH1 co-operates with MUS81 in inducing DNA double-strand breaks and cell death following replication stress. Nat Commun *4*, 1423.

51. Gachechiladze, M., Skarda, J., Soltermann, A., and Joerger, M. (2017). RAD51 as a potential surrogate marker for DNA repair capacity in solid malignancies. Int J Cancer.

52. Gaillard, H., Garcia-Muse, T., and Aguilera, A. (2015). Replication stress and cancer. Nat Rev Cancer *15*, 276-289.

53. German, J. (1995). Bloom's syndrome. Dermatol Clin *13*, 7-18.

54. Glover, T.W., Wilson, T.E., and Arlt, M.F. (2017). Fragile sites in cancer: more than meets the eye. Nat Rev Cancer *17*, 489-501.

55. Godin, S.K., Sullivan, M.R., and Bernstein, K.A. (2016). Novel insights into RAD51 activity and regulation during homologous recombination and DNA replication. Biochem Cell Biol *94*, 407-418.

56. Gravel, S., Chapman, J.R., Magill, C., and Jackson, S.P. (2008). DNA helicases Sgs1 and BLM promote DNA double-strand break resection. Genes Dev *22*, 2767-2772.

57. Haas, K.T., Lee, M., Esposito, A., and Venkitaraman, A.R. (2018). Single-molecule localization microscopy reveals molecular transactions during RAD51 filament assembly at cellular DNA damage sites. Nucleic Acids Res *46*, 2398-2416.

58. Hanada, K., Budzowska, M., Davies, S.L., van Drunen, E., Onizawa, H., Beverloo, H.B., Maas, A., Essers, J., Hickson, I.D., and Kanaar, R. (2007). The structure-specific endonuclease Mus81 contributes to replication restart by generating double-strand DNA breaks. Nat Struct Mol Biol *14*, 1096-1104.

59. Hand, R., and German, J. (1975). A retarded rate of DNA chain growth in Bloom's syndrome. Proc Natl Acad Sci U S A *72*, 758-762.

60. Hashimoto, Y., Puddu, F., and Costanzo, V. (2011). RAD51- and MRE11-dependent reassembly of uncoupled CMG helicase complex at collapsed replication forks. Nat Struct Mol Biol *19*, 17-24.

61. Hashimoto, Y., Ray Chaudhuri, A., Lopes, M., and Costanzo, V. (2010). Rad51 protects nascent DNA from Mre11-dependent degradation and promotes continuous DNA synthesis. Nat Struct Mol Biol *17*, 1305-1311.

62. Hendriks, I.A., Lyon, D., Young, C., Jensen, L.J., Vertegaal, A.C., and Nielsen, M.L. (2017). Site-specific mapping of the human SUMO proteome reveals co-modification with phosphorylation. Nat Struct Mol Biol *24*, 325-336.

63. Hendriks, I.A., and Vertegaal, A.C. (2016). A comprehensive compilation of SUMO proteomics. Nat Rev Mol Cell Biol *17*, 581-595.

64. Higgins, N.P., Kato, K., and Strauss, B. (1976). A model for replication repair in mammalian cells. J Mol Biol *101*, 417-425.

65. Higgs, M.R., Reynolds, J.J., Winczura, A., Blackford, A.N., Borel, V., Miller, E.S., Zlatanou, A., Nieminuszczy, J., Ryan, E.L., Davies, N.J.*, et al.* (2015). BOD1L Is Required to Suppress Deleterious Resection of Stressed Replication Forks. Mol Cell *59*, 462-477.

66. Hilario, J., Amitani, I., Baskin, R.J., and Kowalczykowski, S.C. (2009). Direct imaging of human Rad51 nucleoprotein dynamics on individual DNA molecules. Proc Natl Acad Sci U S A *106*, 361-368.

67. Holliday, R. (2007). A mechanism for gene conversion in fungi. Genet Res *89*, 285-307.

68. Hsiang, Y.H., Hertzberg, R., Hecht, S., and Liu, L.F. (1985). Camptothecin induces protein-linked DNA breaks via mammalian DNA topoisomerase I. J Biol Chem *260*, 14873-14878.

69. Huang, F., and Mazin, A.V. (2014). A small molecule inhibitor of human RAD51 potentiates breast cancer cell killing by therapeutic agents in mouse xenografts. PLoS One *9*, e100993.

70. Huang, F., Motlekar, N.A., Burgwin, C.M., Napper, A.D., Diamond, S.L., and Mazin, A.V. (2011). Identification of specific inhibitors of human RAD51 recombinase using high-throughput screening. ACS Chem Biol *6*, 628-635.

71. Inano, S., Sato, K., Katsuki, Y., Kobayashi, W., Tanaka, H., Nakajima, K., Nakada, S., Miyoshi, H., Knies, K., Takaori-Kondo, A.*, et al.* (2017). RFWD3-Mediated Ubiquitination Promotes Timely Removal of Both RPA and RAD51 from DNA Damage Sites to Facilitate Homologous Recombination. Mol Cell *66*, 622-634.e628.

72. Ira, G., and Haber, J.E. (2002). Characterization of RAD51-independent break-induced replication that acts preferentially with short homologous sequences. Mol Cell Biol *22*, 6384-6392.

73. Irwin, J.J., Sterling, T., Mysinger, M.M., Bolstad, E.S., and Coleman, R.G. (2012). ZINC: a free tool to discover chemistry for biology. J Chem Inf Model *52*, 1757-1768.

74. Jacome, A., Gutierrez-Martinez, P., Schiavoni, F., Tenaglia, E., Martinez, P., Rodriguez-Acebes, S., Lecona, E., Murga, M., Mendez, J., Blasco, M.A.*, et al.* (2015). NSMCE2 suppresses cancer and aging in mice independently of its SUMO ligase activity. EMBO J *34*, 2604-2619.

75. Jeggo, P.A., Pearl, L.H., and Carr, A.M. (2016). DNA repair, genome stability and cancer: a historical perspective. Nat Rev Cancer *16*, 35-42.

76. Kawashima, Y., Yamaguchi, N., Teshima, R., Narahara, H., Yamaoka, Y., Anai, H., Nishida, Y., and Hanada, K. (2017). Detection of DNA double-strand breaks by pulsed-field gel electrophoresis. Genes Cells *22*, 84-93.

77. Keskin, H., Shen, Y., Huang, F., Patel, M., Yang, T., Ashley, K., Mazin, A.V., and Storici, F. (2014). Transcript-RNA-templated DNA recombination and repair. Nature *515*, 436-439.

78. Keskin, H., and Storici, F. (2018). An Approach to Detect and Study DNA Double-Strand Break Repair by Transcript RNA Using a Spliced-Antisense RNA Template. Methods Enzymol *601*, 59-70.

79. Khan, Q.A., Kohlhagen, G., Marshall, R., Austin, C.A., Kalena, G.P., Kroth, H., Sayer, J.M., Jerina, D.M., and Pommier, Y. (2003). Position-specific trapping of topoisomerase II by benzo[a]pyrene diol epoxide adducts: implications for interactions with intercalating anticancer agents. Proc Natl Acad Sci U S A *100*, 12498-12503.

80. Kitao, H., Iimori, M., Kataoka, Y., Wakasa, T., Tokunaga, E., Saeki, H., Oki, E., and Maehara, Y. (2018). DNA replication stress and cancer chemotherapy. Cancer Sci *109*, 264-271.

81. Kliszczak, M., Stephan, A.K., Flanagan, A.M., and Morrison, C.G. (2012). SUMO ligase activity of vertebrate Mms21/Nse2 is required for efficient DNA repair but not for Smc5/6 complex stability. DNA repair *11*, 799-810.

82. Lambert, S., Mizuno, K., Blaisonneau, J., Martineau, S., Chanet, R., Freon, K., Murray, J.M., Carr, A.M., and Baldacci, G. (2010). Homologous recombination restarts blocked replication forks at the expense of genome rearrangements by template exchange. Mol Cell *39*, 346-359.

83. Lebel, M., and Monnat, R.J., Jr. (2018). Werner syndrome (WRN) gene variants and their association with altered function and age-associated diseases. Ageing research reviews *41*, 82-97.

84. Lemacon, D., Jackson, J., Quinet, A., Brickner, J.R., Li, S., Yazinski, S., You, Z., Ira, G., Zou, L., Mosammaparast, N.*, et al.* (2017). MRE11 and EXO1 nucleases degrade reversed forks and elicit MUS81-dependent fork rescue in BRCA2-deficient cells. Nat Commun *8*, 860.

85. Leung, J.W., Ghosal, G., Wang, W., Shen, X., Wang, J., Li, L., and Chen, J. (2013). Alpha thalassemia/mental retardation syndrome X-linked gene product ATRX is required for proper replication restart and cellular resistance to replication stress. J Biol Chem *288*, 6342-6350.

86. Liang, J., Li, B.Z., Tan, A.P., Kolodner, R.D., Putnam, C.D., and Zhou, H. (2018). SUMO E3 ligase Mms21 prevents spontaneous DNA damage induced genome rearrangements. PLoS genetics *14*, e1007250.

87. Liang, Y.C., Lee, C.C., Yao, Y.L., Lai, C.C., Schmitz, M.L., and Yang, W.M. (2016). SUMO5, a Novel Poly-SUMO Isoform, Regulates PML Nuclear Bodies. Sci Rep *6*, 26509.

88. Liberi, G., Maffioletti, G., Lucca, C., Chiolo, I., Baryshnikova, A., Cotta-Ramusino, C., Lopes, M., Pellicioli, A., Haber, J.E., and Foiani, M. (2005). Rad51-dependent DNA structures accumulate at damaged replication forks in sgs1 mutants defective in the yeast ortholog of BLM RecQ helicase. Genes Dev *19*, 339-350.

89. Liu, Y., Nielsen, C.F., Yao, Q., and Hickson, I.D. (2014). The origins and processing of ultra fine anaphase DNA bridges. Curr Opin Genet Dev *26*, 1-5.

90. Lucas, I., Germe, T., Chevrier-Miller, M., and Hyrien, O. (2001). Topoisomerase II can unlink replicating DNA by precatenane removal. EMBO J *20*, 6509-6519.

91. Lynch, H.T., Snyder, C.L., Shaw, T.G., Heinen, C.D., and Hitchins, M.P. (2015). Milestones of Lynch syndrome: 1895-2015. Nat Rev Cancer *15*, 181-194.

92. Lyu, Y.L., Kerrigan, J.E., Lin, C.P., Azarova, A.M., Tsai, Y.C., Ban, Y., and Liu, L.F. (2007). Topoisomerase IIbeta mediated DNA double-strand breaks: implications in doxorubicin cardiotoxicity and prevention by dexrazoxane. Cancer Res *67*, 8839-8846.

93. Ma, C.J., Gibb, B., Kwon, Y., Sung, P., and Greene, E.C. (2017). Protein dynamics of human RPA and RAD51 on ssDNA during assembly and disassembly of the RAD51 filament. Nucleic Acids Res *45*, 749-761.

94. Mayle, R., Campbell, I.M., Beck, C.R., Yu, Y., Wilson, M., Shaw, C.A., Bjergbaek, L., Lupski, J.R., and Ira, G. (2015). DNA REPAIR. Mus81 and converging forks limit the mutagenicity of replication fork breakage. Science *349*, 742-747.

95. McEntee, K., Weinstock, G.M., and Lehman, I.R. (1979). Initiation of general recombination catalyzed in vitro by the recA protein of Escherichia coli. Proc Natl Acad Sci U S A *76*, 2615-2619.

96. Mendez, J., and Stillman, B. (2000). Chromatin association of human origin recognition complex, cdc6, and minichromosome maintenance proteins during the cell cycle: assembly of prereplication complexes in late mitosis. Mol Cell Biol *20*, 8602-8612.

97. Menolfi, D., Delamarre, A., Lengronne, A., Pasero, P., and Branzei, D. (2015). Essential Roles of the Smc5/6 Complex in Replication through Natural Pausing Sites and Endogenous DNA Damage Tolerance. Mol Cell *60*, 835-846.

98. Michelini, F., Pitchiaya, S., Vitelli, V., Sharma, S., Gioia, U., Pessina, F., Cabrini, M., Wang, Y., Capozzo, I., Iannelli, F.*, et al.* (2017). Damage-induced lncRNAs control the DNA damage response through interaction with DDRNAs at individual double-strand breaks. Nat Cell Biol *19*, 1400-1411.

99. Mijic, S., Zellweger, R., Chappidi, N., Berti, M., Jacobs, K., Mutreja, K., Ursich, S., Ray Chaudhuri, A., Nussenzweig, A., Janscak, P.*, et al.* (2017). Replication fork reversal triggers fork degradation in BRCA2-defective cells. Nat Commun *8*, 859.

100. Minocha, A., and Long, B.H. (1984). Inhibition of the DNA catenation activity of type II topoisomerase by VP16-213 and VM26. Biochem Biophys Res Commun *122*, 165-170.

101. Mizuno, K., Lambert, S., Baldacci, G., Murray, J.M., and Carr, A.M. (2009). Nearby inverted repeats fuse to generate acentric and dicentric palindromic chromosomes by a replication template exchange mechanism. Genes Dev *23*, 2876-2886.

102. Mohebi, S., Mizuno, K., Watson, A., Carr, A.M., and Murray, J.M. (2015). Checkpoints are blind to replication restart and recombination intermediates that result in gross chromosomal rearrangements. Nat Commun *6*, 6357.

103. Moreno, A., Carrington, J.T., Albergante, L., Al Mamun, M., Haagensen, E.J., Komseli, E.S., Gorgoulis, V.G., Newman, T.J., and Blow, J.J. (2016). Unreplicated DNA remaining from unperturbed S phases passes through mitosis for resolution in daughter cells. Proc Natl Acad Sci U S A *113*, E5757-5764.

104. Mosmann, T. (1983). Rapid colorimetric assay for cellular growth and survival: application to proliferation and cytotoxicity assays. J Immunol Methods *65*, 55-63.

105. Murai, J., Huang, S.Y., Das, B.B., Renaud, A., Zhang, Y., Doroshow, J.H., Ji, J., Takeda, S., and Pommier, Y. (2012). Trapping of PARP1 and PARP2 by Clinical PARP Inhibitors. Cancer Res *72*, 5588-5599.

106. Naim, V., and Rosselli, F. (2009). The FANC pathway and BLM collaborate during mitosis to prevent micro-nucleation and chromosome abnormalities. Nat Cell Biol *11*, 761-768.

107. Natale, V., and Raquer, H. (2017). Xeroderma pigmentosum-Cockayne syndrome complex. Orphanet J Rare Dis *12*, 65.

108. Nepal, M., Che, R., Zhang, J., Ma, C., and Fei, P. (2017). Fanconi Anemia Signaling and Cancer. Trends in cancer *3*, 840-856.

109. Nitiss, J.L. (2009). Targeting DNA topoisomerase II in cancer chemotherapy. Nat Rev Cancer *9*, 338-350.

110. O'Connor, M.J. (2015). Targeting the DNA Damage Response in Cancer. Mol Cell *60*, 547-560.

111. Ogawa, T., Yu, X., Shinohara, A., and Egelman, E.H. (1993). Similarity of the yeast RAD51 filament to the bacterial RecA filament. Science *259*, 1896-1899.

112. Olive, P.L., and Banath, J.P. (2006). The comet assay: a method to measure DNA damage in individual cells. Nat Protoc *1*, 23-29.

113. Ouyang, K.J., Woo, L.L., Zhu, J., Huo, D., Matunis, M.J., and Ellis, N.A. (2009). SUMO modification regulates BLM and RAD51 interaction at damaged replication forks. PLoS Biol *7*, e1000252.

114. Parplys, A.C., Seelbach, J.I., Becker, S., Behr, M., Jend, C., Mansour, W.Y., Joosse, S., Stuerzbecher, H.W., Pospiech, H., Petersen, C.*, et al.* (2015a). High levels of RAD51 perturb DNA replication elongation and cause unscheduled origin firing due to impaired CHK1 activation. Cell Cycle, 0.

115. Parplys, A.C., Seelbach, J.I., Becker, S., Behr, M., Wrona, A., Jend, C., Mansour, W.Y., Joosse, S.A., Stuerzbecher, H.W., Pospiech, H.*, et al.* (2015b). High levels of RAD51 perturb DNA replication elongation and cause unscheduled origin firing due to impaired CHK1 activation. Cell Cycle *14*, 3190-3202.

116. Payne, F., Colnaghi, R., Rocha, N., Seth, A., Harris, J., Carpenter, G., Bottomley, W.E., Wheeler, E., Wong, S., Saudek, V.*, et al.* (2014). Hypomorphism in human NSMCE2 linked to primordial dwarfism and insulin resistance. J Clin Invest *124*, 4028-4038.

117. Pepe, A., and West, S.C. (2014). Substrate specificity of the MUS81-EME2 structure selective endonuclease. Nucleic Acids Res *42*, 3833-3845.

118. Petermann, E., Orta, M.L., Issaeva, N., Schultz, N., and Helleday, T. (2010). Hydroxyurea-stalled replication forks become progressively inactivated and require two different RAD51-mediated pathways for restart and repair. Mol Cell *37*, 492-502.

119. Pichler, A., Knipscheer, P., Oberhofer, E., van Dijk, W.J., Korner, R., Olsen, J.V., Jentsch, S., Melchior, F., and Sixma, T.K. (2005). SUMO modification of the ubiquitin-conjugating enzyme E2-25K. Nat Struct Mol Biol *12*, 264-269.

120. Pommier, Y., Sun, Y., Huang, S.N., and Nitiss, J.L. (2016). Roles of eukaryotic topoisomerases in transcription, replication and genomic stability. Nat Rev Mol Cell Biol *17*, 703-721.

121. Pond, K.W., de Renty, C., Yagle, M.K., and Ellis, N.A. (2019). Rescue of collapsed replication forks is dependent on NSMCE2 to prevent mitotic DNA damage. PLoS genetics *15*, e1007942.

122. Potts, P.R. (2009). The Yin and Yang of the MMS21-SMC5/6 SUMO ligase complex in homologous recombination. DNA repair *8*, 499-506.

123. Potts, P.R., Porteus, M.H., and Yu, H. (2006). Human SMC5/6 complex promotes sister chromatid homologous recombination by recruiting the SMC1/3 cohesin complex to double-strand breaks. EMBO J *25*, 3377-3388.

124. Potts, P.R., and Yu, H. (2005). Human MMS21/NSE2 is a SUMO ligase required for DNA repair. Mol Cell Biol *25*, 7021-7032.

125. Potts, P.R., and Yu, H. (2007). The SMC5/6 complex maintains telomere length in ALT cancer cells through SUMOylation of telomere-binding proteins. Nat Struct Mol Biol *14*, 581-590.

126. Pourquier, P., Waltman, J.L., Urasaki, Y., Loktionova, N.A., Pegg, A.E., Nitiss, J.L., and Pommier, Y. (2001). Topoisomerase I-mediated cytotoxicity of N-methyl-N'-nitro-N-nitrosoguanidine: trapping of topoisomerase I by the O6-methylguanine. Cancer Res *61*, 53-58.

127. Quinet, A., and Vindigni, A. (2018). Superfast DNA replication causes damage in cancer cells. Nature *559*, 186-187.

128. Reverter, D., and Lima, C.D. (2005). Insights into E3 ligase activity revealed by a SUMO-RanGAP1-Ubc9-Nup358 complex. Nature *435*, 687-692.

129. Rodriguez, M.S., Dargemont, C., and Hay, R.T. (2001). SUMO-1 conjugation in vivo requires both a consensus modification motif and nuclear targeting. J Biol Chem *276*, 12654-12659.

130. Rothblum-Oviatt, C., Wright, J., Lefton-Greif, M.A., McGrath-Morrow, S.A., Crawford, T.O., and Lederman, H.M. (2016). Ataxia telangiectasia: a review. Orphanet J Rare Dis *11*, 159.

131. Ryan, A.J., Squires, S., Strutt, H.L., and Johnson, R.T. (1991). Camptothecin cytotoxicity in mammalian cells is associated with the induction of persistent double strand breaks in replicating DNA. Nucleic Acids Res *19*, 3295-3300.

132. Rydberg, B. (2000). Radiation-induced heat-labile sites that convert into DNA double-strand breaks. Radiat Res *153*, 805-812.

133. Saini, N., Ramakrishnan, S., Elango, R., Ayyar, S., Zhang, Y., Deem, A., Ira, G., Haber, J.E., Lobachev, K.S., and Malkova, A. (2013). Migrating bubble during break-induced replication drives conservative DNA synthesis. Nature *502*, 389-392.

134. Saitoh, H., and Hinchey, J. (2000). Functional heterogeneity of small ubiquitin-related protein modifiers SUMO-1 versus SUMO-2/3. J Biol Chem *275*, 6252-6258.

135. Saleh, E.M., El-Awady, R.A., Anis, N., and El-Sharkawy, N. (2012). Induction and repair of DNA double-strand breaks using constant-field gel electrophoresis and apoptosis as predictive markers for sensitivity of cancer cells to cisplatin. Biomed Pharmacother *66*, 554-562.

136. Sarangi, P., Steinacher, R., Altmannova, V., Fu, Q., Paull, T.T., Krejci, L., Whitby, M.C., and Zhao, X. (2015). Sumoylation influences DNA break repair partly by increasing the solubility of a conserved end resection protein. PLoS genetics *11*, e1004899.

137. Schlacher, K., Christ, N., Siaud, N., Egashira, A., Wu, H., and Jasin, M. (2011). Double-strand break repair-independent role for BRCA2 in blocking stalled replication fork degradation by MRE11. Cell *145*, 529-542.

138. Shah Punatar, R., Martin, M.J., Wyatt, H.D., Chan, Y.W., and West, S.C. (2017). Resolution of single and double Holliday junction recombination intermediates by GEN1. Proc Natl Acad Sci U S A *114*, 443-450.

139. Shibata, T., Cunningham, R.P., DasGupta, C., and Radding, C.M. (1979). Homologous pairing in genetic recombination: complexes of recA protein and DNA. Proc Natl Acad Sci U S A *76*, 5100-5104.

140. Sidorova, J.M., Kehrli, K., Mao, F., and Monnat, R., Jr. (2013). Distinct functions of human RECQ helicases WRN and BLM in replication fork recovery and progression after hydroxyurea-induced stalling. DNA repair *12*, 128-139.

141. Sidorova, J.M., Li, N., Schwartz, D.C., Folch, A., and Monnat, R.J., Jr. (2009). Microfluidic-assisted analysis of replicating DNA molecules. Nat Protoc *4*, 849-861.

142. Solinger, J.A., Kiianitsa, K., and Heyer, W.D. (2002). Rad54, a Swi2/Snf2-like recombinational repair protein, disassembles Rad51:dsDNA filaments. Mol Cell *10*, 1175-1188.

143. Sollier, J., Driscoll, R., Castellucci, F., Foiani, M., Jackson, S.P., and Branzei, D. (2009). The Saccharomyces cerevisiae Esc2 and Smc5-6 proteins promote sister chromatid junction-mediated intra-S repair. Mol Biol Cell *20*, 1671-1682.

144. Streich, F.C., Jr., and Lima, C.D. (2016). Capturing a substrate in an activated RING E3/E2-SUMO complex. Nature *536*, 304-308.

145. Strumberg, D., Pilon, A.A., Smith, M., Hickey, R., Malkas, L., and Pommier, Y. (2000). Conversion of topoisomerase I cleavage complexes on the leading strand of ribosomal DNA into 5'-phosphorylated DNA double-strand breaks by replication runoff. Mol Cell Biol *20*, 3977-3987.

146. Stubbe, J., and van der Donk, W.A. (1995). Ribonucleotide reductases: radical enzymes with suicidal tendencies. Chem Biol *2*, 793-801.

147. Sullivan, M.R., and Bernstein, K.A. (2018). RAD-ical New Insights into RAD51 Regulation. Genes *9*.

148. Sundin, O., and Varshavsky, A. (1980). Terminal stages of SV40 DNA replication proceed via multiply intertwined catenated dimers. Cell *21*, 103-114.

149. Tapia-Alveal, C., Lin, S.J., and O'Connell, M.J. (2014). Functional interplay between cohesin and Smc5/6 complexes. Chromosoma *123*, 437-445.

150. Tatham, M.H., Rodriguez, M.S., Xirodimas, D.P., and Hay, R.T. (2009). Detection of protein SUMOylation in vivo. Nat Protoc *4*, 1363-1371.

151. Thangavel, S., Berti, M., Levikova, M., Pinto, C., Gomathinayagam, S., Vujanovic, M., Zellweger, R., Moore, H., Lee, E.H., Hendrickson, E.A.*, et al.* (2015). DNA2 drives processing and restart of reversed replication forks in human cells. J Cell Biol *208*, 545-562.

152. Toledo, L.I., Altmeyer, M., Rask, M.B., Lukas, C., Larsen, D.H., Povlsen, L.K., Bekker-Jensen, S., Mailand, N., Bartek, J., and Lukas, J. (2013). ATR prohibits replication catastrophe by preventing global exhaustion of RPA. Cell *155*, 1088-1103.

153. van Gent, D.C., Hoeijmakers, J.H., and Kanaar, R. (2001). Chromosomal stability and the DNA double-stranded break connection. Nat Rev Genet *2*, 196-206.

154. Verver, D.E., Zheng, Y., Speijer, D., Hoebe, R., Dekker, H.L., Repping, S., Stap, J., and Hamer, G. (2016). Non-SMC Element 2 (NSMCE2) of the SMC5/6 Complex Helps to Resolve Topological Stress. Int J Mol Sci *17*.

155. Villwock, S.K., and Aparicio, O.M. (2014). Two-dimensional agarose gel electrophoresis for analysis of DNA replication. Methods Mol Biol *1205*, 329-340.

156. Wang, A.T., Kim, T., Wagner, J.E., Conti, B.A., Lach, F.P., Huang, A.L., Molina, H., Sanborn, E.M., Zierhut, H., Cornes, B.K.*, et al.* (2015). A Dominant Mutation in Human RAD51 Reveals Its Function in DNA Interstrand Crosslink Repair Independent of Homologous Recombination. Mol Cell *59*, 478-490.

157. Wang, L., Wansleeben, C., Zhao, S., Miao, P., Paschen, W., and Yang, W. (2014). SUMO2 is essential while SUMO3 is dispensable for mouse embryonic development. EMBO reports *15*, 878-885.

158. Watanabe, K., Pacher, M., Dukowic, S., Schubert, V., Puchta, H., and Schubert, I. (2009). The STRUCTURAL MAINTENANCE OF CHROMOSOMES 5/6 complex promotes sister chromatid alignment and homologous recombination after DNA damage in Arabidopsis thaliana. Plant Cell *21*, 2688-2699.

159. Whitby, M.C., Osman, F., and Dixon, J. (2003). Cleavage of model replication forks by fission yeast Mus81-Eme1 and budding yeast Mus81-Mms4. J Biol Chem *278*, 6928-6935.

160. Willetts, N.S., Clark, A.J., and Low, B. (1969). Genetic location of certain mutations conferring recombination deficiency in Escherichia coli. J Bacteriol *97*, 244-249.

161. Witkiewicz, A.K., McMillan, E.A., Balaji, U., Baek, G., Lin, W.C., Mansour, J., Mollaee, M., Wagner, K.U., Koduru, P., Yopp, A.*, et al.* (2015). Whole-exome sequencing of pancreatic cancer defines genetic diversity and therapeutic targets. Nat Commun *6*, 6744.

162. Wlodek, D., Banath, J., and Olive, P.L. (1991). Comparison between pulsed-field and constant-field gel electrophoresis for measurement of DNA double-strand breaks in irradiated Chinese hamster ovary cells. Int J Radiat Biol *60*, 779-790.

163. Wu, N., Kong, X., Ji, Z., Zeng, W., Potts, P.R., Yokomori, K., and Yu, H. (2012). Scc1 sumoylation by Mms21 promotes sister chromatid recombination through counteracting Wapl. Genes Dev *26*, 1473-1485.

164. Xaver, M., Huang, L., Chen, D., and Klein, F. (2013). Smc5/6-Mms21 prevents and eliminates inappropriate recombination intermediates in meiosis. PLoS genetics *9*, e1004067.

165. Xing, J., Apedo, A., Tymiak, A., and Zhao, N. (2004). Liquid chromatographic analysis of nucleosides and their mono-, di- and triphosphates using porous graphitic carbon stationary phase coupled with electrospray mass spectrometry. Rapid Commun Mass Spectrom *18*, 1599-1606.

166. Xu, J., He, Y., Qiang, B., Yuan, J., Peng, X., and Pan, X.M. (2008). A novel method for high accuracy sumoylation site prediction from protein sequences. BMC Bioinformatics *9*, 8.

167. Ying, S., Minocherhomji, S., Chan, K.L., Palmai-Pallag, T., Chu, W.K., Wass, T., Mankouri, H.W., Liu, Y., and Hickson, I.D. (2013). MUS81 promotes common fragile site expression. Nat Cell Biol *15*, 1001-1007.

168. Zellweger, R., Dalcher, D., Mutreja, K., Berti, M., Schmid, J.A., Herrador, R., Vindigni, A., and Lopes, M. (2015). Rad51-mediated replication fork reversal is a global response to genotoxic treatments in human cells. J Cell Biol *208*, 563-579.

169. Zhang, C.Z., Spektor, A., Cornils, H., Francis, J.M., Jackson, E.K., Liu, S., Meyerson, M., and Pellman, D. (2015). Chromothripsis from DNA damage in micronuclei. Nature *522*, 179-184.

170. Zhang, F.P., Mikkonen, L., Toppari, J., Palvimo, J.J., Thesleff, I., and Janne, O.A. (2008). Sumo-1 function is dispensable in normal mouse development. Mol Cell Biol *28*, 5381-5390.

171. Zhao, X., and Blobel, G. (2005). A SUMO ligase is part of a nuclear multiprotein complex that affects DNA repair and chromosomal organization. Proc Natl Acad Sci U S A *102*, 4777-4782.

172. Zhu, J., Zhu, S., Guzzo, C.M., Ellis, N.A., Sung, K.S., Choi, C.Y., and Matunis, M.J. (2008). Small ubiquitin-related modifier (SUMO) binding determines substrate recognition and paralog-selective SUMO modification. J Biol Chem *283*, 29405-29415.